

D3.1: Data-set on soil parameters

Project Contractual Details

Project Acronym INF⁴INiTY

Project Title: Integrated Designs for Future Floating Offshore Wind Farm Technology

Project No.: 101136087

Call: HORIZON-CL5-2023-D3-01
Topic: HORIZON-CL5-2023-D3-01-05

Project Coordinator: Technische Universität Braunschweig

Project Start Date: January 1, 2024
Project End Date: December 31, 2027

Duration: 48 months

Document Details

Due Date of Deliverable: 30-06-2025(M18)

Actual Submission Date: 30-06-2025
Lead Partner for Deliverable: IBW PAN

Contributing Partner(s): GICON, BM SUMER, DTU-C, WIKKI, LUH, PoliTO

PU - Public

Associated Work Package: WP 3
Associated Task(s): Task 3.1
Issue Number: D3.1

Prepared by: Krystyna Kazimierowicz-Frankowska

Verified by: Gael Verao Fernández

History of Changes

Dissemination Level:

Version	Date	Change	Contributor(s)
1.0	18-06-2025	First Draft	Krystyna Kazimierowicz- Frankowska
1.1	24-06-2025	Corrections	Gael Verao Fernández
2.0	27-06-2025	Final Version	Krystyna Kazimierowicz- Frankowska





Executive Summary

The objective of the testing program was to determine the geotechnical characteristics of soil samples collected from three marine regions: the Baltic Sea, the Scottish Sea, and the Adriatic Sea. For each of the above-mentioned regions, samples were taken from two locations. In total, preliminary tests were carried out for six types of soil. The experimental campaign began with a detailed microscopic examination and grain size distribution analysis to classify the soils. Based on the results, five of them were found to meet the initially adopted criteria (these are non-cohesive soils) and were subjected to a detailed testing procedure (a full set of monotonic and cyclic triaxial tests was performed). Soil samples marked with the symbol Adriatic 1 were identified as cohesive and therefore not suitable for liquefaction-related testing.

Subsequent testing involved monotonic and cyclic triaxial shear tests to determine mechanical and index properties, liquefaction potential, and elastic parameters based on seismic wave velocities. A database of soil characteristics was compiled to support the development of surrogate soils with scaled properties for further use in physical and numerical modelling. Detailed results of the most significant tests performed are included in the appendixes attached to the report.



Table of Contents

E>	ecutive	Summary	2
1	Intro	duction	8
2	Expe	rimental programme and methodology	9
	2.1	Basic soil properties	9
	2.2	Triaxial tests	11
	2.2.1	Main goals of tests	11
	2.2.2	Triaxial apparatus	11
	2.2.3	Sample preparation, test procedure	11
	2.2.4	Measurement of shear wave velocity	12
3	Test	Results	12
	3.1	Testing programme	12
	3.2	Monotonic triaxial tests	12
	3.3	Cyclic triaxial tests	21
	3.4	Elastic modulus	26
4	Cond	lusions	28
5	Refe	rences	29
6	Appe	endixes	30
	6.1	Appendix nr 1 - Triaxial tests: Summary of testing program	30
	6.2	Appendix nr 2 - Results of soil samples collected from Baltic Sea; Soil type: Baltic 1	34
	6.3	Appendix nr 3 - Results of soil samples collected from Baltic Sea; Soil type: Baltic 2	46
	6.4	Appendix nr 4 - Results of soil samples collected from Baltic Sea; Soil type: Scottish 1	60
	6.5	Appendix nr 5 - Results of soil samples collected from Baltic Sea; Soil type: Scottish 2	69
	6.6	Appendix nr 6 - Results of soil samples collected from Adriatic Sea; Soil type: Adriatic 1	79
	6.7	Appendix nr 7 - Results of soil samples collected from Adriatic Sea; Soil type: Adriatic 2	81
	6.8	Appendix nr 8 - Triaxial tests: Elastic modulus	86



List of Figures

- 1. Fig. 1 Sampling locations: Baltic Sea (a); Scottish Sea (b); Adriatic Sea (c)
- 2. Fig. 2 The view of soil grains under the microscope: Baltic Sea (a); Scottish Sea (b); Adriatic Sea (c)
- 3. Fig. 3 Grain size distribution curves
- 4. Fig.4. Triaxial apparatus: scheme (a), general view (b)
- 5. Fig.5 Typical shape of steady state line
- 6. Fig. 6 Stress paths for sand collected from Baltic Sea (Baltic 1)
- 7. Fig.7 Steady state line position for sand collected from Baltic Sea (Baltic 1)
- 8. Fig.8 Stress paths for sand collected from Baltic Sea (Baltic 2)
- 9. Fig.9 Steady state line position for sand collected from Baltic Sea (Baltic 2)
- 10. Fig.10 Stress paths for sand collected from Scottish Sea (Scottish 1)
- 11. Fig.11 Position of points on the steady-state line for sand collected from Scottish Sea (Scottish 1)
- 12. Fig.12 Stress paths for sand collected from Scottish Sea (Scottish 2)
- 13. Fig.13 Position of points on the steady-state line for sand collected from Scottish Sea (Scottish 2)
- 14. Fig.14 Results of monotonic test carried out on cohesive sample collected from Adriatic Sea (Adriatic 1): stress path
- 15. Fig.15 Results of monotonic test carried out on cohesive sample collected from Adriatic Sea (Adriatic 1): stress deviator and volumetric strain versus vertical strain.
- 16. Fig.16 Stress paths for sand collected from Adriatic Sea (Adriatic 2)
- 17. Fig.17 Position of points correspond to steady state of deformation (b) for sand collected from Adriatic Sea (Adriatic 2)
- 18. Fig.18 Comparison of the position of the steady-state line for different types of sand (collected from Baltic, Scottish and Adriatic Sea)
- 19. Fig.19 Cyclic loading stress paths for sand collected from Baltic Sea (Baltic 1)
- 20. Fig.20 Cyclic loading stress paths for sand collected from Baltic Sea (Baltic 2)
- 21. Fig.21 Cyclic loading stress paths for sand collected from Scottish Sea (Scottish 1)
- 22. Fig.22 Cyclic loading stress paths for sand collected from Scottish Sea (Scottish 2)
- 23. Fig.23 Cyclic loading stress paths for sand collected from Adriatic Sea (Adriatic 2)
- 24. Fig.24 Typical results of cyclic triaxial compression test made on contractive sample stress spaces
- 25. Fig.25 Typical results of cyclic triaxial compression test made on contractive sample: generation of pore-water pressure and changes of axial strain versus number of loading cycles





- 26. Fig.26 Normalized amplitude of the shear stress vs. the number of cycles to liquefaction results for the five types of soil samples
- 27. Fig.27 Initial changes of the stress deviator $q = \sigma_{z0} \sigma_{x0}$ as a function of the axial strain ϵz
- 28. Fig.28 Calculated values of modulus E as functions of the initial effective stress σ^\prime_0
- 29. Fig. 29 Calculated values of Poisson's ratios as functions of the initial effective stress σ_0 '



List of Tables

1. Table 1. Soils properties



List of Appendixes

- 1. Appendix nr 1 Triaxial tests: Summary of testing program
- 2. Appendix nr 2 Results of soil samples collected from Baltic Sea; Soil type: Baltic 1
- 3. Appendix nr 3 Results of soil samples collected from Baltic Sea; Soil type: Baltic 2
- 4. Appendix nr 4 Results of soil samples collected from Baltic Sea; Soil type: Scottish 1
- 5. Appendix nr 5 Results of soil samples collected from Baltic Sea; Soil type: Scottish 2
- 6. Appendix nr 6 Results of soil samples collected from Adriatic Sea; Soil type: Adriatic 1
- 7. Appendix nr 7 Results of soil samples collected from Adriatic Sea; Soil type: Adriatic 2
- 8. Appendix nr 8 Triaxial tests: Elastic modulus



1 Introduction

The general objective of the performed work was to collect soil samples from three different locations – (1) the Baltic Sea, (2) the Scottish Sea, and (3) the Adriatic Sea – and subsequently determinate their basic geotechnical characteristics. During the first project meeting, specific guidelines regarding the sampling strategy were established. It was decided to focus on investigating non-cohesive soils since one of the key parameters to be determined during tests was the susceptibility to liquefaction. This phenomenon occurs only in non-cohesive soils. Therefore, the soil samples were collected from locations where, based on available information, such non-cohesive soils were expected to be present (see Fig. 1).

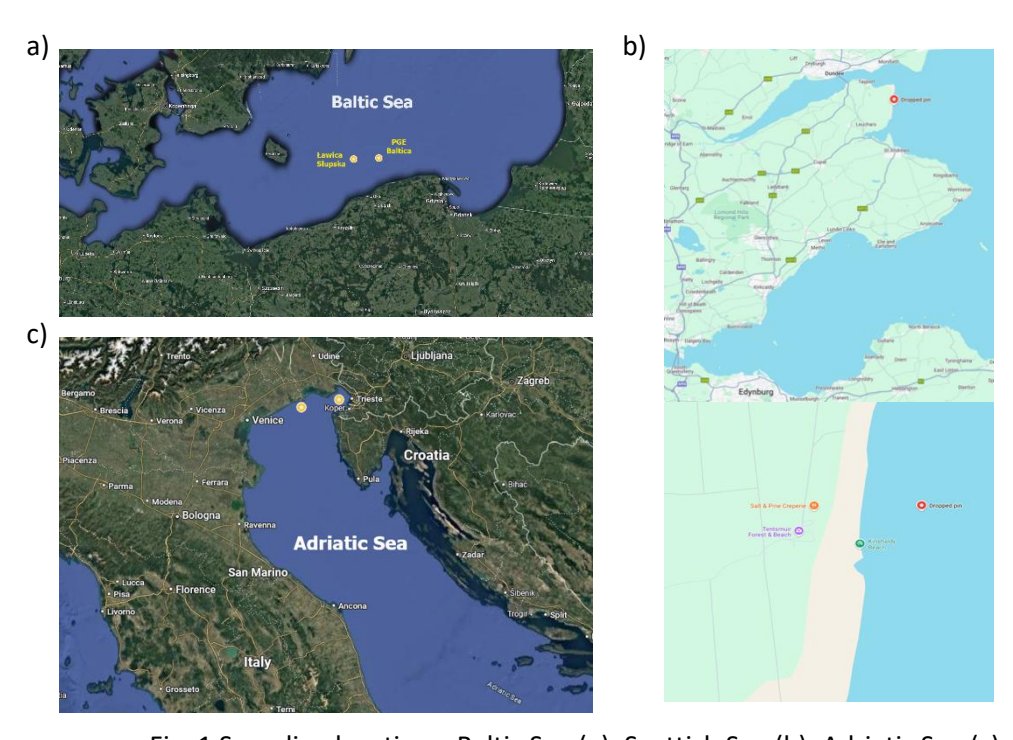


Fig. 1 Sampling locations: Baltic Sea (a); Scottish Sea (b); Adriatic Sea (c)

Having compiled the soil samples, a database of geotechnical characteristics of the soils at the three test sites was constructed. The main objective was achieved through determining the geotechnical characteristics of investigated soil samples (i.e., soil index and mechanical properties, susceptibility to liquefaction, elastic constants based on seismic waves' velocities) via a series of monotonic and cyclic triaxial shear tests.

This task was carried out over a period of 18 months (from Month 1 to Month 18) and involved the participation of eight project partners (L: IBW PAN; P: GICON, BM SUMER, DTU-C, WIKKI, LUH, PoliTO), each contributing in a specific way. For example, PoliTO provided access to relevant soil databases, while BM SUMER, LUH, and DTUC contributed expertise gained from earlier scaled geotechnical and morphodynamic studies, helping to define the requirements for the surrogate soils. At the same time, WIKKI played a key role in facilitating the transfer of geotechnical knowledge into the domain of numerical modelling.



2 Experimental programme and methodology

2.1 Basic soil properties

The experimental testing program began with a detailed microscopic examination of the soil samples collected for analysis (Fig.2) and identification of the types of soils collected. For this purpose, particle size distribution curves were determined (Fig. 3). The grain size distribution curves were determined using conventional sieve analysis for the fraction that was larger than 0.063 mm and using the hydro suspension method for the soil with a grain size smaller than 0.063 mm. The results of the tests performed show that in five cases the soil samples that were used in the tests could be classified as sand (Baltic Sea 1; Baltic Sea 2, Scottish Sea 1, Scottish Sea 2, Adriatic Sea 2). In one case (Adriatic 1), the soil samples collected were identified as cohesive soil. Therefore, it did not meet the criteria set for the type of soils intended for investigation. Therefore, only a limited scope of testing was carried out for this soil (see Appendix 6) – the basic soil parameters were determined, and a triaxial test was performed under monotonic loading.



Fig. 2 The view of soil grains under the microscope: Baltic Sea (a); Scottish Sea (b); Adriatic Sea (c)



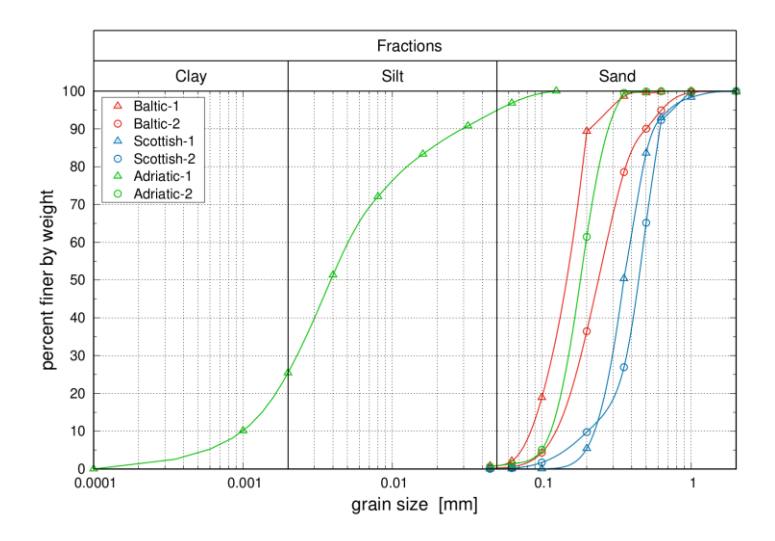


Fig. 3 Grain size distribution curves

Then, in order to determine the basic physical and mechanical parameters for the soil that was used in the experiments, several standard tests were carried out. Table 1 summarizes main physical and mechanical characteristics of investigated soil samples. The parameter d_{50} is the grain size at which 50% of the soil is finer. The values of e_{max} and e_{min} are the extreme values of the void ratio, corresponding to the loosest and densest states of the soil, respectively. The angle of internal friction was determined from tests performed in the triaxial apparatus for the "geotechnical" stress path (vertical effective stress increased, cell pressure kept constant). In the case of soil samples taken from the Adriatic Sea 1 location, not all the parameters listed in Table 1 were determined. This was due to the different type of soil (cohesive soil) as explained above.

Table 1. Soils properties

Cond	d ₅₀	$ ho_{\sf d,max}$	$oldsymbol{ ho}_{\sf d,min}$	e _{min}	e _{max}	φ	ρς
Sand	[mm]	[t/m³]	[t/m³]	[-]	[-]	[deg]	[g/cm ³]
Baltic Sea 1	0.144	1.681	1.345	0.576	0.970	31.8	2.65
Baltic Sea 2	0.250	1.741	1.390	0.522	0.906	33.0	2.67
Scottish Sea 1	0.354	1.642	1.362	0.631	0.966	34.6	2.69
Scottish Sea 2	0.443	1.751	1.404	0.564	0.950	33.0	2.74
Adriatic Sea 1	0.004						2.69
Adriatic Sea 2	0.181	1.687	1.394	0.652	0.999	33.9	2.79

 d_{50} – median grain size, $ho_{d_{max/min}}$ – maximum/minimum dry density; $e_{min/max}$ – minimum/ maximum void ratio; φ – friction angle, ho_{S} – particle density





2.2 Triaxial tests

2.2.1 Main goals of tests

The main objective of triaxial tests was to determine more advanced parameters of the tested soils. The focus was primarily on assessing the soils' susceptibility to liquefaction. For this purpose, both monotonic and cyclic tests were conducted. The results obtained from the triaxial tests were also used to determine the elastic constants of the tested soils, such as Young's modulus and Poisson's ratio.

2.2.2 Triaxial apparatus

All triaxial tests were carried out using a computer controlled triaxial testing system manufactured by GDS Instruments Ltd. (Fig.4). The system consisted of a triaxial cell of the Bishop and Wesley type with internal load cell, housing specimens of 38 mm in diameter and 80 mm in height, digital pressure-volume controllers for controlling cell and back pressures, as well as axial load, and data acquisition system linked to a desktop computer. The volume change (during drained tests) or the pore-water pressure (during undrained tests) of the sample was measured by one of the controllers, which was able to either control back pressure while measuring volume change, or control volume change while measuring pore-water pressure. The tests were performed in both strain and load controlled modes, including cyclic loading. A single test consisted of four main stages: (1) preparation of the specimen to the desired density, (2) saturation to the required value of B Scampton's coefficient playing with back pressure, (3) consolidation to the presumed confining pressure and (4) final loading.

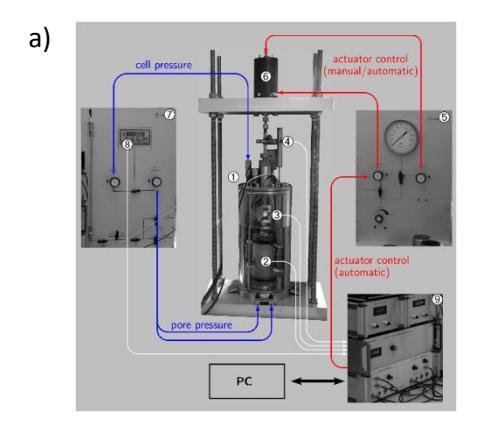




Fig.4. Triaxial apparatus: scheme (a), general view (b)

2.2.3 Sample preparation, test procedure

All samples were prepared in a membrane-lined split mould either by moist tampling (MT) or by air pluviation (AP) methods. The first method led to a relatively uniform – very loose – samples which revealed contractive behaviour when sheared, whereas the second method rendered denser samples exhibiting dilative character. The split mould was attached to the lower platen of the cell and the membrane held to the inside of the mould by vacuum. In the case of moist compacted samples five pre-weighted portions of sand were mixed with de-aired water to give about a 3 to 5% water content. Each portion of sand was then compacted into the mould to a predetermined height corresponding to the desired void ratio. Wet pluviated samples were





prepared from the sand which had first been mixed with de-aired water and then spooned into the mould filled initially with 30% of de-aired water. The mould was tapped gently to densify the sample, if necessary, to obtain the required weight of soil in the mould. Once the sample was in the mould and closed by the top platen, a vacuum pressure of the order of 15 kPa was applied. It allowed easy assembling of the triaxial cell or gauges for local measurement of horizontal and radial strains to control the void ratio change during saturation and consolidation stages, without disturbance of the sample and preserving the initial void ratio, particularly in very loose samples. After assembling the triaxial cell and filling it with de-aired water the vacuum pressure was then replaced by the same confining pressure.

2.2.4 Measurement of shear wave velocity

Measurement of the velocity of seismic wave (V_s – Table 1 – Appendix 1) was carried out after completion of consolidation process. Piezoelectric bender elements were used to induce shear waves being propagated through the specimen. The wave passage time was measured. Velocity was calculated knowing the distance between piezoelectric elements. Wave frequency varied between 6 kHz and 20 kHz and was adjusted to obtain the best soil response. In order to determine the wave passage time more accurately, very asymmetrical sinusoidal signal was used.

3 Test Results

3.1 Testing programme

The testing programme was summarised in Table 1 (Appendix 1). Within the frame of the experimental programme two main types of tests were carried out, namely: monotonic compression triaxial (MT) and cyclic triaxial tests (CT) for various initial states of the specimens and loading conditions. Test conditions varied considerably and included drained (13) and undrained (28) conditions for 38 specimens prepared by moist compaction method, two by air pluviation and one by slurry deposition. The general aim of experimental work was to study the undrained response of saturated non-cohesive soils to monotonic and cyclic loading.

3.2 Monotonic triaxial tests

In order to determine the liquefaction susceptibility of soil, the position of steady-state line was selected. The concept of steady state of deformation for sands originated from Casagrande's idea of "critical void ratio" (Green & Fergusson 1971) and was later extended by critical state concept proposed by Schofield and Wroth (1968) for clays. It was Castro who first termed the ultimate constant state the sample of loose sand reaches during monotonic triaxial shearing in undrained conditions, after rapid drop of shear strength from peak shear resistance to the residual value, as the steady state (Castro 1975; Lipiński 2000).

On the basis of Castro's extensive experimental work, Poulos (1981) defined the steady state of deformation for any mass of particles as the state in which the mass is continuously deforming at constant volume, constant normal effective stress, constant shear stress, and constant velocity. The steady state is achieved only after orientation of all particles has reached a statically steady-state condition and after all particle breakage, if any, is complete, so that the shear stress needed to continue deformation and its velocity remains constant (Sawicki & Kazimierowicz-Frankowska, 2015). Such state corresponds to residual constant shear strength which, in this case, is identified with liquefaction of the soil.



The term "steady state" is used to reflect the steady-state flow of liquefied sand, whereas the term "deformation" is used to emphasize that the steady state exists only when deformation is ongoing (Poulos 1981). Steady state of deformation is described by two parameters: void ratio and mean effective stress during steady state. The pairs of these values corresponding to steady state, when plotted in the void ratio—mean effective stress space (presented in semi-logarithmic scale e - log p'), are located along the common line designated as steady state line. Typical steady state line has been schematically shown in Fig.5. The mean effective stress is defined as:

$$\sigma_0' = \frac{\sigma_1' + 2\sigma_3'}{3}$$

where σ_1' is vertical effective stress, and σ_3' is horizontal effective stress.

It can be noticed that the value of mean effective stress may change completely the behaviour of any granular material which e.g. when in dense state and subjected to sufficiently high pressures may behave similarly to loose material.

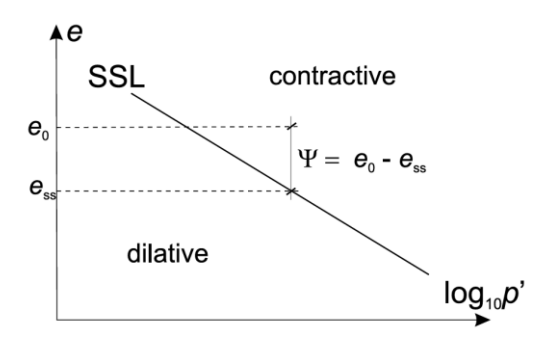


Fig.5 Typical shape of steady state line



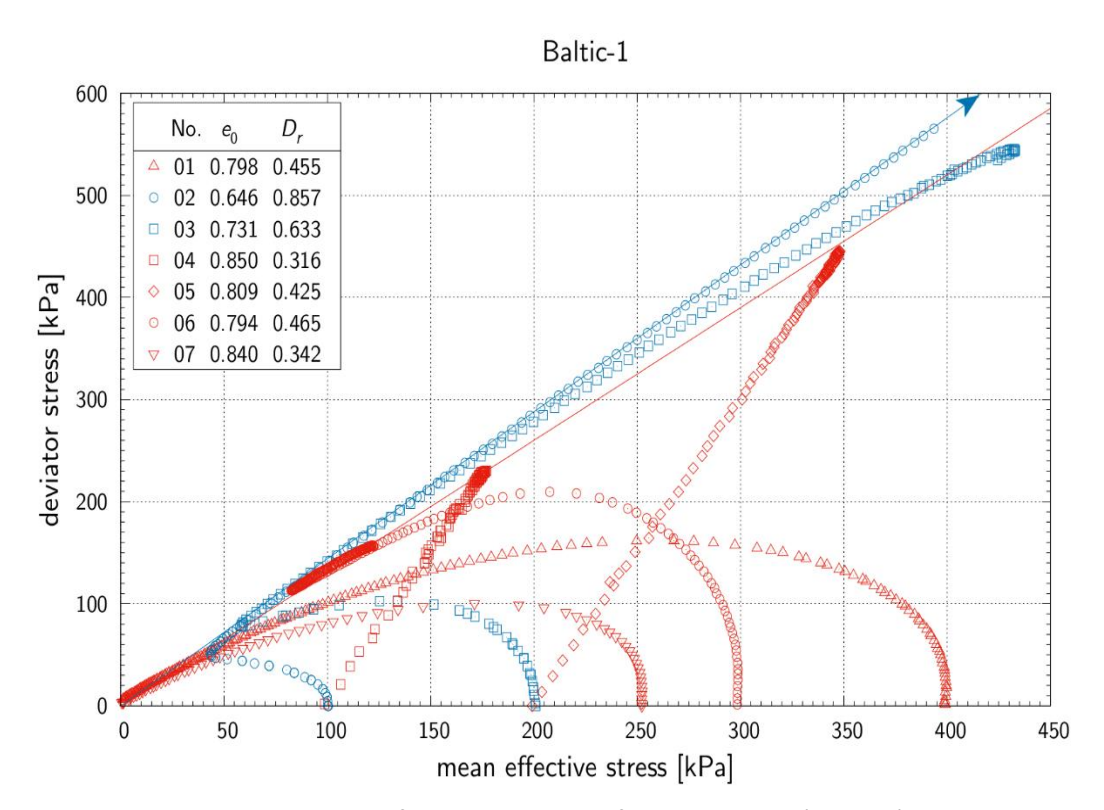


Fig.6 Stress paths for sand collected from Baltic Sea (Baltic 1).

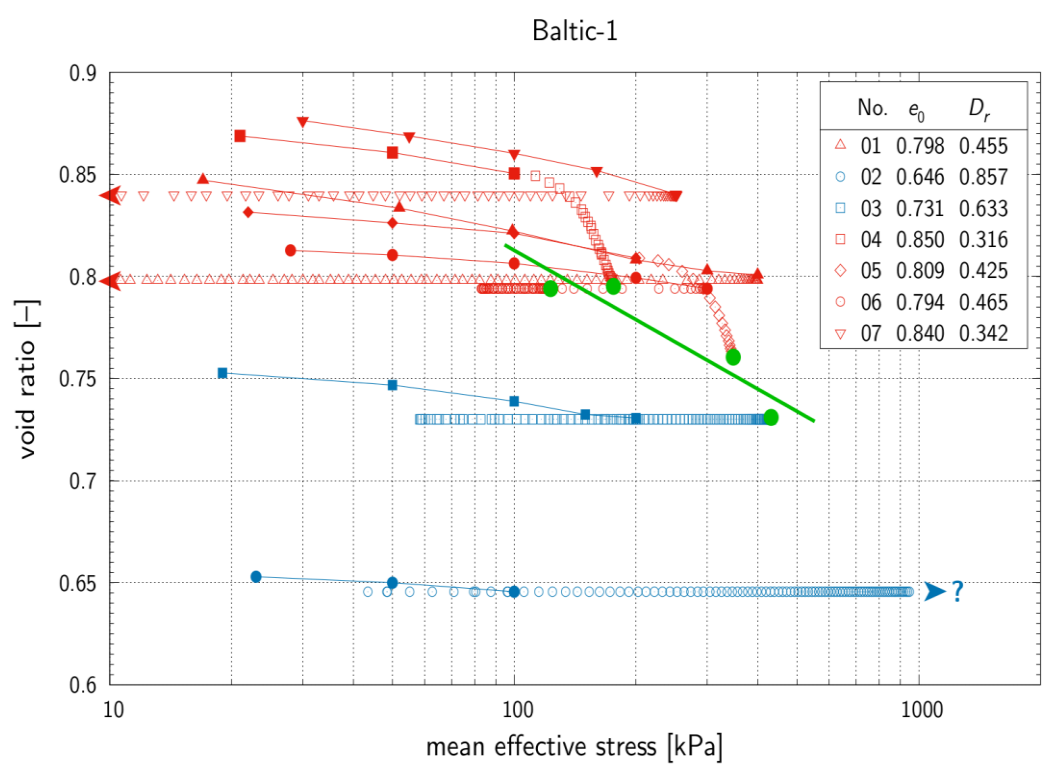


Fig.7 Steady state line position for sand collected from Baltic Sea (Baltic 1).





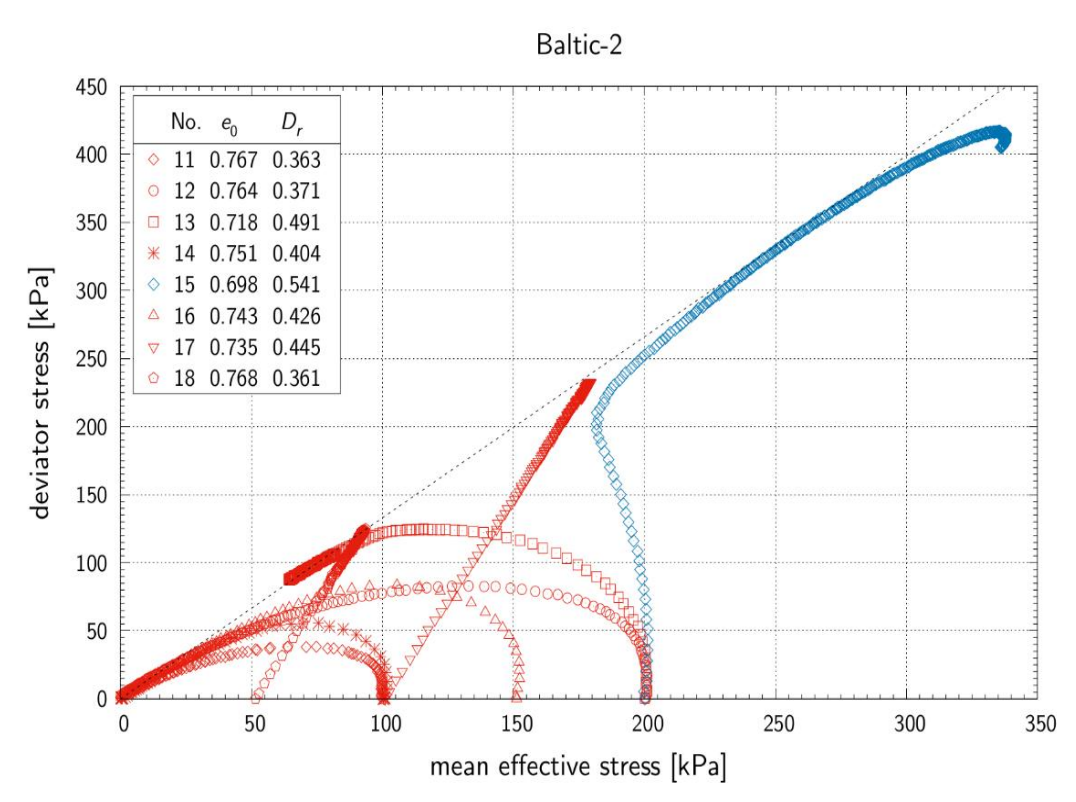


Fig.8 Stress paths for sand collected from Baltic Sea (Baltic 2).

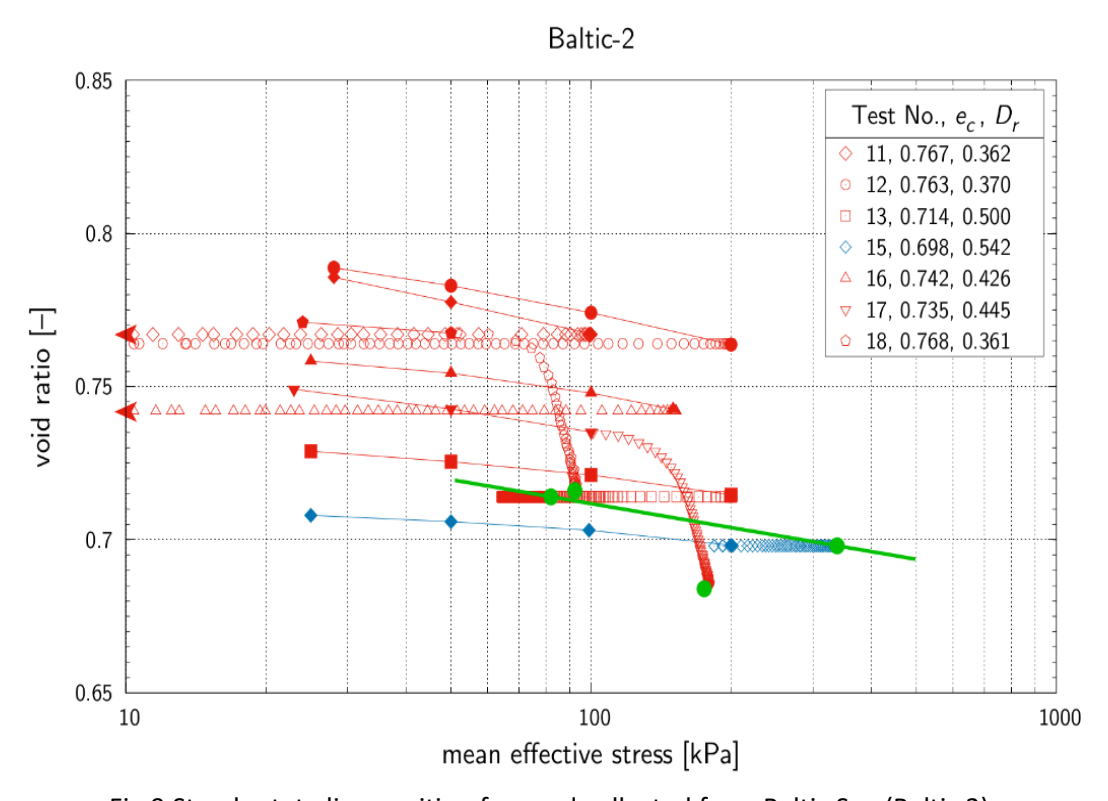


Fig.9 Steady state line position for sand collected from Baltic Sea (Baltic 2).





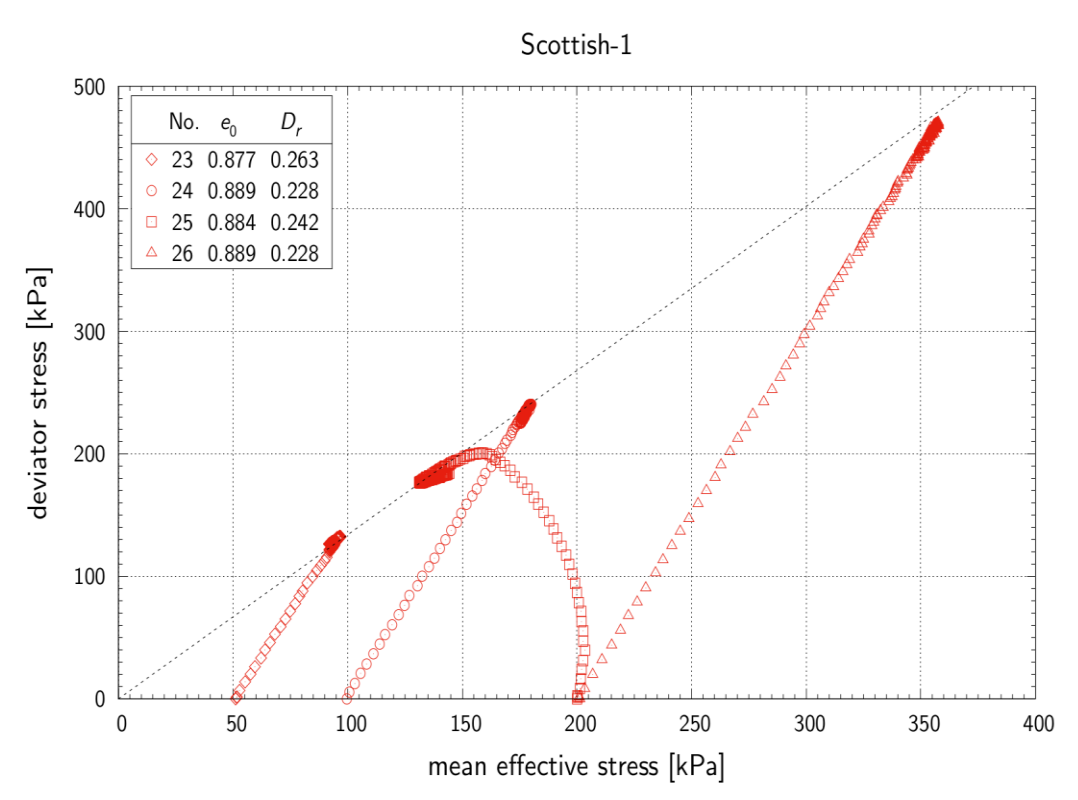


Fig.10 Stress paths for sand collected from Scottish Sea (Scottish 1).

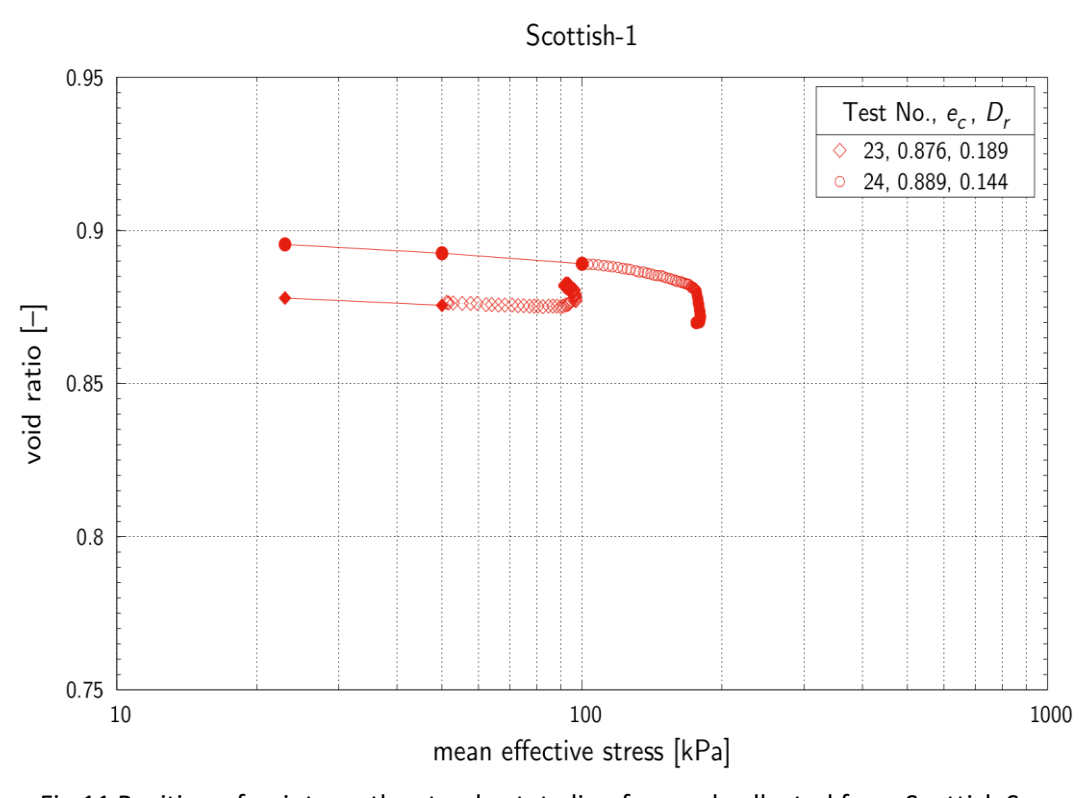


Fig.11 Position of points on the steady-state line for sand collected from Scottish Sea (Scottish 1).





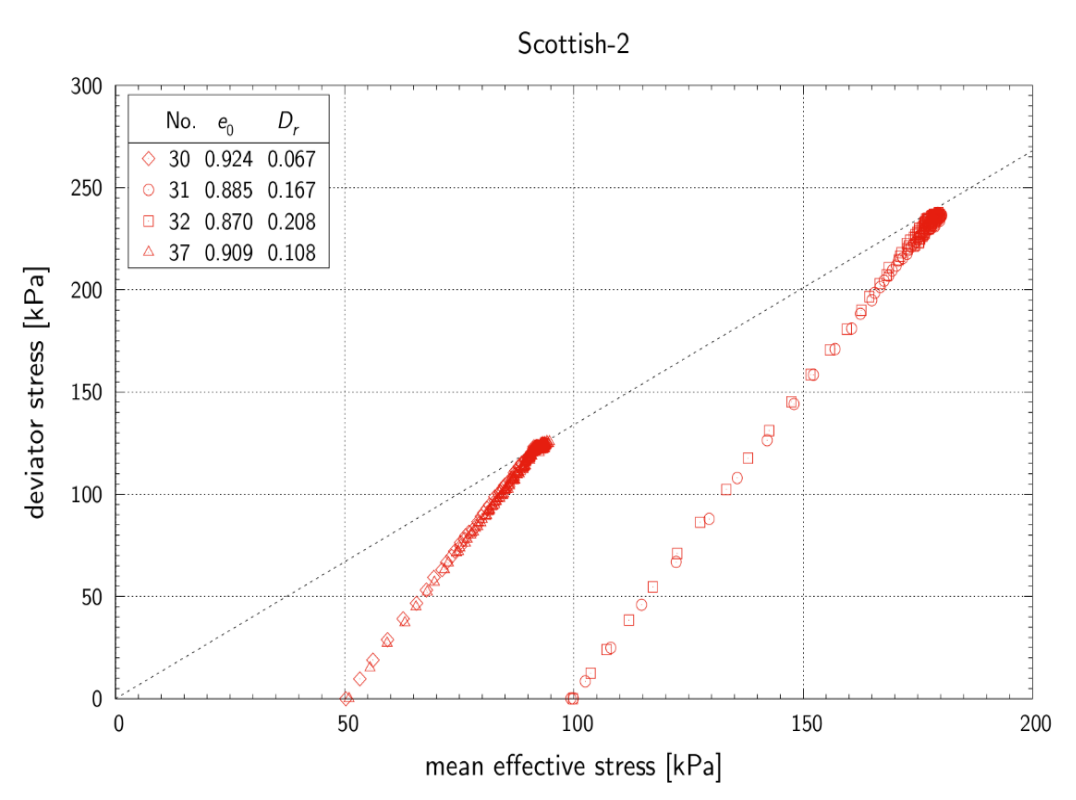


Fig.12 Stress paths for sand collected from Scottish Sea (Scottish 2).

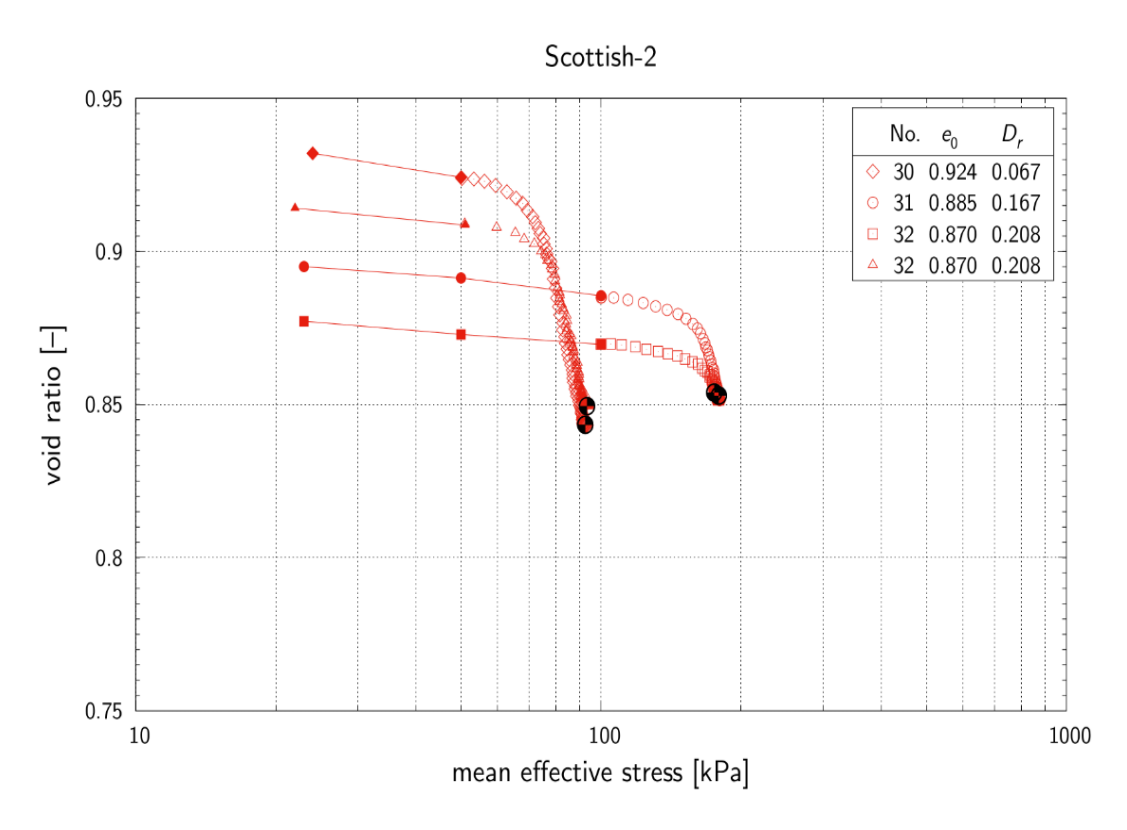


Fig.13 Position of points correspond to steady state of deformation for sand collected from Scottish Sea (Scottish 2).





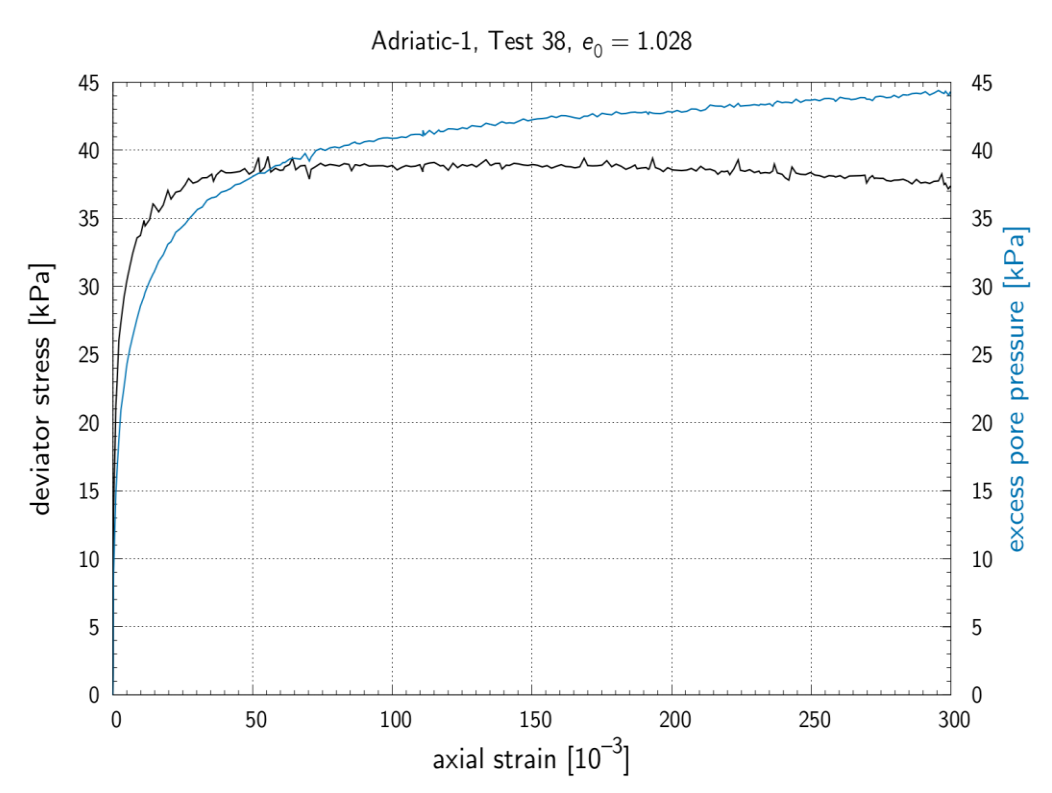


Fig.14 Results of monotonic test carried out on cohesive sample collected from Adriatic Sea (Adriatic 1): stress path.

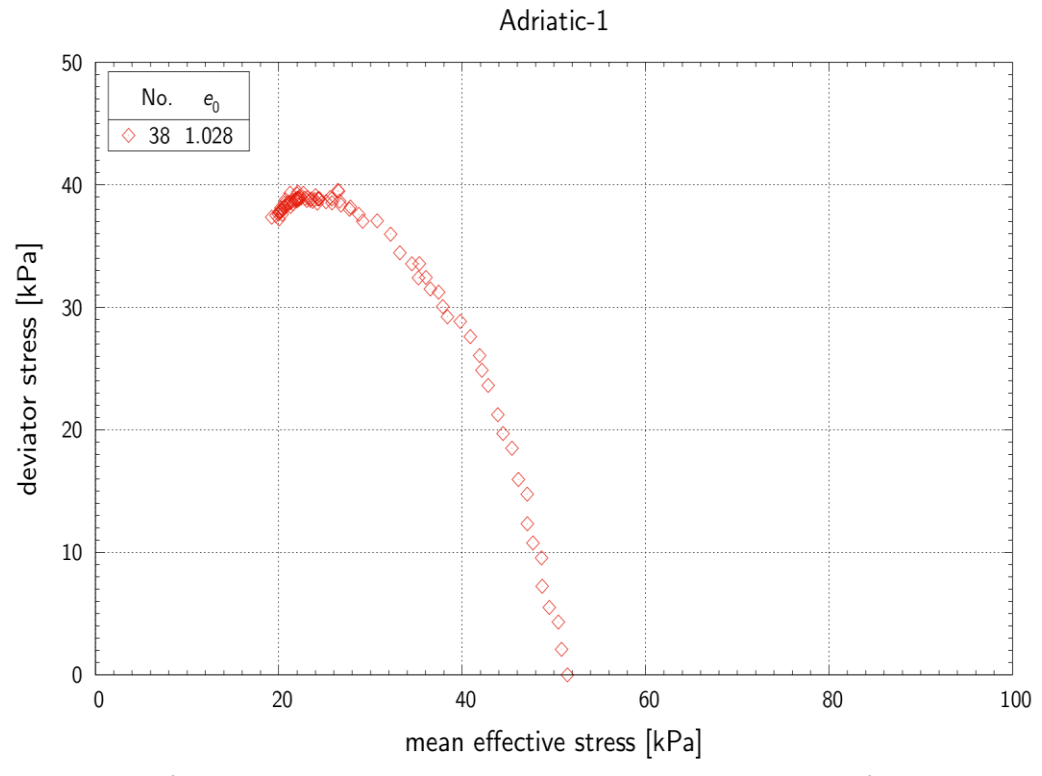


Fig.15 Results of monotonic test carried out on cohesive sample collected from Adriatic Sea (Adriatic 1): stress deviator and volumetric strain versus vertical strain.





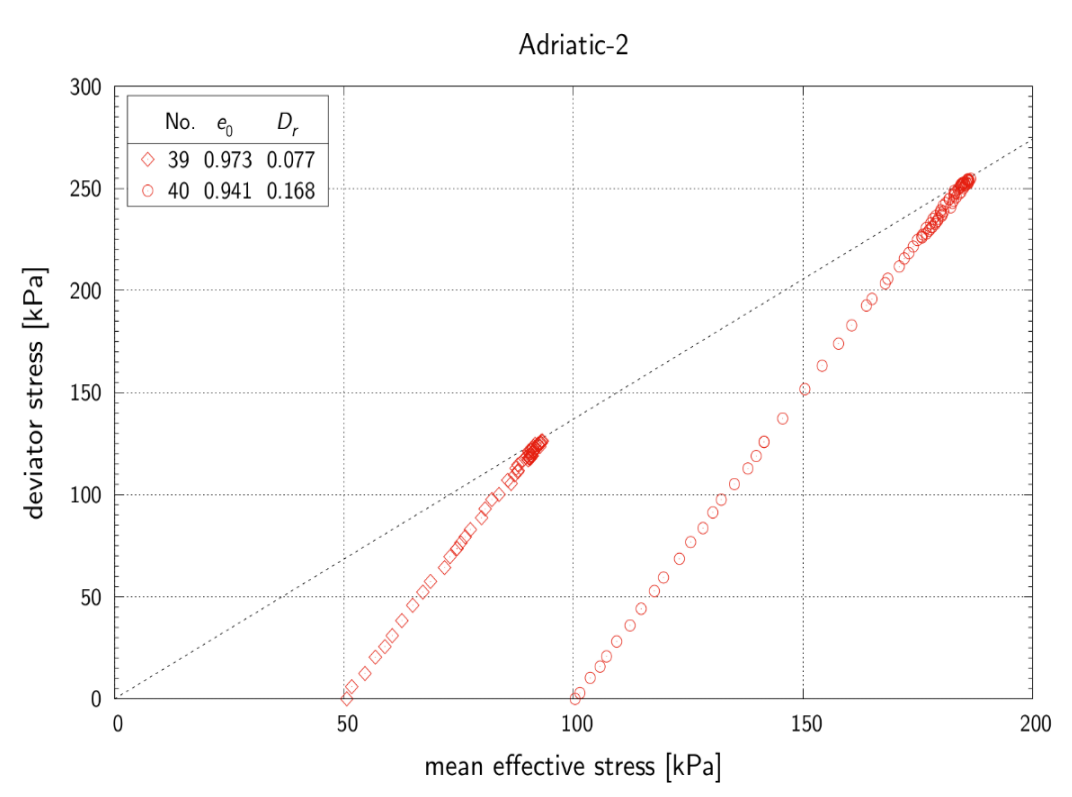


Fig.16 Stress paths for sand collected from Adriatic Sea (Adriatic 2).

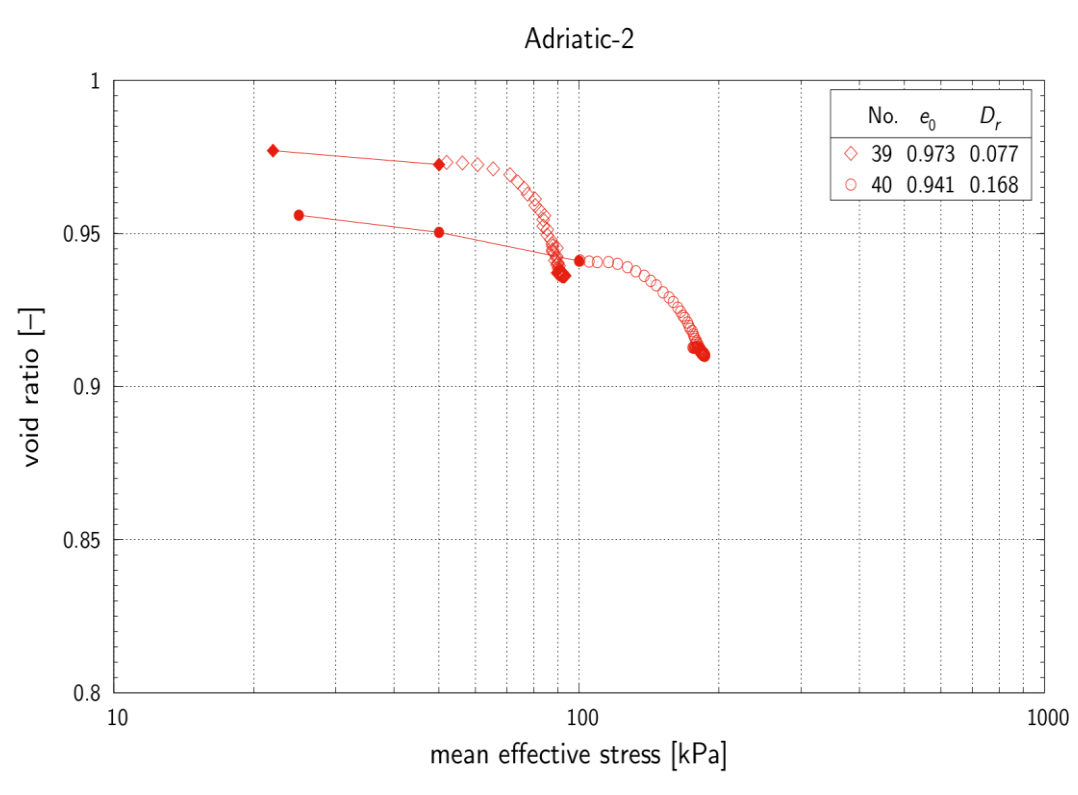


Fig.17 Position of points correspond to steady state of deformation for sand collected from Adriatic Sea (Adriatic 2).





The steady-state lines were determined on the base of results of a series of monotonic triaxial tests, which were performed on samples characterised by different initial relative densities. Both undrained as well as drained tests were carried out for various initial states of the sand (see Table 1 – Appendix 1). The samples were sheared in strain-controlled mode at a strain rate varying from 10 to 12 mm/h. All monotonic tests were being conducted up to the end of range of the piston's vertical movement, which corresponded to approximately 30% of vertical strain of the sample tested. In the case of undrained conditions (zero volume change), during shearing axial load and pore water pressure versus axial strain were monitored (at confining pressure kept constant). In drained tests, the volume change of the sample was measured either directly by local gauges installed on it or by measuring the volume of water sucked or expelled from the sample during shearing. The details can be found in Świdziński & Mierczyński (2002).

During the tests, different stress paths were applied. Their courses for the soil samples are shown in Fig. 6 (soil: Baltic 1); Fig.8 (soil: Baltic 2); Fig.10 (soil: Scottish 1); Fig.12 (soil: Scottish 2); Fig.14 (soil: Adriatic 1); Fig.16 (soil: Adriatic 2). The positions of steady state lines obtained for investigated soils are drawn in Fig.7 (soil: Baltic 1); Fig.9 (soil: Baltic 2); Fig.11 (soil: Scottish 1); Fig.13 (soil: Scottish 2); Fig.17 (soil: Adriatic 2). The zones of the contractive behaviour of soils during shearing are above the steady state lines. The steady state estimated for tests is marked with green dots. The results obtained for contractive specimens are presented in red, and for the dilative ones in blue. Liquefaction does not take place in initially dilative soils, but only in contractive ones. A comparison of the position of the steady-state line for different types of non-cohesive soils is presented in Fig. 18. Therefore, from data presented in Fig.18 one can recognize the initial state of soil, defined by its initial void ratio e and the initial value of the mean effective stress p_0 ', in which liquefaction may appear. Detailed results of all conducted tests (divided according to the types of tested samples) are included in the appendixes. For the cohesive soil (Adriatic 1), the position of the steady-state line was not determined, as cohesive soils are not susceptible to liquefaction.

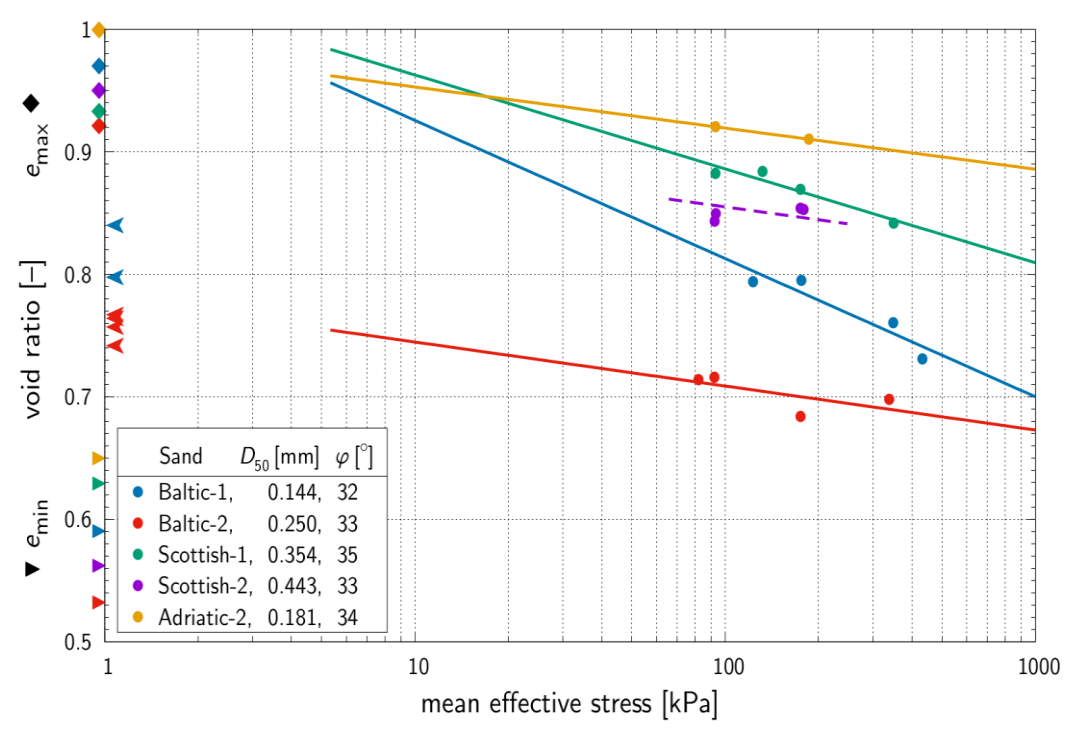


Fig.18 Comparison of the position of the steady-state line for different types of sand (collected from Baltic, Scottish and Adriatic Sea).





3.3 Cyclic triaxial tests

In cyclic triaxial compression tests, the samples were first consolidated to the desired confining pressure and then slightly loaded to the assumed average stress deviator just to have reference level for cyclic loading above the hydrostatic line. During the test, pore-water pressure, as well as axial deformation, were measured in a function of loading cycles. Due to constrains of the triaxial system used, the period of a single loading cycle was relatively long varying from 1 minute to 2 minutes. In the case of cyclic loading, the tests were carried out under controlled stress conditions. During the tests, different stress paths were applied. Their courses for the soil samples are shown in Figs. 19-23.

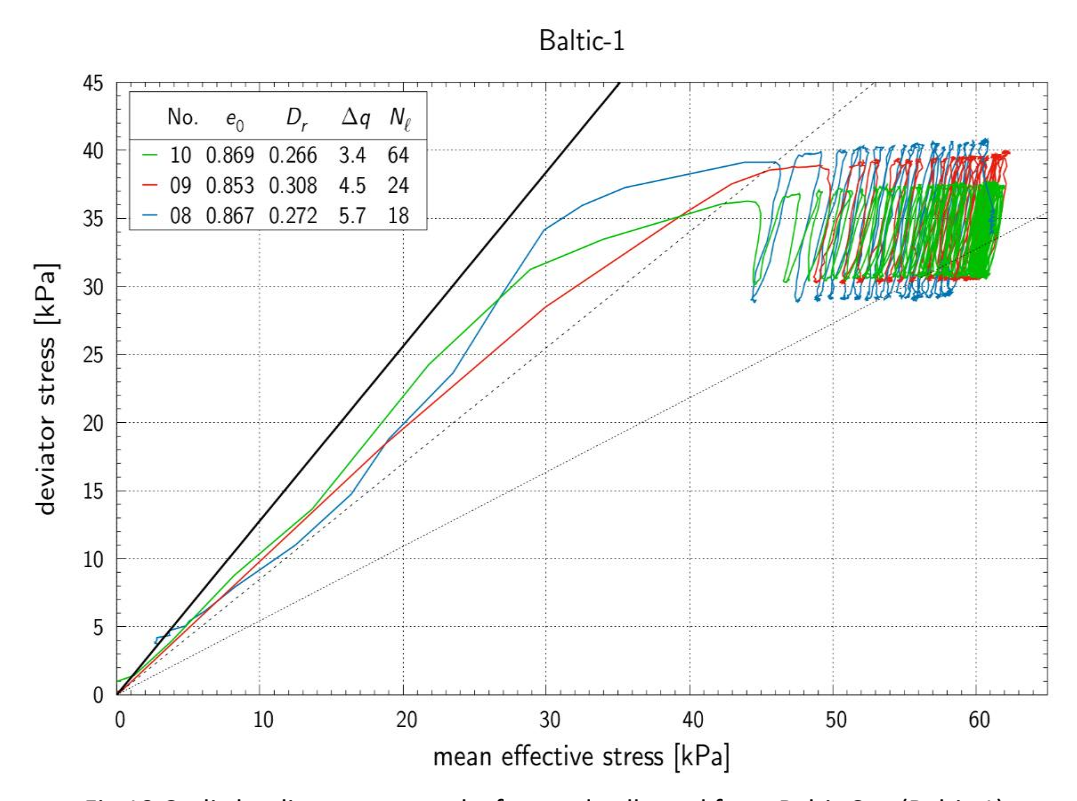


Fig.19 Cyclic loading - stress paths for sand collected from Baltic Sea (Baltic 1)



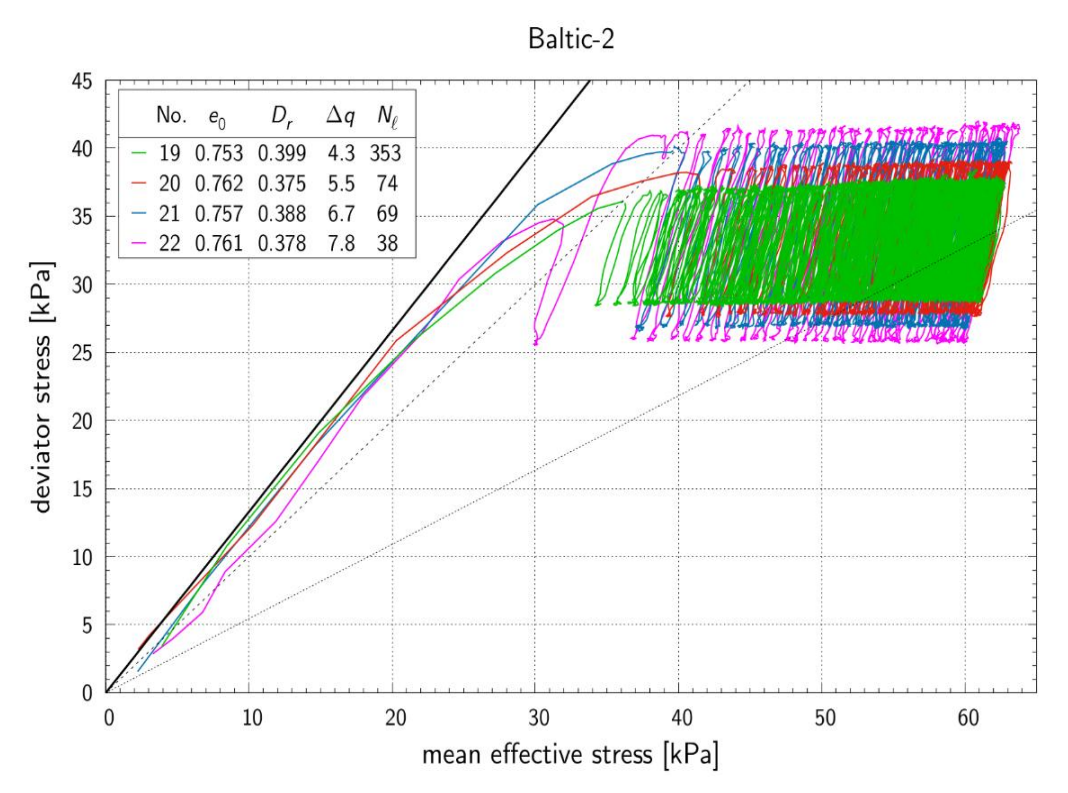


Fig. 20 Cyclic loading - stress paths for sand collected from Baltic Sea (Baltic 2)

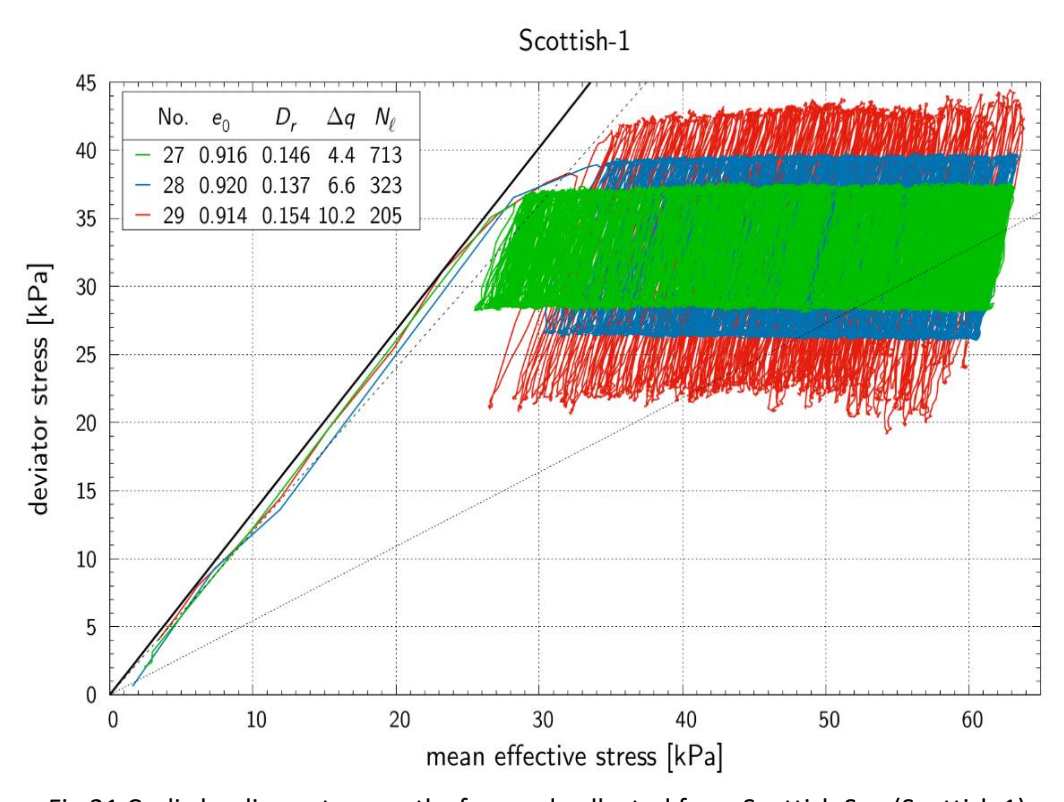


Fig.21 Cyclic loading - stress paths for sand collected from Scottish Sea (Scottish 1)





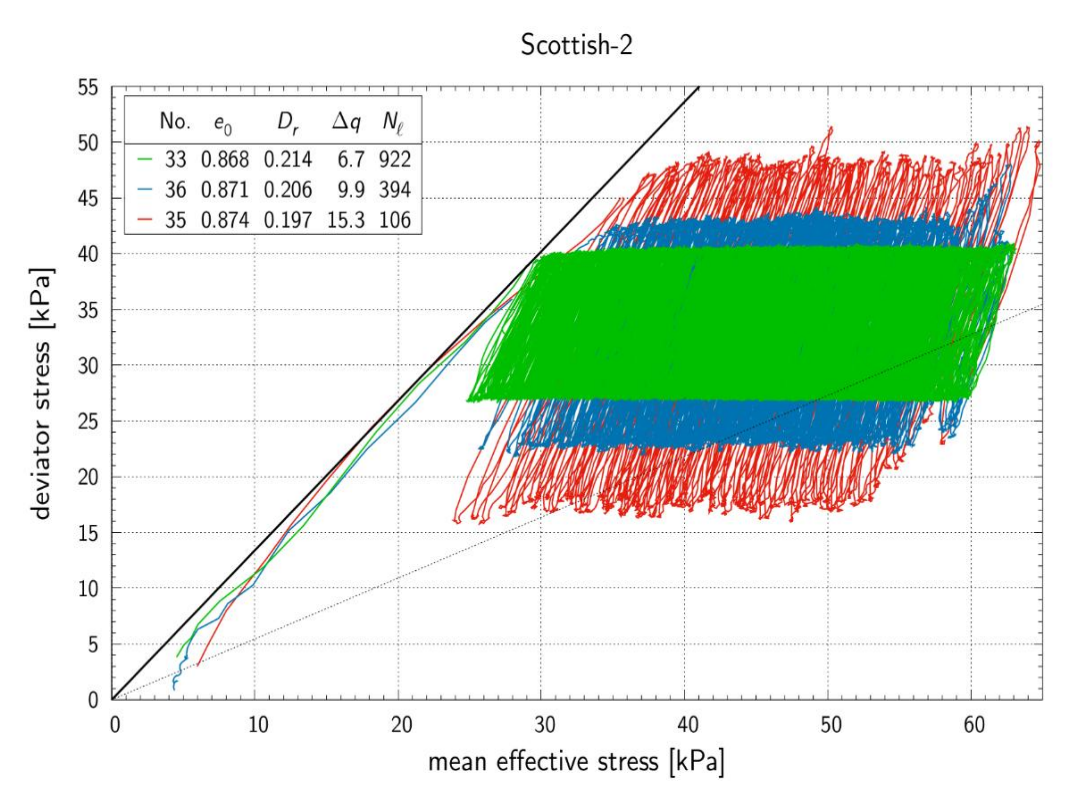


Fig.22 Cyclic loading - stress paths for sand collected from Scottish Sea (Scottish 2)

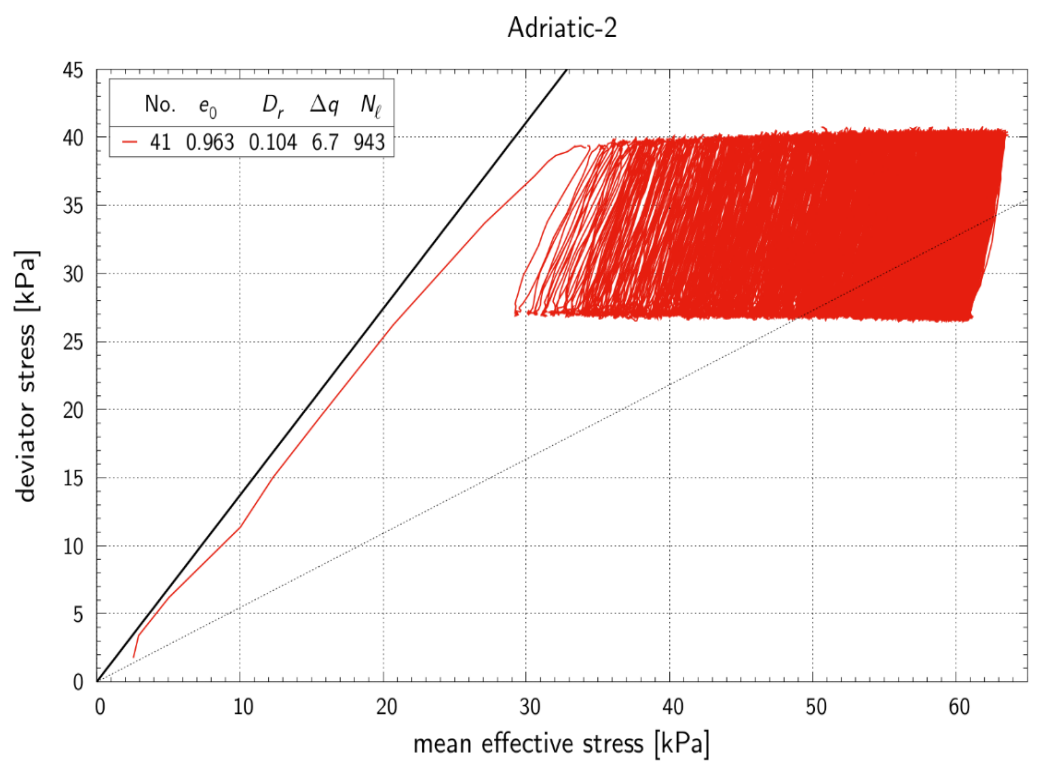


Fig.23 Cyclic loading - stress paths for sand collected from Adriatic Sea (Adriatic 2)





Typical results of cyclic compression tests for contractive samples are shown in Figs. 24-25. Fig.24 shows the realization of cyclic triaxial compression tests in stress space. In Fig.25, the response is expressed in terms of pore-water pressure generation and the change of axial strain depending on the number of loading cycles. In cycle 64 of loading, rapid increase of pore-water pressure was observed, which was accompanied by a sudden drop in shear strength to zero effective stress and large increase of axial strain up to complete collapse of the specimen. Such behaviour is typical for the liquefaction phenomenon. Fig. 26 summarizes the most important information obtained from the cyclic triaxial tests. The relationship between the number of cycles to liquefaction NI and the normalized amplitude of cyclic loading $(\Delta q/2\sigma 3c')$ is presented. It is evident that the number of cycles required for liquefaction increased as the amplitude of cyclic vertical stress decreased and as the average consolidation pressure increased.

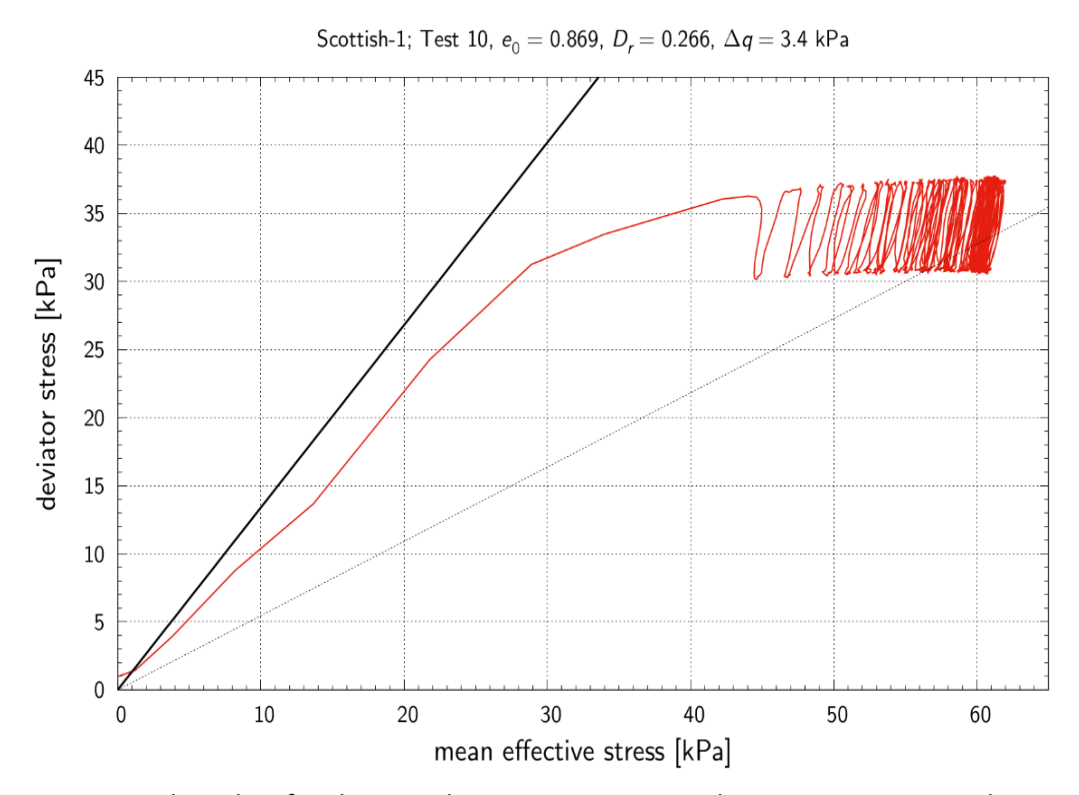


Fig.24 Typical results of cyclic triaxial compression test made on contractive sample - stress spaces.



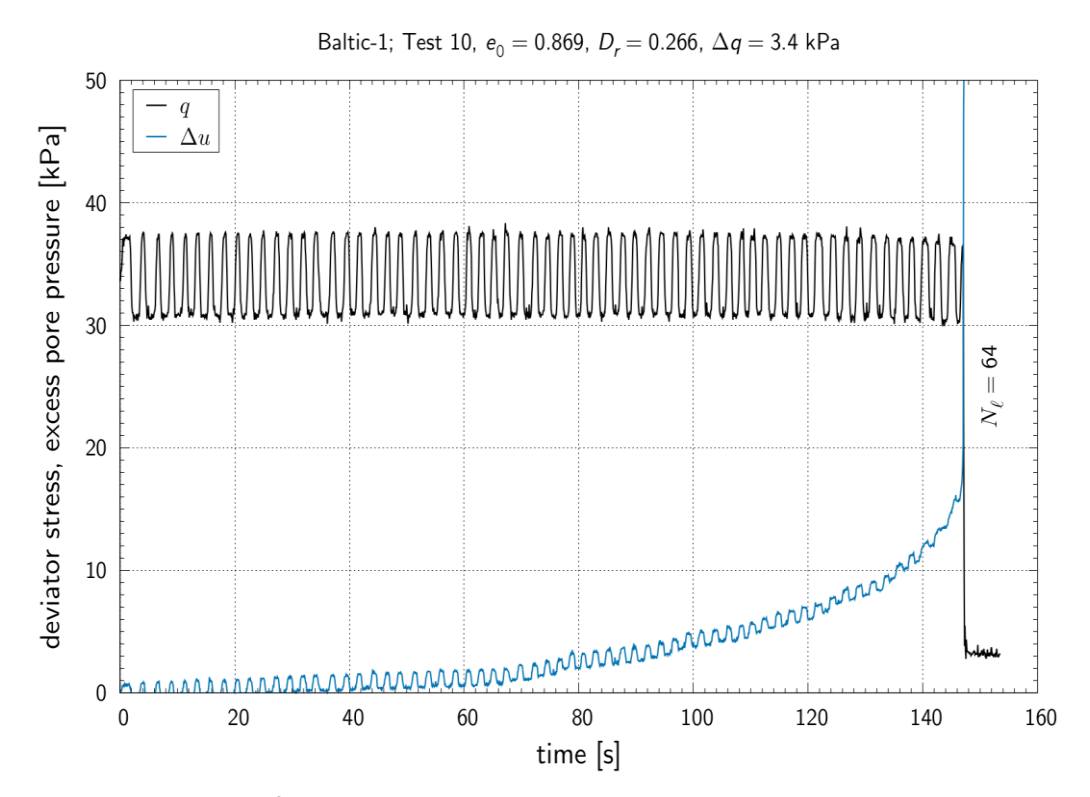


Fig.25 Typical results of cyclic triaxial compression test made on contractive sample: generation of pore-water pressure and changes of axial strain versus number of loading cycles.

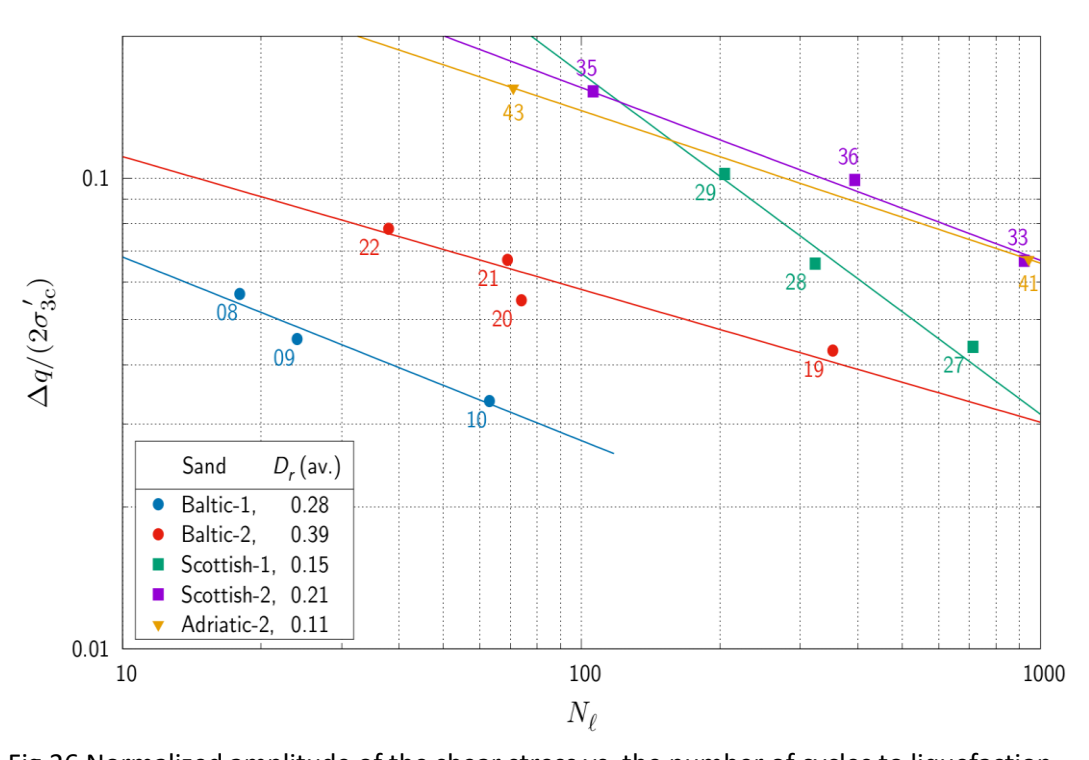


Fig.26 Normalized amplitude of the shear stress vs. the number of cycles to liquefaction - results for the five types of soil samples.





3.4 Elastic modulus

The elastic moduli of the tested soils were calculated based on the results of monotonic triaxial tests, which were conducted under the following conditions:

- Isotopically consolidated saturated specimens: $\sigma_z^0{}_0 = \sigma_x^0{}_0 = \sigma_0^0$, where: $\sigma_z^0{} \text{axial}$ (vertical) effective stress, $\sigma_x^0{} \text{radial}$ (horizontal) effective stress, $\sigma_0^0{} = (\sigma_z^0{} + 2\sigma_x^0{})/3$ initial mean effective stress.
- "Standard geotechnical path" axial compression (with constant strain rate) and constant horizontal effective stress $\sigma_x^0 = \sigma_0^0$.

The results of the initial changes of the stress deviator $q = \sigma_z^0 - \sigma_x^0$ as a function of axial strain are presented in Fig. 27. They were then approximated by the following function:

$$q(\varepsilon_z) = a\log(1 + b\varepsilon_z) + c\varepsilon_z$$

The Young's modulus is defined as:

$$E = \left(\frac{d\sigma_z^i}{d\varepsilon_z}\right)_{\varepsilon_z = 0} = \left(\frac{dq}{d\varepsilon_z}\right)_{\varepsilon_z = 0} = ab + c$$

Fig.28 shows the calculated values of modulus E as functions of the initial effective stress and an example of simple approximation ($\sigma_{ref}^{0} = 100$ kPa is introduced to obtain a dimensionless base of the power function used for approximations).



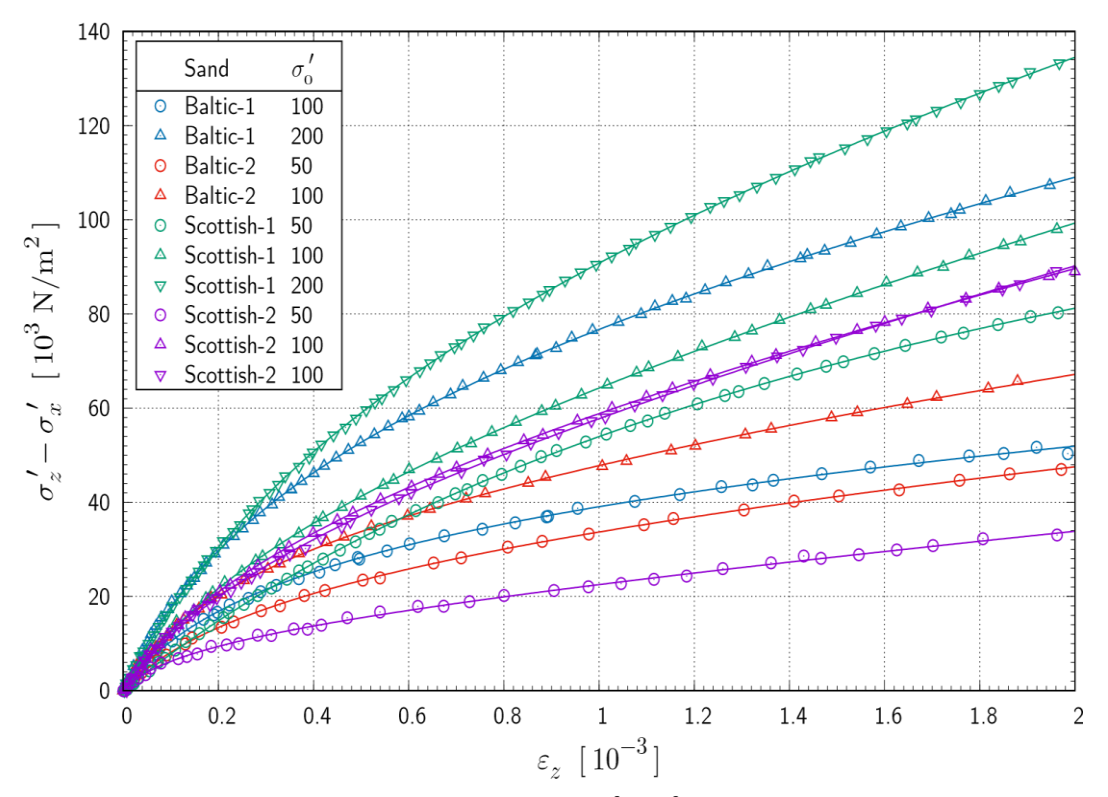


Fig.27 Initial changes of the stress deviator $q = \sigma_z^0 - \sigma_x^0$ as a function of the axial strain ε_z

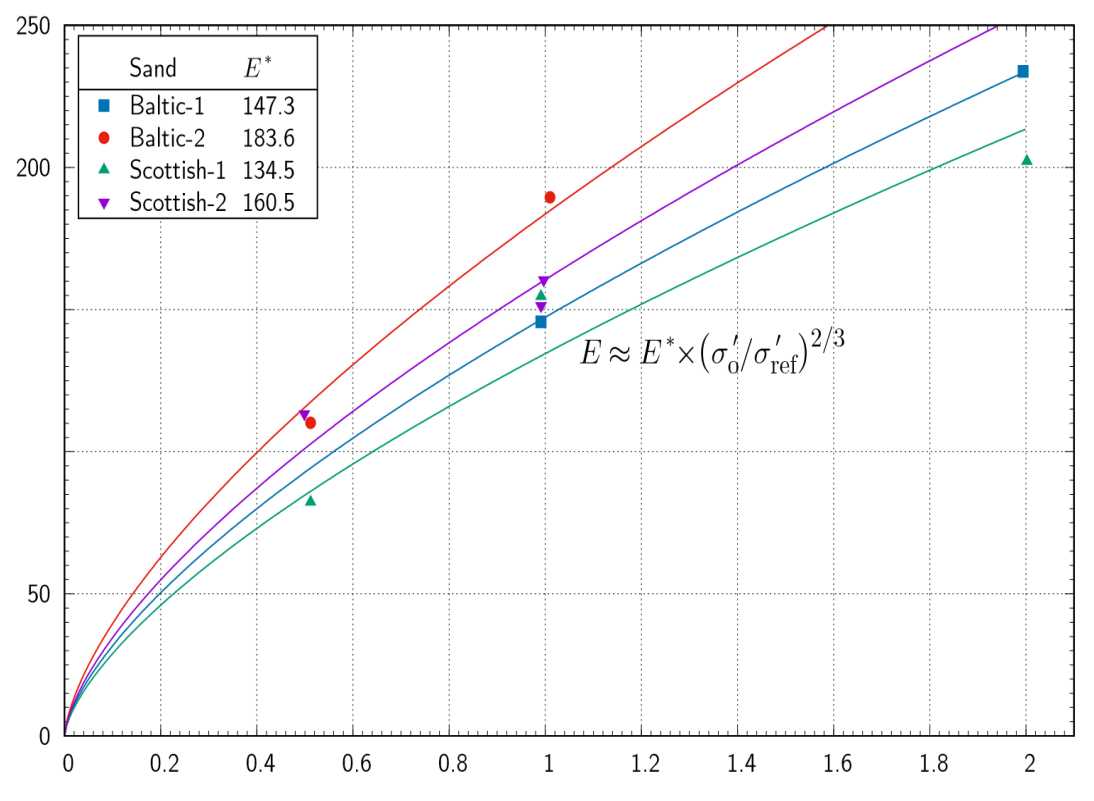


Fig.28 Calculated values of modulus E as functions of the initial effective stress σ_0 .



Similar procedure was applied to calculate the values of Poisson's ratios, and a detailed description of the partial results is provided in Appendix 8. Calculated values of Poisson's ratios as functions of the initial effective stress σ_0^0 are presented in Fig.29.

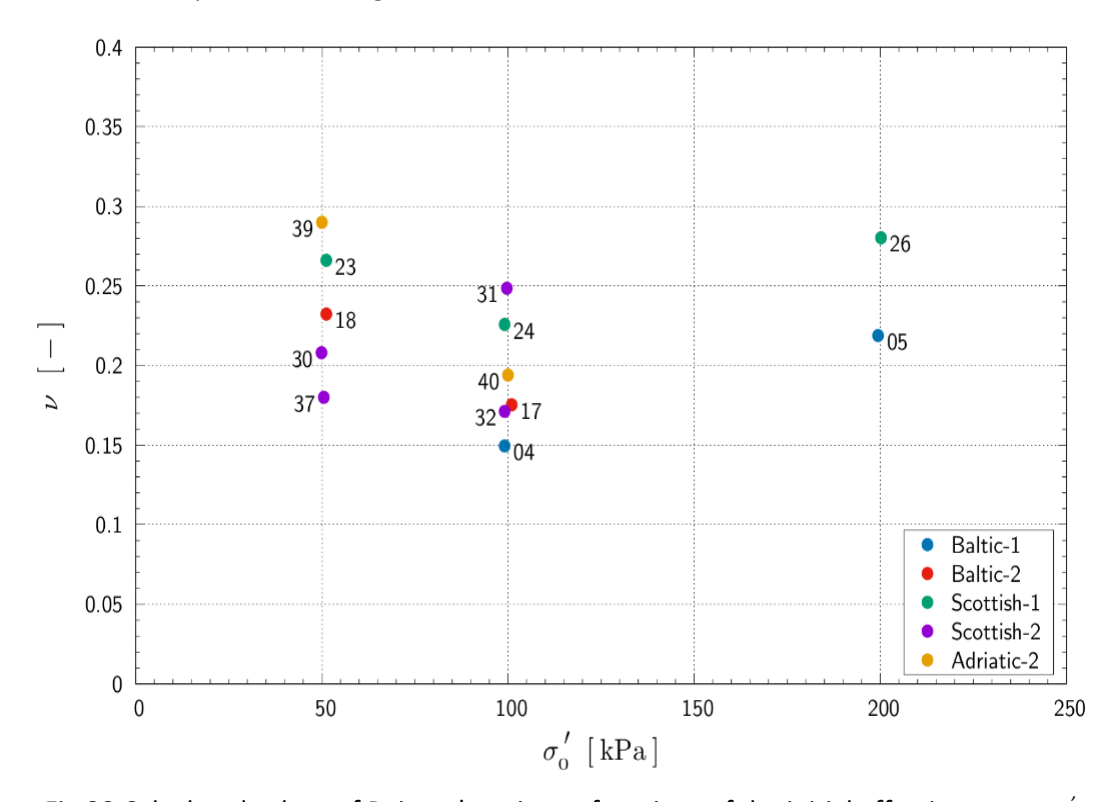


Fig.29 Calculated values of Poisson's ratios as functions of the initial effective stress σ_0 .

4 Conclusions

The objective of the testing program was to determine the geotechnical characteristics of soil samples collected from three marine regions: the Baltic Sea, the Scottish Sea, and the Adriatic Sea. For each of the above-mentioned regions, samples were taken from two locations. In total, preliminary tests were carried out for six types of soil. The experimental campaign began with a detailed microscopic examination and grain size distribution analysis to classify the soils. Based on the results, five of them were found to meet the initially adopted criteria (these are non-cohesive soils) and were subjected to a detailed testing procedure (a full set of monotonic and cyclic triaxial tests was performed). Soil samples marked with the symbol Adriatic 1 were identified as cohesive and therefore not suitable for liquefaction-related testing.

Subsequent testing involved monotonic and cyclic triaxial shear tests to determine mechanical and index properties, liquefaction potential, and elastic parameters based on seismic wave velocities. A database of soil characteristics was compiled to support the development of surrogate soils with scaled properties for further use in physical and numerical modelling. Detailed results of the most significant tests performed are included in the appendixes attached to the report.



5 References

- Castro G. (1975), Liquefaction and Cyclic Mobility of Saturated Sands, J. Geotech. Engrg. ASCE, Vol. 101, No. GT6, 551–569.
- Green P. A., Ferguson P. A. S. (1971), On Liquefaction Phenomena, by Professor A. Casagrande: Report of Lecture, Geotechnique, XXI, 3, 197–202.
- Lipiński M. J. (2000), Undrained Response of Cohesionless Soils to Monotonic Loadings, PhD thesis, Faculty of Hydro and Environmental Engineering, Gdańsk Technical University.
- Poulos S. J. (1981), The Steady State of Deformation, J. Geotech. Engrg. ASCE, Vol. 107, No. GT5, 501-516
- Sawicki, A., K., Kazimierowicz-Frankowska. 2015. *Geotechnical Aspects of Multi-Use* 512 *Offshore Platforms*, IBW PAN, Gdańsk.
- Świdziński W., Mierczyński J. (2002), On the Measurement of Strains in the Triaxial Test, Arch. of Hydro-Engineering and Environ. Mech., Vol. 49, No. 1, 23–41.



6 Appendixes

6.1 Appendix nr 1 - Triaxial tests: Summary of testing program

Table 6.1.1a Summary of testing program – Baltic Seabed.

	Sand			Test results													
No Location	Depth	<i>d</i> ₅₀	Preparation	<i>e</i> ₀	<i>D</i> _r	p_0'	9 0	V s	Test	Δq	q peak	q max	q res	N₂	Reaction		
Location	[m]	[mm]	method	[-]	[-]	[kPa]	[kPa]	[m/s]	type	[kPa]	[kPa]	[kPa]	[kPa]	[-]	type		
1			MT	0.798	0.455	400	0	213	M-U	-	162	-	0	-	C-L		
2			AP	0.646	0.857	100	0	158	M-U	-	-	_*	-	-	D-SH		
3			AP	0.731	0.633	200	0	193	M-U	-	103	545	0	-	D-SSL		
4 P			MT	0.850	0.316	100	0	149	M-D	-	-	230	-	-	C-SSL		
Sea 16.!	3.0-3.3	0.144	MT	0.809	0.425	200	0	179	M-D	-	-	445	-	-	C-SSL		
2 Baltic (55.05 N,	3.0-3.3	0.144	MT	0.794	0.465	300	0	210	M-U	-	210	-	157	-	C-LL/SSL		
7 B 9:00			MT	0.840	0.342	250	0	206	M-U	-	100	-	0	-	C-L		
8			MT	0.862	0.266	61	34	139	C-U	5.7	-	-	0	18	C-L		
9					MT	0.853	0.308	61	34	136	C-U	4.6	-	-	0	23	C-L
10			MT	0.869	0.266	61	34	135	C-U	3.4	-	-	0	64	C-L		
11			MT	0.767	0.363	100	0	151	M-U	_	38	_	0	_	C-L		
12 🔐			MT	0.763	0.371	200	0	186	M-U	_	83	_	0	_	C-L		
a 2 81 7.11 2.11			MT	0.714	0.491	200	0	197	M-U	_	125	-	106	-	C-LL/SSL		
13	1.1-2.1	0.250	MT	0.751	0.404	100	0	164	M-U	_	55	_	0	_	C-L		
Balt 5.06			MT	0.698	0.541	200	0	184	M-U	_	_	417	_	_	D-SSL		
16			MT	0.742	0.426	150	0	183	M-U	_	83.5	_	0	_	C-L		
17			MT	0.735	0.445	100	0	167	M-D	_	_	232.6	_	_	C-SSL		



18	MT	0.768	0.361	50	0	147	M-D	-	_	123.6	_	_	C-SSL
19	MT	0.753	0.399	61	33	151	C-U	4.3	_	_	0	353	C-L
20	MT	0.762	0.375	61	34	165	C-U	5.5	_	_	0	74	C-L
21	MT	0.757	0.388	61	34	164	C-U	6.7	_	_	0	69	C-L
22	MT	0.761	0.378	61	34	162	C-U	7.8	_	_	0	38	C-L

^{*} test interrupted after the measured axial force exceeded the sensor range.





Table 6.1.1b Summary of testing program – Scottish Seabed and Adriatic Sea.

	San	nd		I	nitial con	ditions			Test results								
No	Location	<i>d</i> ₅0	Preparation	<i>e</i> 0	<i>D</i> r	p ′0	9 0	V s	Test	Δq	<i>q</i> peak	q max	<i>G</i> res	N₂	Reaction		
	Location	[mm]	method	[-]	[-]	[kPa]	[kPa]	[m/s]	type	[kPa]	[kPa]	[kPa]	[kPa]	[-]	type		
23			MT	0.877	0.263	50	0	137	M-D	_	_	132.5	_	_	D-SSL		
24			MT	0.889	0.144	100	0	168	M-D	_	_	240	_	_	C-SSL		
25	Sea 1		MT	0.884	0.159	200	0	194	M-U	-	201		182	_	C-SSL		
26	s ys	0.354	MT	0.889	0.144	200	0	198	M-D	_	_	470	_	_	C-SSL		
27	Scottish	0	MT	0.916	0.146	61	33	127	C-U	4.4	_	_	0	713	C-L		
28	01		MT	0.920	0.137	61	34	166	C-U	6.6	_	_	0	323	C-L		
29			MT	0.914	0.154	61	33	164	C-U	10.2	_	_	0	205	C-L		
30			MT	0.924	0.067	50	0	148	M-D	_	_	123.6	-	_	C-SSL		
31			MT	0.885	0.167	100	0	159	M-D	_	_	237.5	_	_	C-SSL		
32	2		MT	0.870	0.208	100	0	170	M-D	_	_	237.3	_	_	C-SSL		
33	Sea	43	MT	0.868	0.214	61	34	162	C-U	6.7	_	_	0	922	C-L		
34	Scottish	0.443	MT	0.868	0.214	61	34	161	C-U	10.2	_	_	0	1123	C-L		
35	Sco		MT	0.874	0.197	61	34	165	C-U	15.3	_	_	0	106	C-L		
36			MT	0.871	0.206	61	34	152	C-U	9.9	-	-	0	394	C-L		
37			MT	0.909	0.108	50	0	_	M-D		_	125.2	_	_	C-SSL		
38	Adriatic Sea 1	0.004	SD	1.170		50	0		M-U	_	_	39	_	_	C-L		





39		MT	0973	0.077	50	0	149	M-D	_	-	125	118	-	C-SSL
40 Adria	atic 0.181	MT	0.941	0.168	100	0	184	M-D	_	_	255	225	_	C-SSL
41 Sea	a 2	MT	0.963	0.104	61	33	158	C-U	6.7	_	_	0	943	C-L
43		MT	0.959	0.116	61	33	155	C-U	11.5	-	-	_	71	C-L

 d_{50} – median grain size, preparation method – **A**ir **P**luviation/**M**oist **T**amping, e_0 – void ratio after consolidation, D_f – relative density p_0' – initial mean effective stress, q_0 – initial deviator stress, V_s – shear wave velocity, Test type – **C**yclic/**M**onotonic-**D**rained/**U**ndrained Δq – cyclic loading amplitude, q_{peak} – local maximum in the range of small values of axial strain (less than 1%)

 q_{max} – maximum value during the test, q_{res} – residual value after liquefaction, N_{t} – number of cycles to liquefaction



6.2 Appendix nr 2 - Results of soil samples collected from Baltic Sea; Soil type: Baltic 1

1. Sampling locations and View of the samples under the microscope.



Fig.6.2.1 Sampling location.

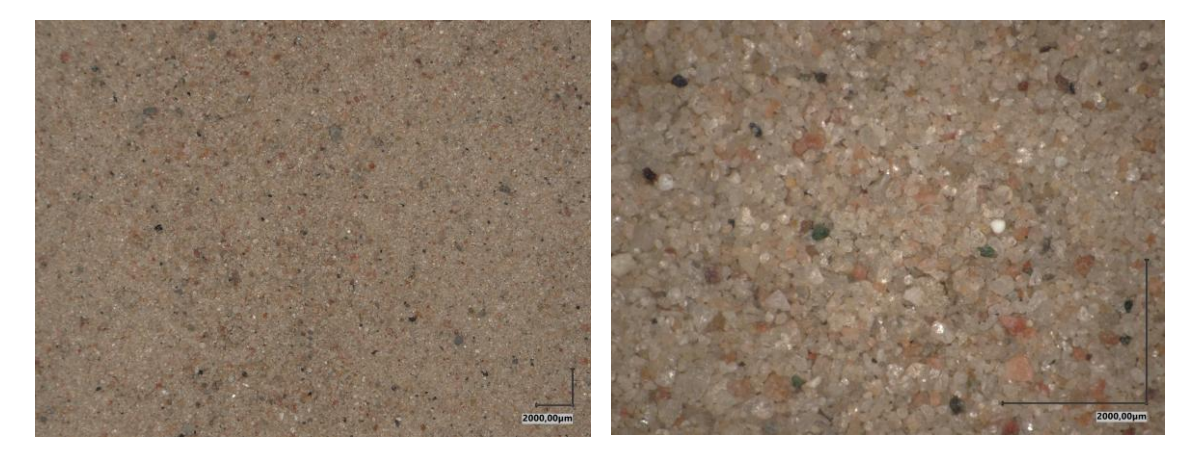


Fig.6.2.2 View of the samples under the microscope.



2. Results of monotonic triaxial tests.

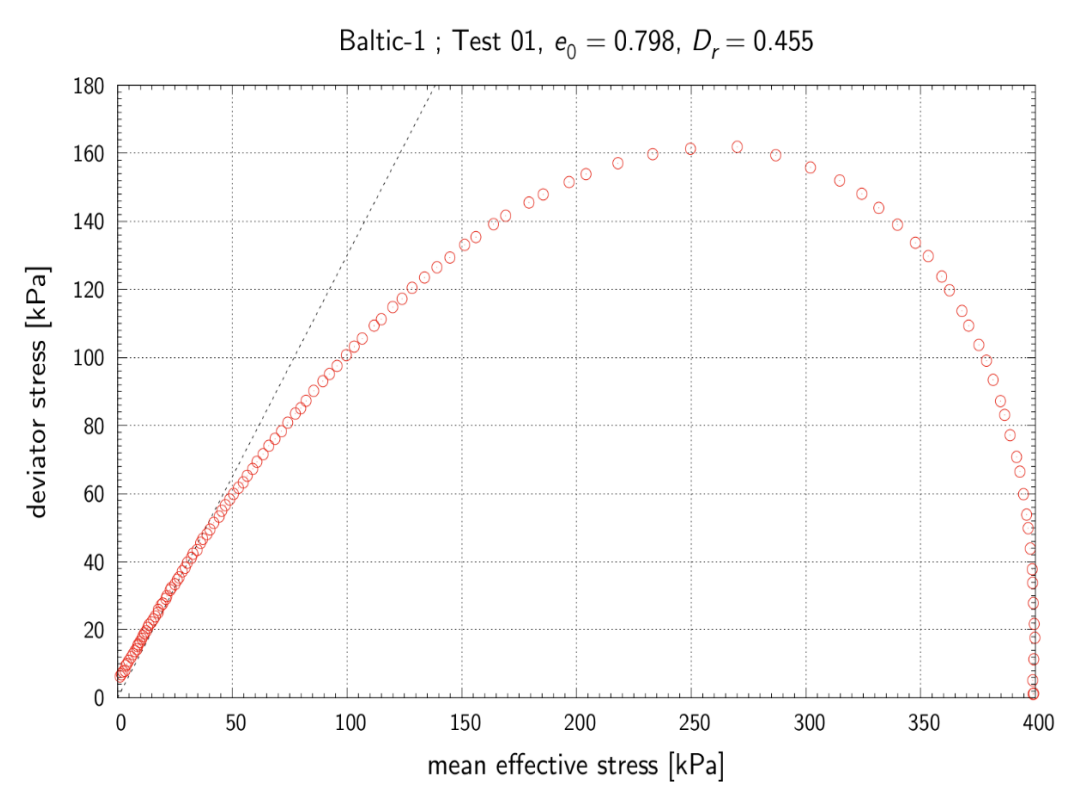


Fig.6.2.3 Results of monotonic test: stress path - sample no 1.

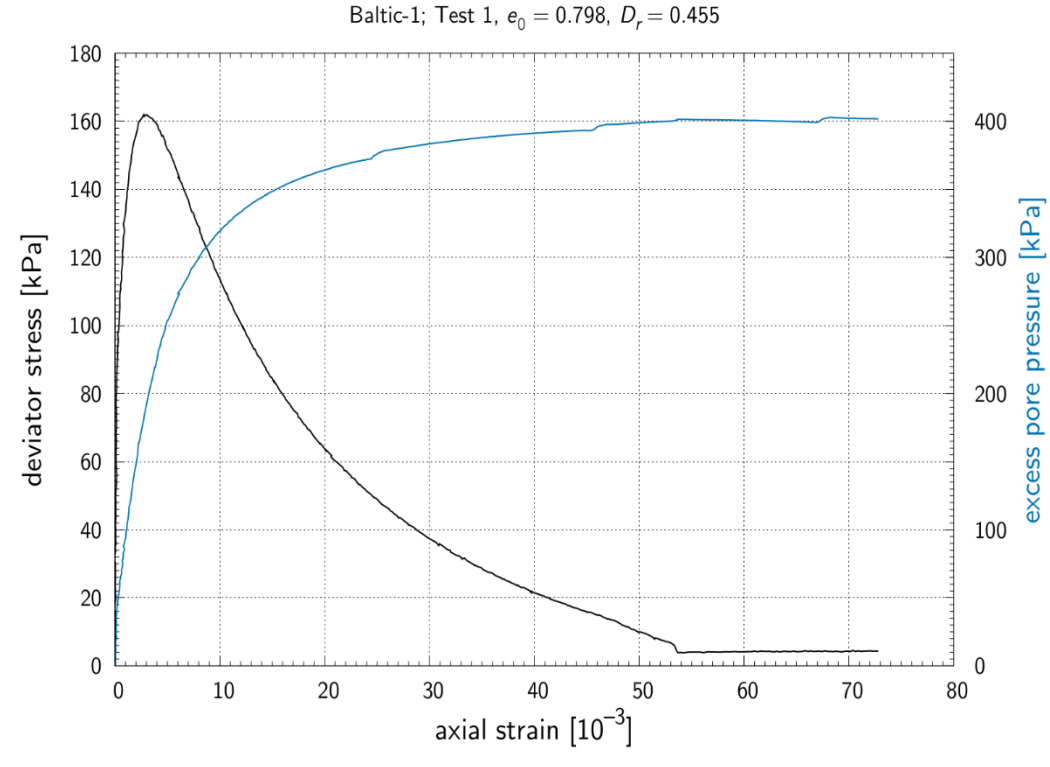


Fig.6.2.4 Results of monotonic test: response of soil sample: deviator stress vs. vertical strain – sample no 1.



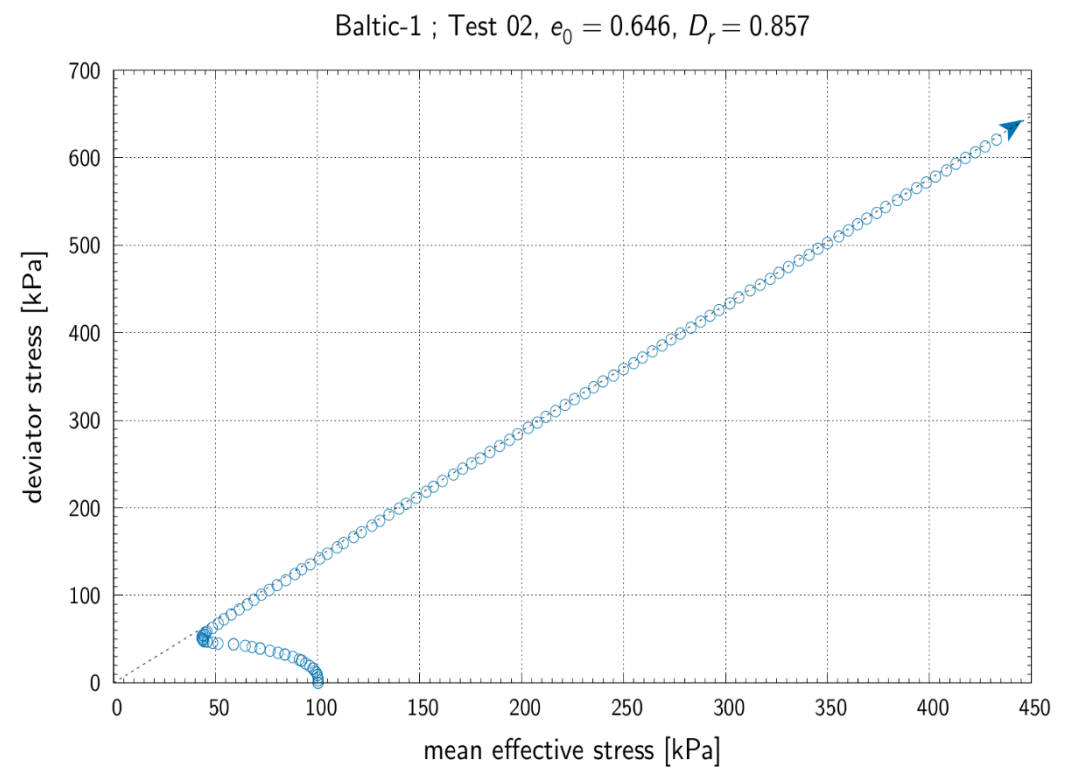


Fig. 6.2.5 Results of monotonic test: stress path - sample no 2.

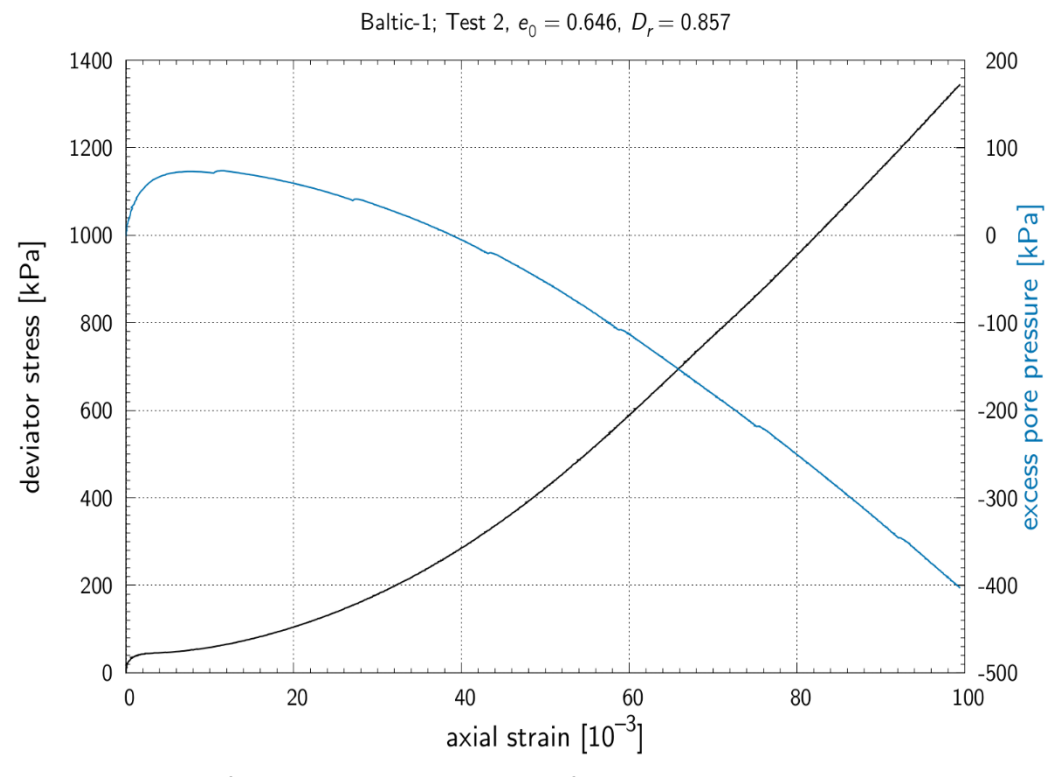


Fig.6.2.6 Results of monotonic test: response of soil sample: deviator stress vs. vertical strain – sample no 2.





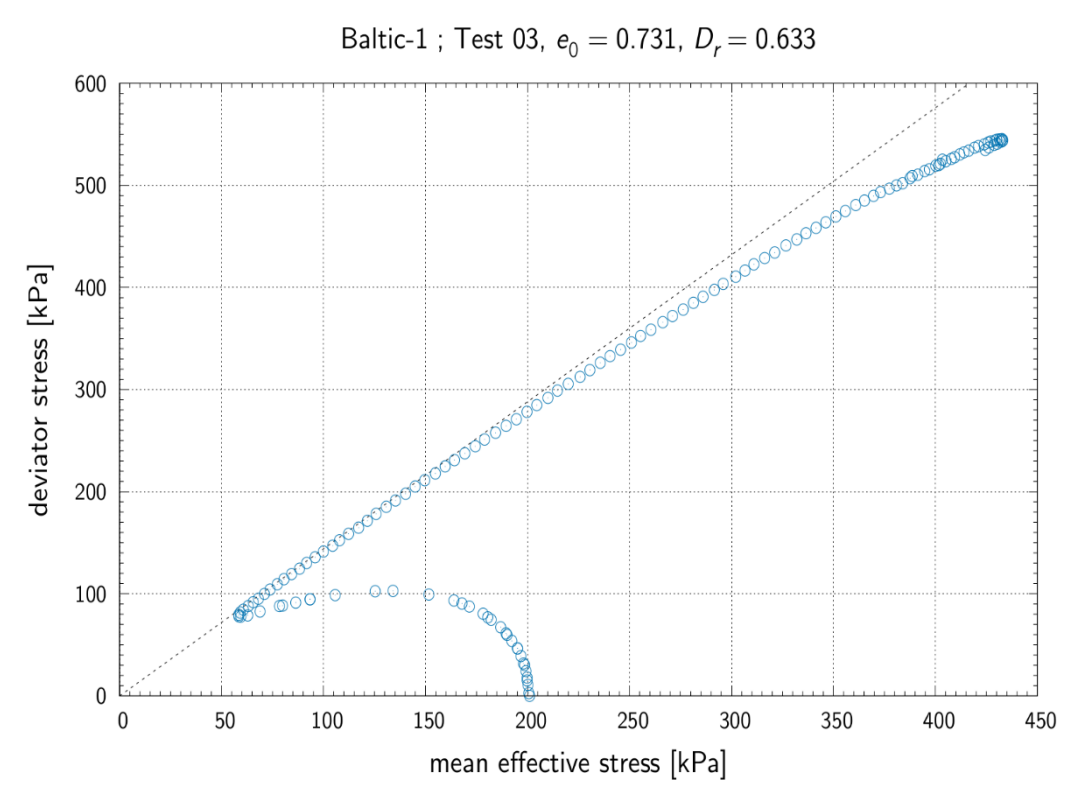


Fig.6.2.7 Results of monotonic test: stress path - sample no 3.

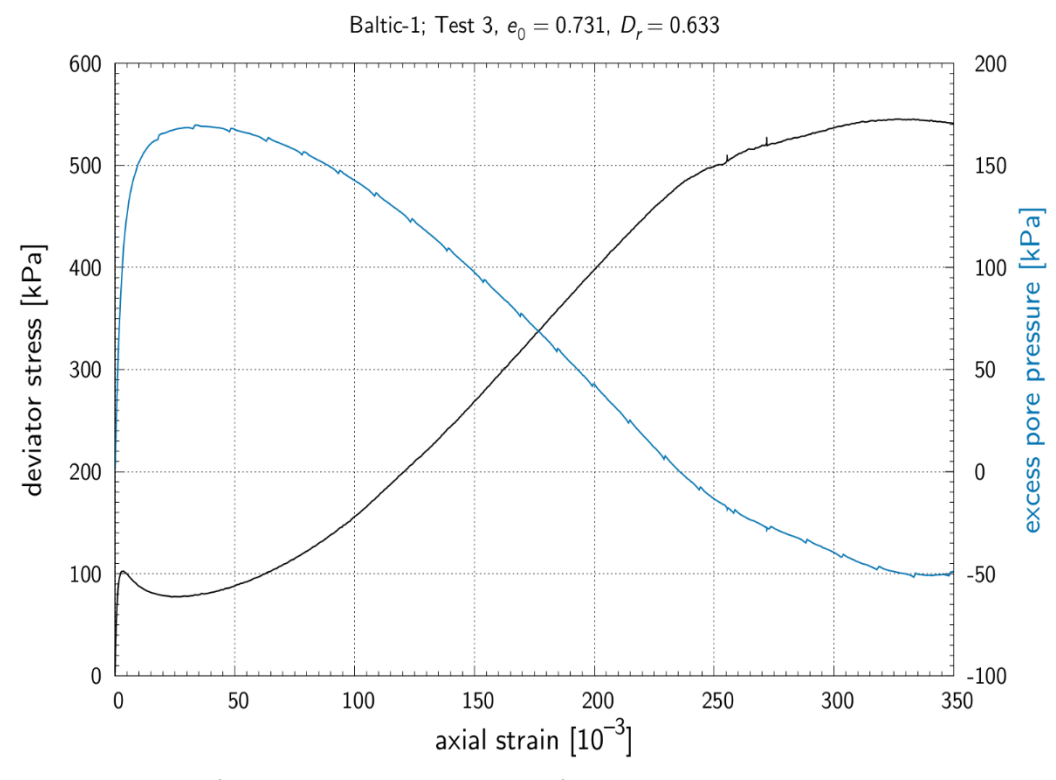


Fig.6.2.8 Results of monotonic test: response of soil sample: deviator stress vs. vertical strain – sample no 3.





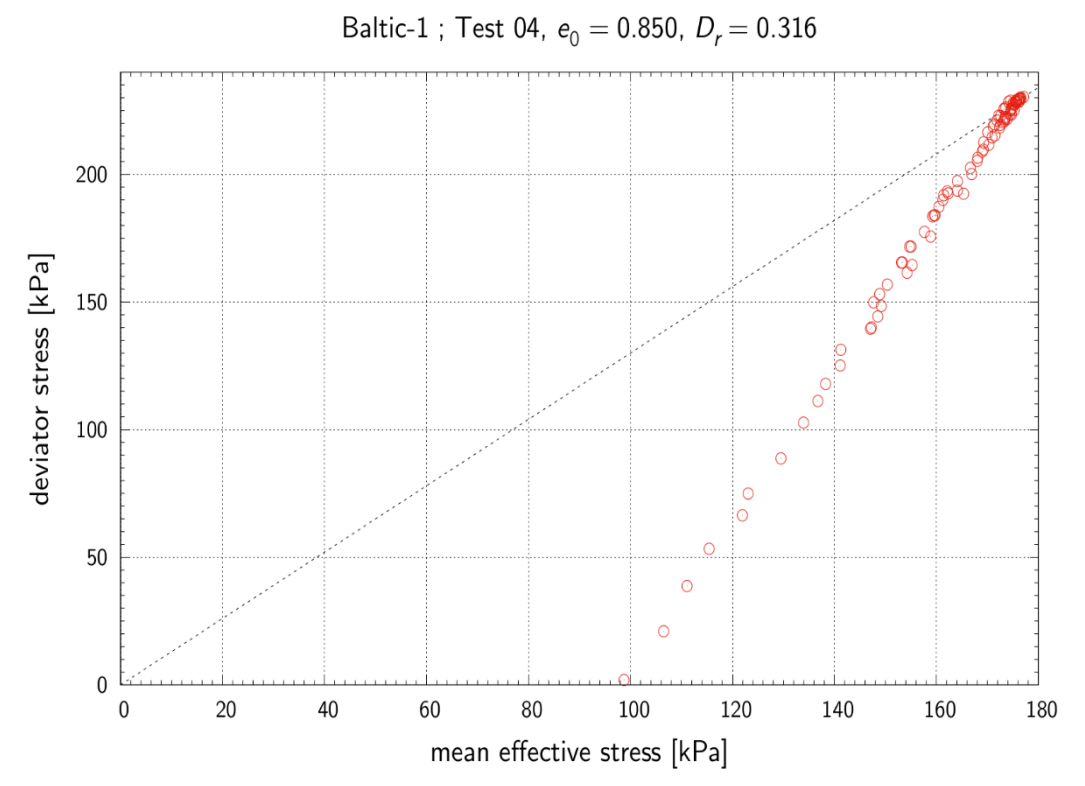


Fig.6.2.9 Results of monotonic test: stress path - sample no 4.

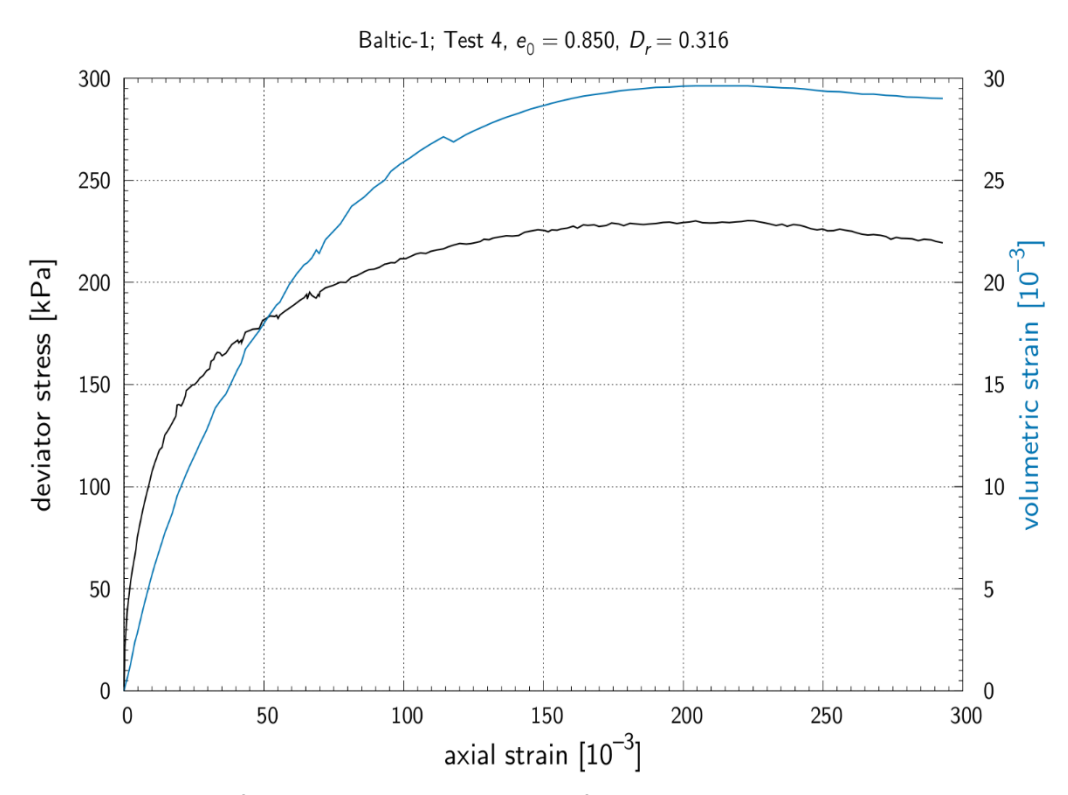


Fig.6.2.10 Results of monotonic test: response of soil sample: deviator stress vs. vertical strain – sample no 4.





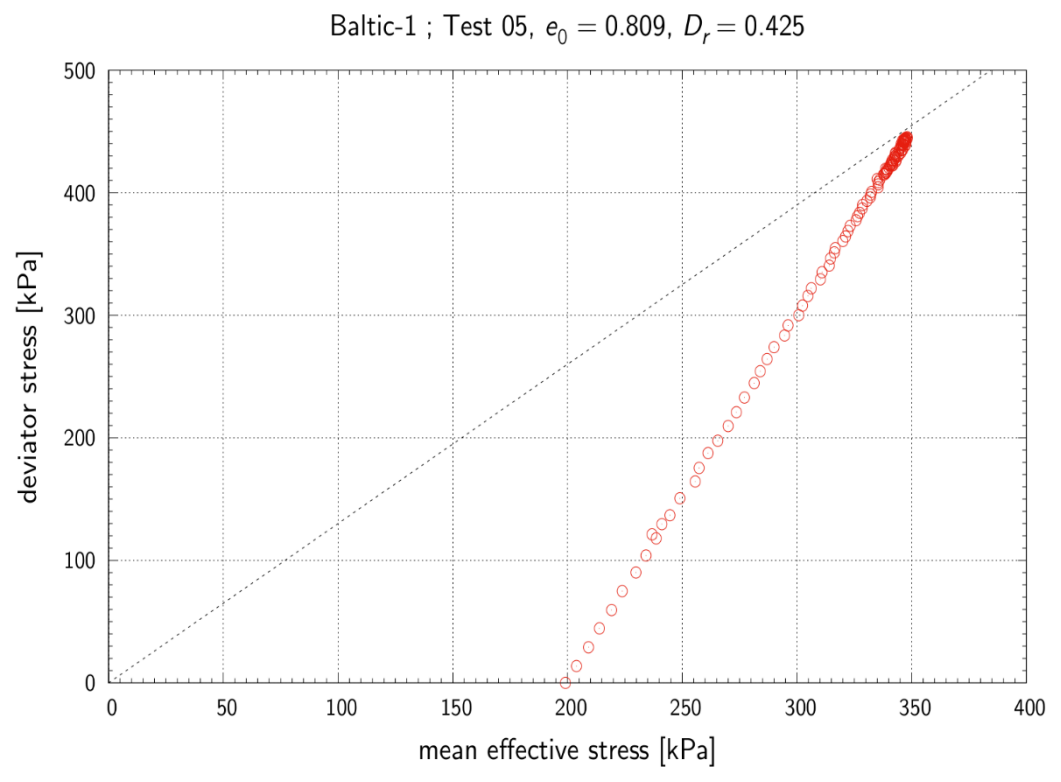


Fig.6.2.11 Results of monotonic test: stress path - sample no 5.

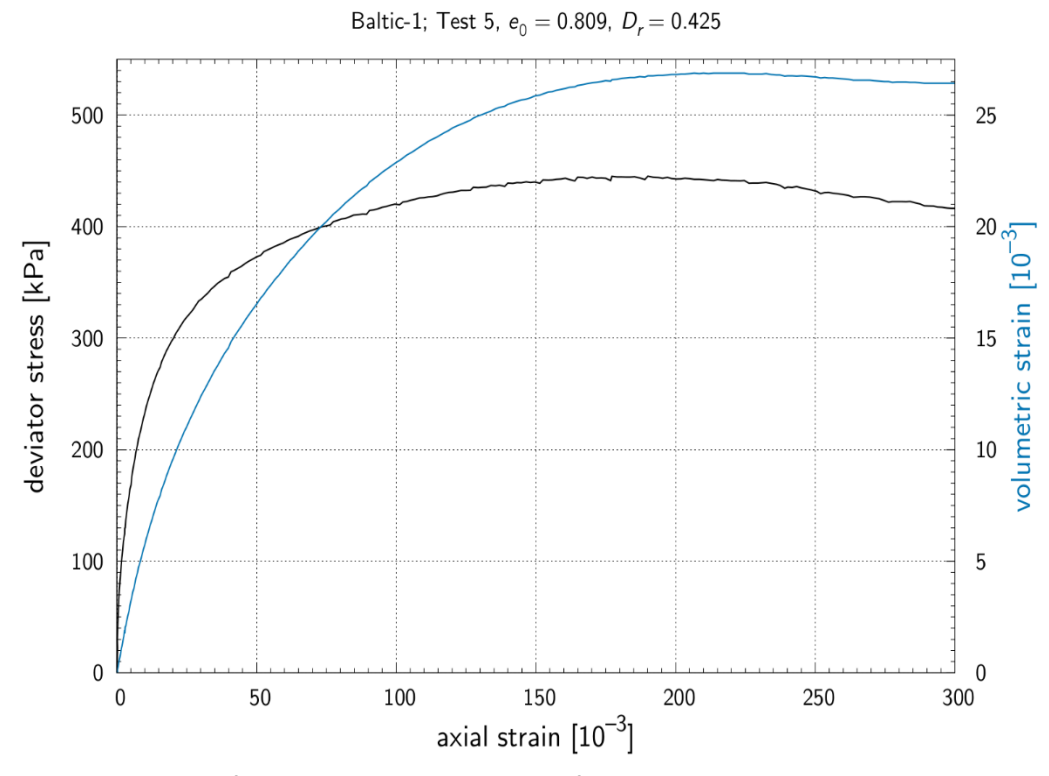


Fig.6.2.12 Results of monotonic test: response of soil sample: deviator stress vs. vertical strain – sample no 5.





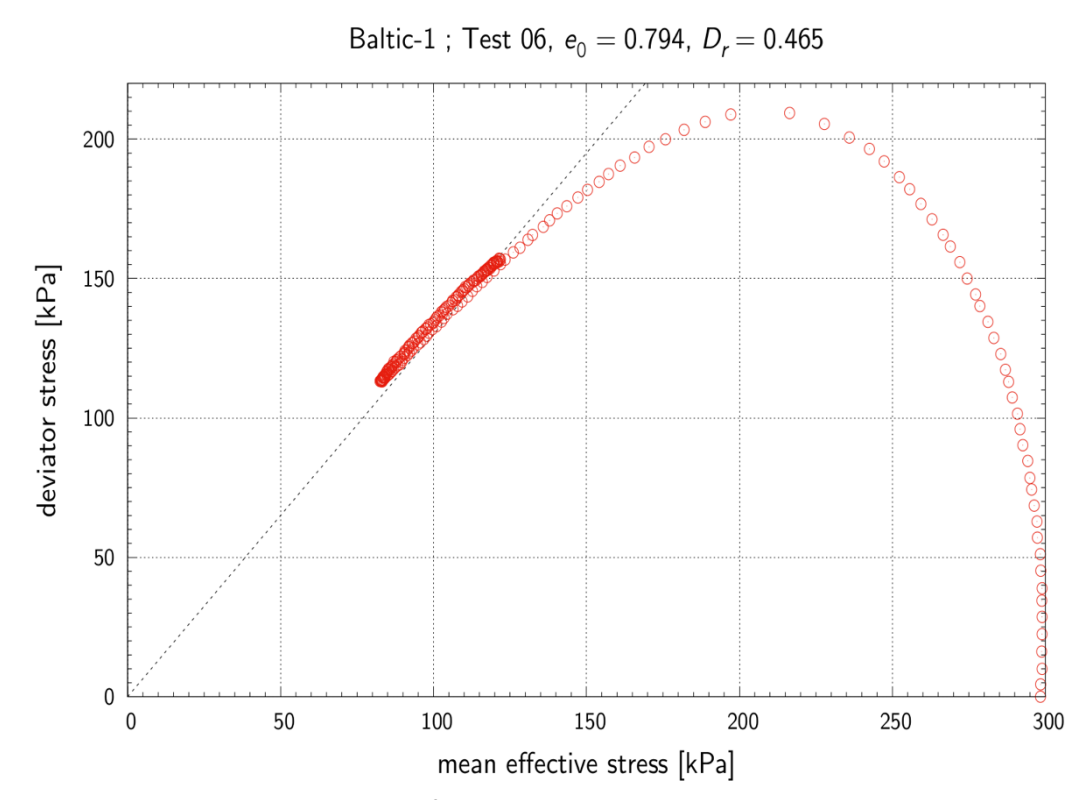


Fig.6.2.13 Results of monotonic test: stress path - sample no 6.

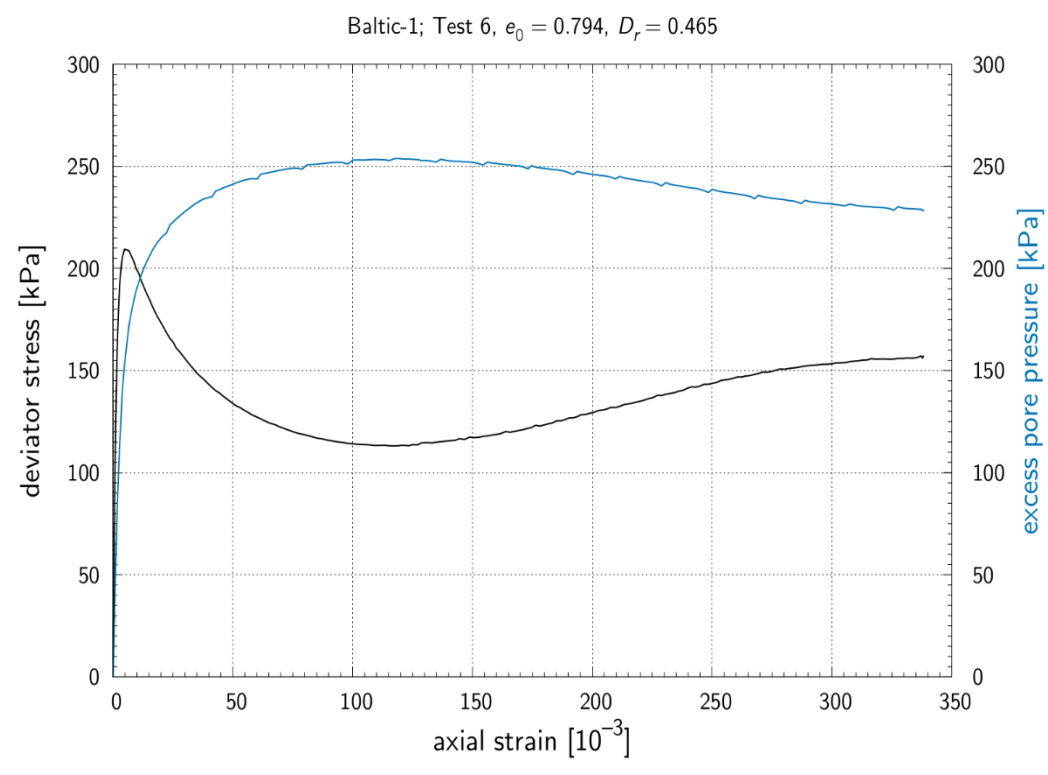


Fig.6.2.14 Results of monotonic test: response of soil sample: deviator stress vs. vertical strain – sample no 6.





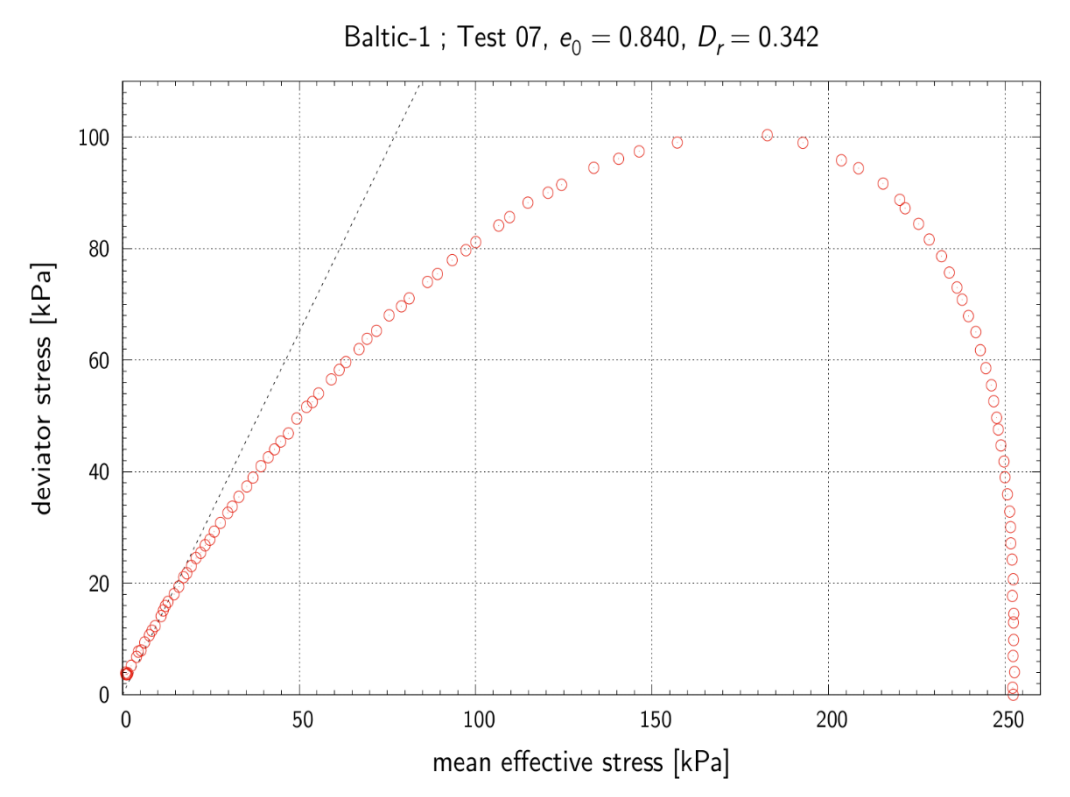


Fig.6.2.15 Results of monotonic test: stress path - sample no 7.

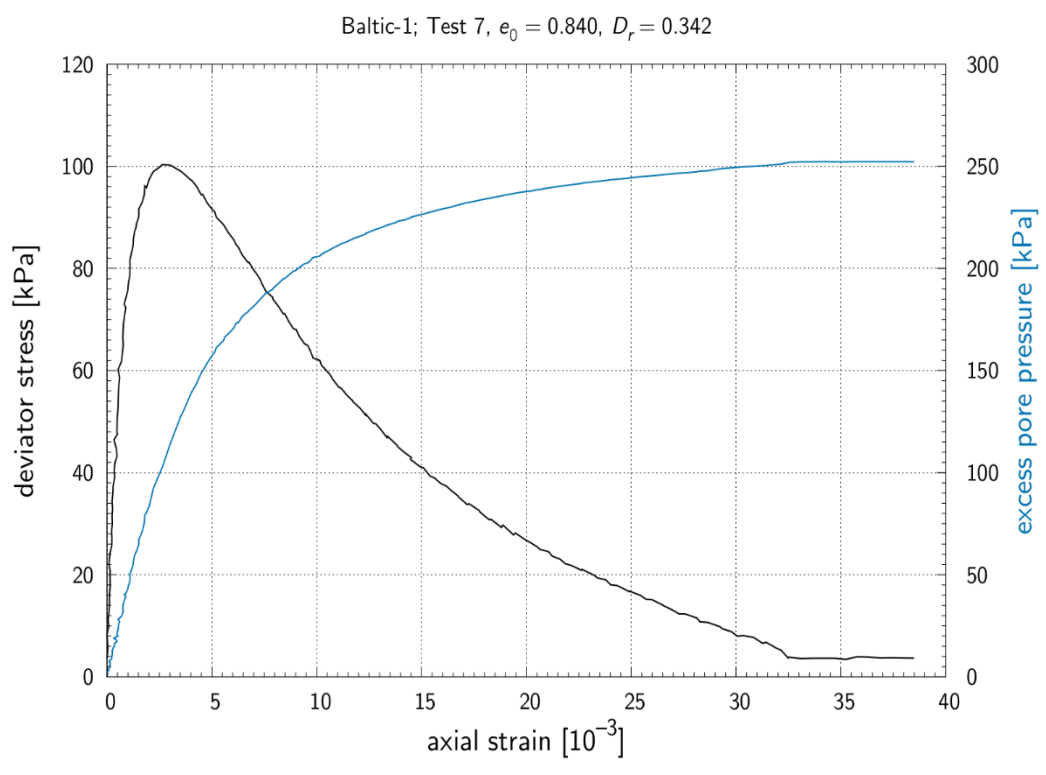


Fig. 6.2.16 Results of monotonic test: response of soil sample: deviator stress vs. vertical strain – sample no 7.





3. Results of cyclic triaxial tests.

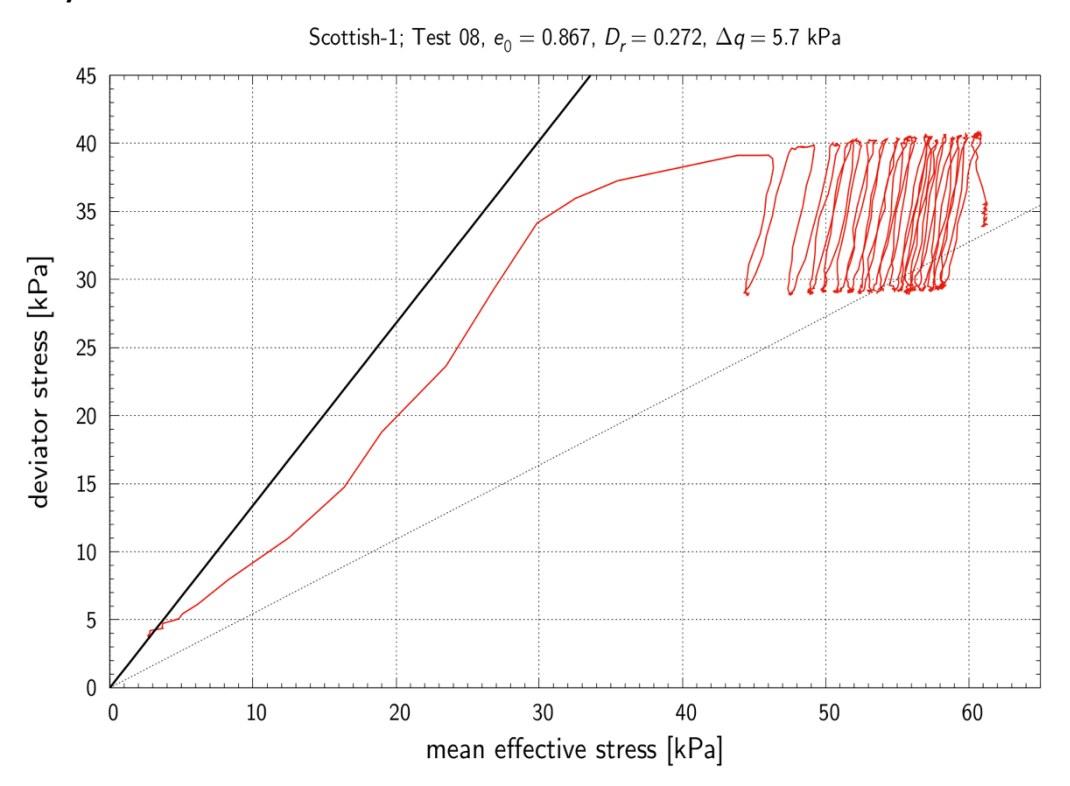


Fig.6.2.17 Results of cyclic test: stress path - sample no 8.

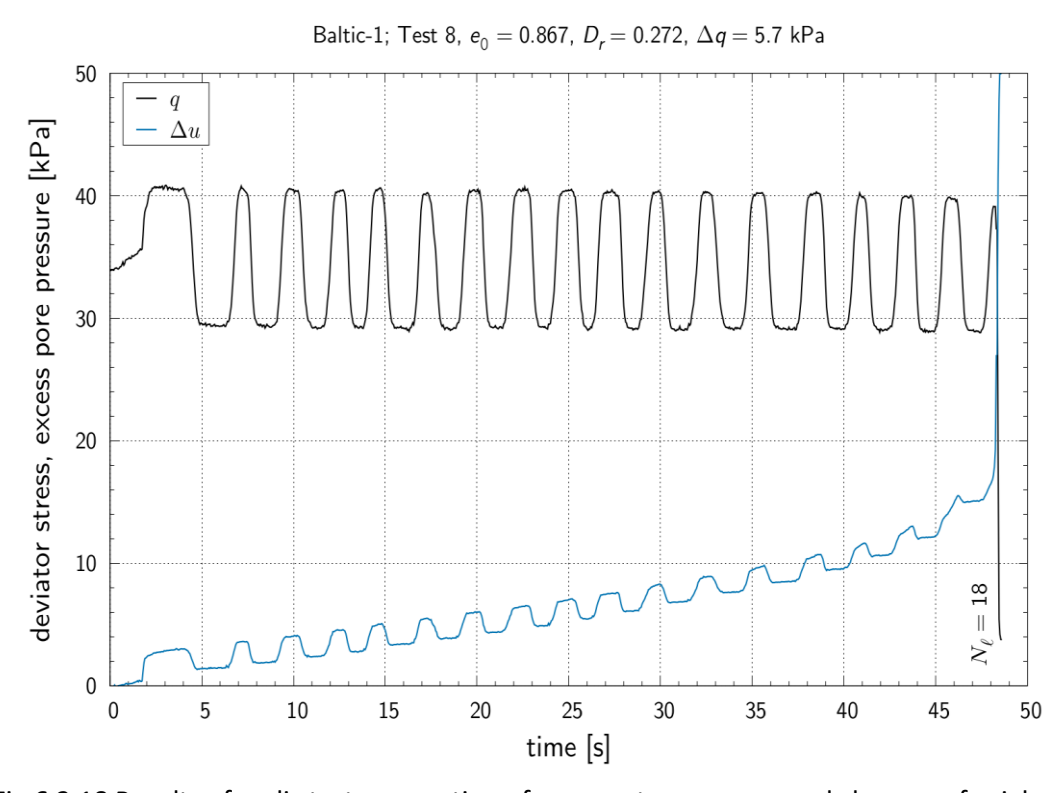


Fig.6.2.18 Results of cyclic test: generation of pore-water pressure and changes of axial strain versus number of loading cycles – sample no 8.





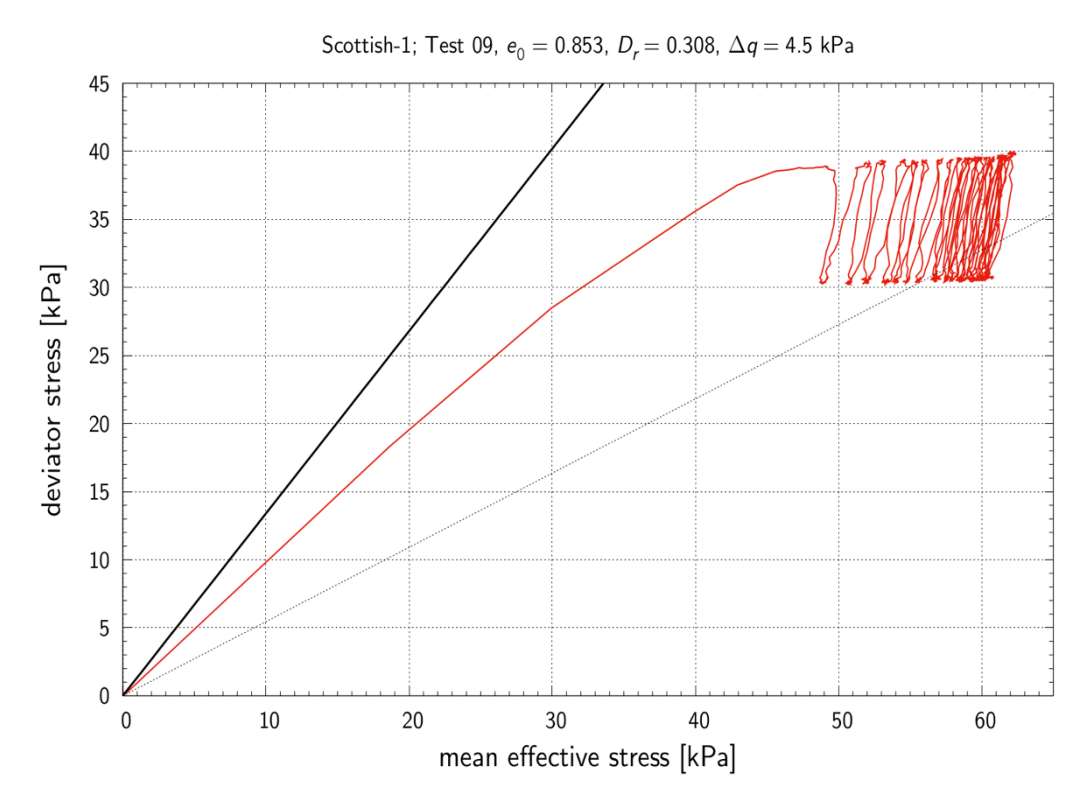


Fig.6.2.19 Results of cyclic test: stress path - sample no 9.

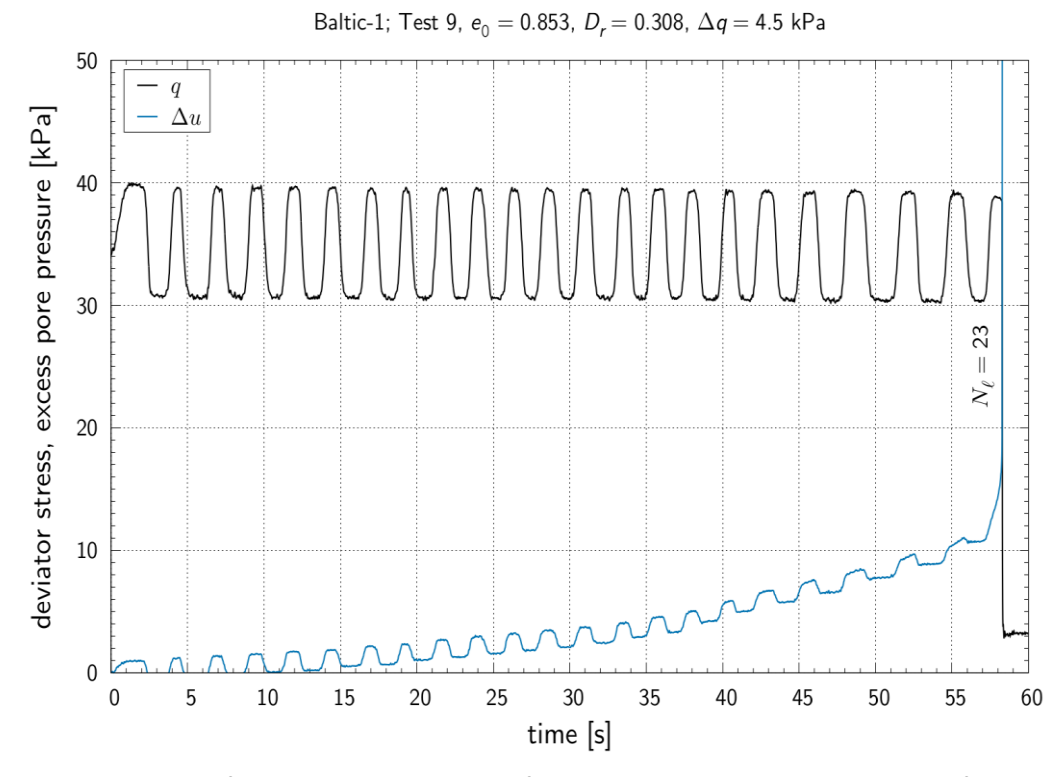


Fig.6.2.20 Results of cyclic test: generation of pore-water pressure and changes of axial strain versus number of loading cycles – sample no 9.





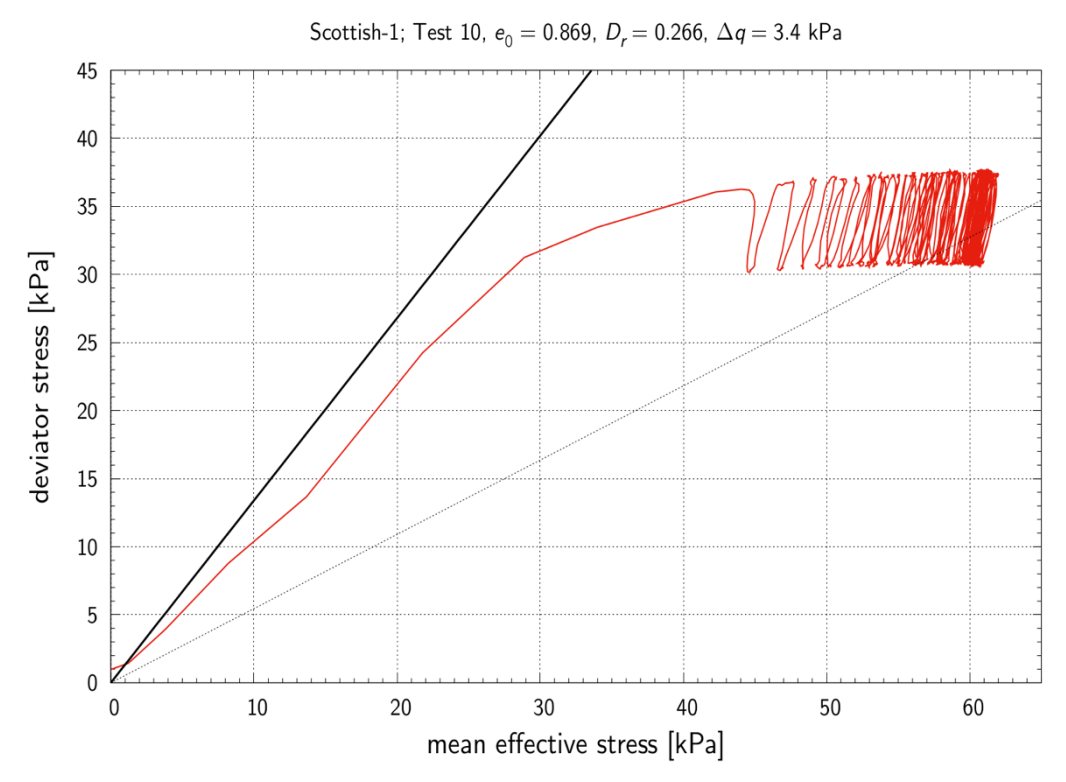


Fig.6.2.21 Results of cyclic test: stress path - sample no 10.

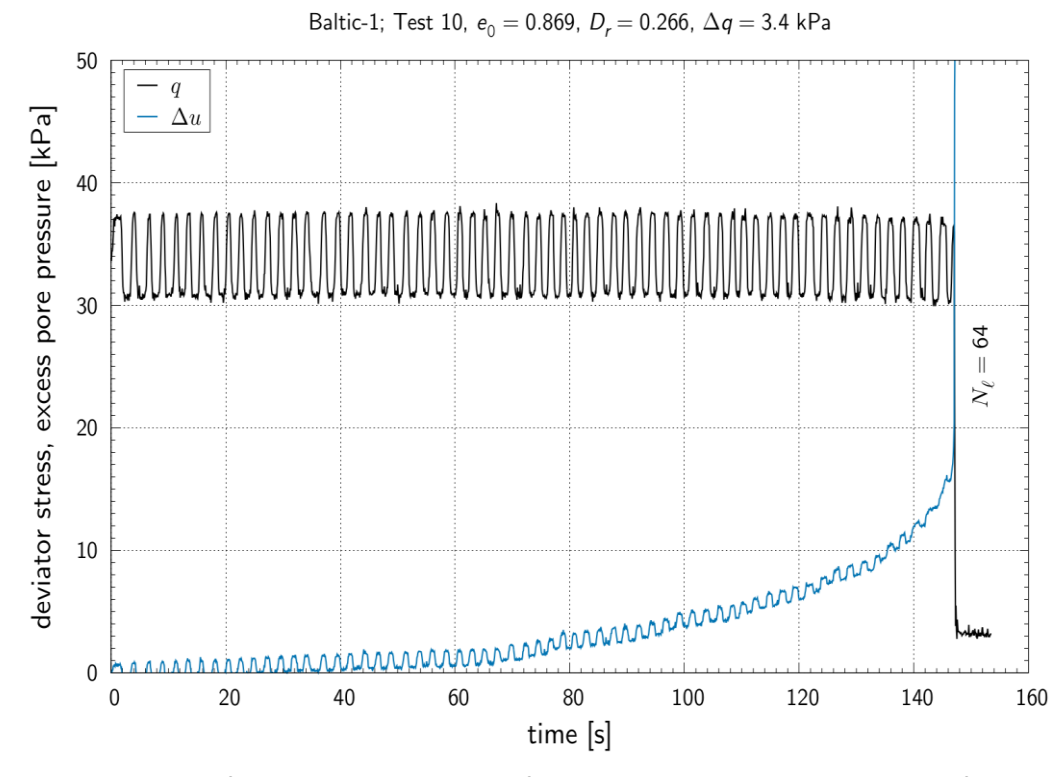


Fig.6.2.22 Results of cyclic test: generation of pore-water pressure and changes of axial strain versus number of loading cycles – sample no 10.





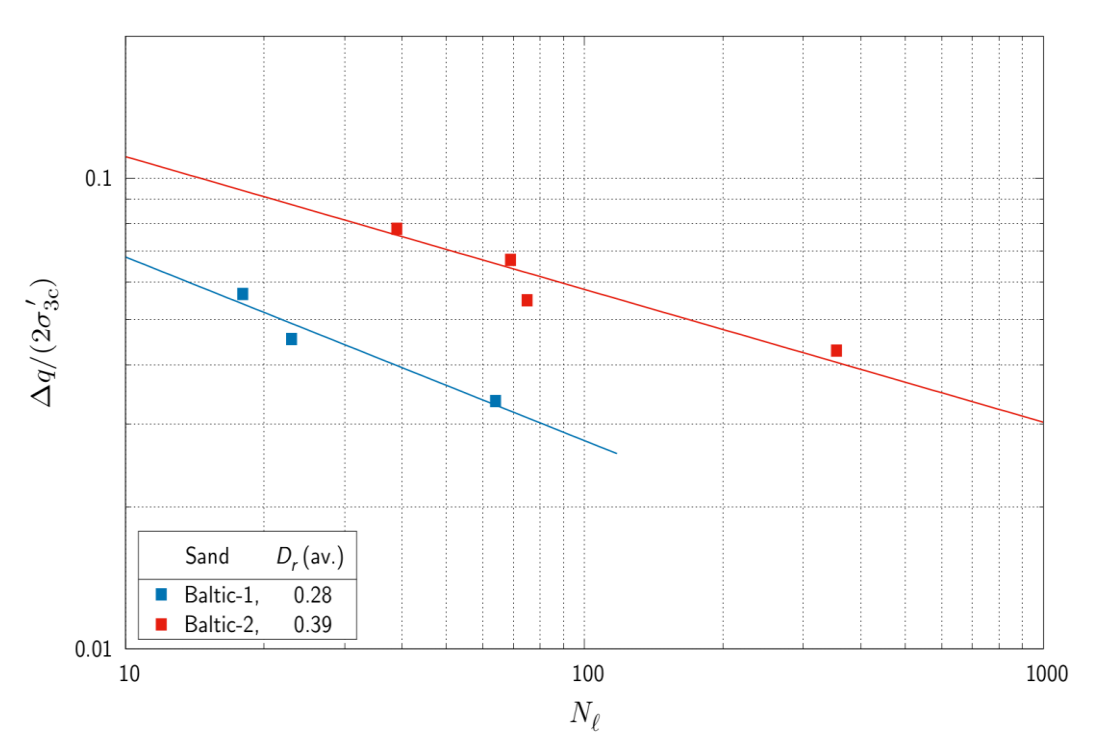


Fig.6.2.23 Normalized amplitude of the shear stress vs. the number of cycles to liquefaction.



6.3 Appendix nr 3 - Results of soil samples collected from Baltic Sea; Soil type: Baltic 2

1. Sampling locations and View of the samples under the microscope.



Fig.6.3.1 Sampling location.



Fig.6.3.2 View of the samples under the microscope.



2. Results of monotonic triaxial tests.

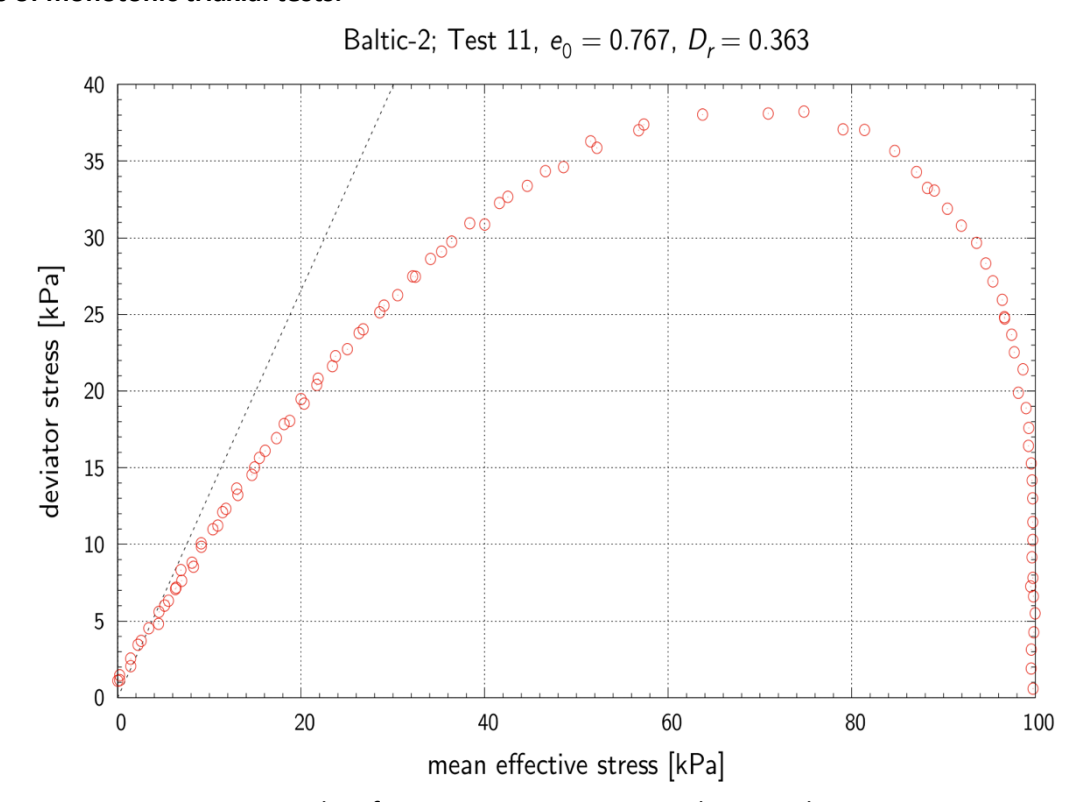


Fig.6.3.3 Results of monotonic test: stress path – sample no 11.

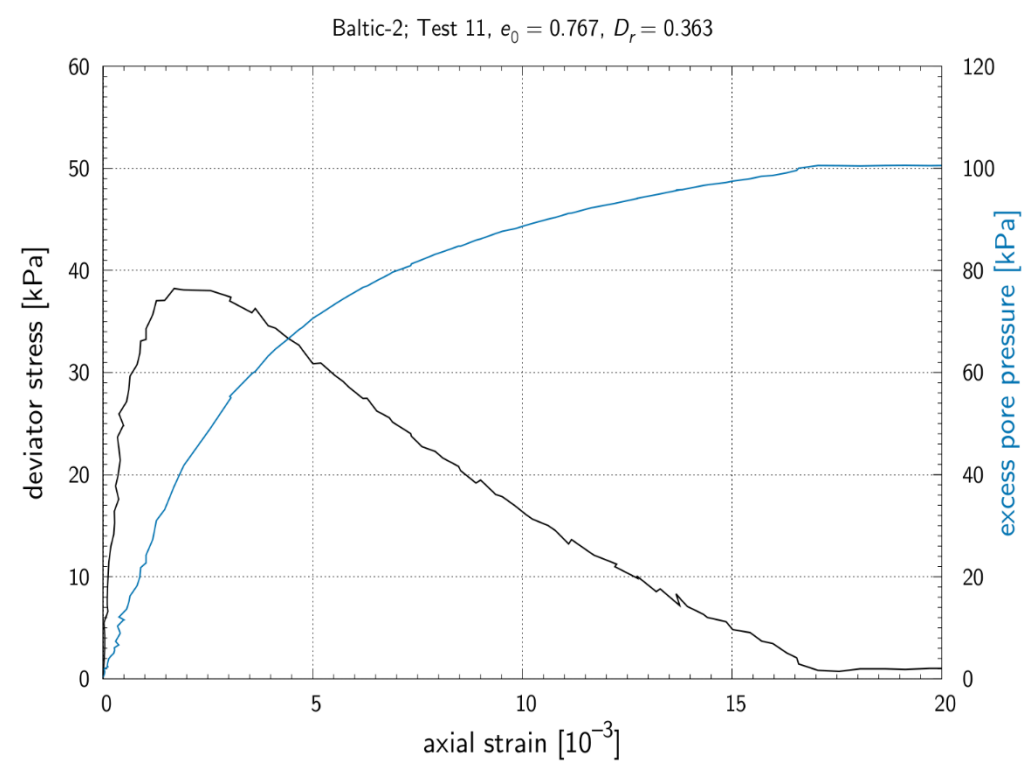


Fig.6.3.4 Results of monotonic test: response of soil sample: deviator stress vs. vertical strain – sample no 11.





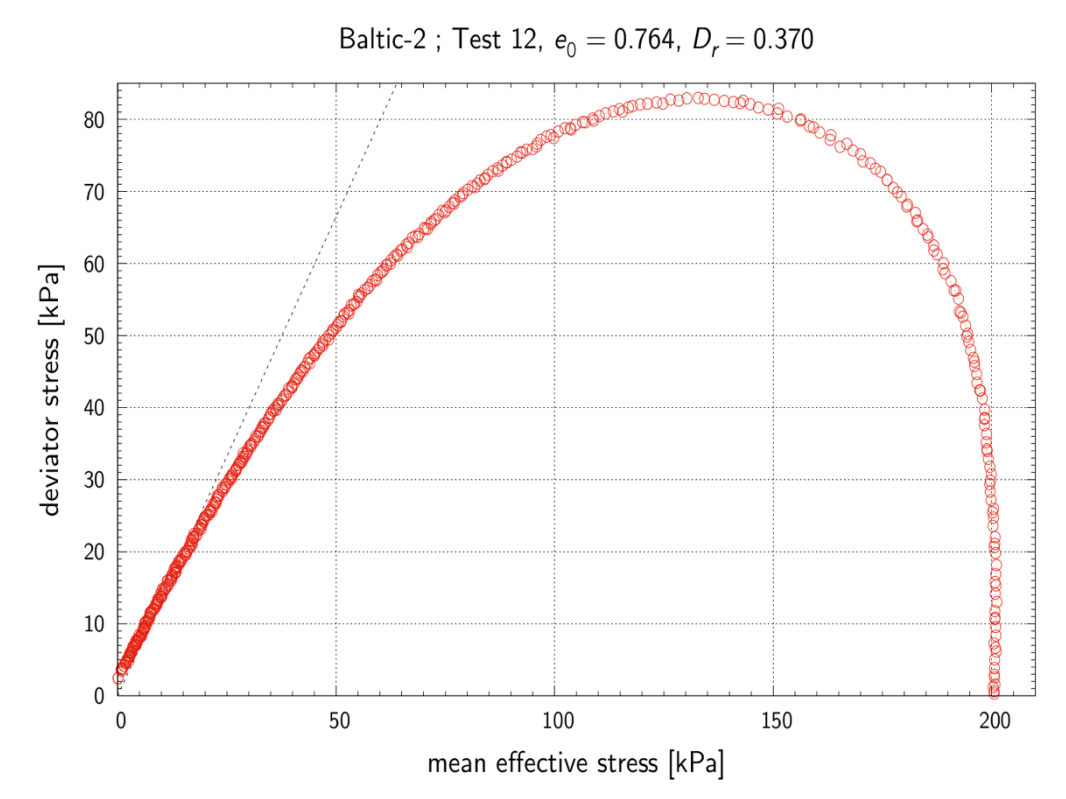


Fig.6.3.5 Results of monotonic test: stress path – sample no 12.

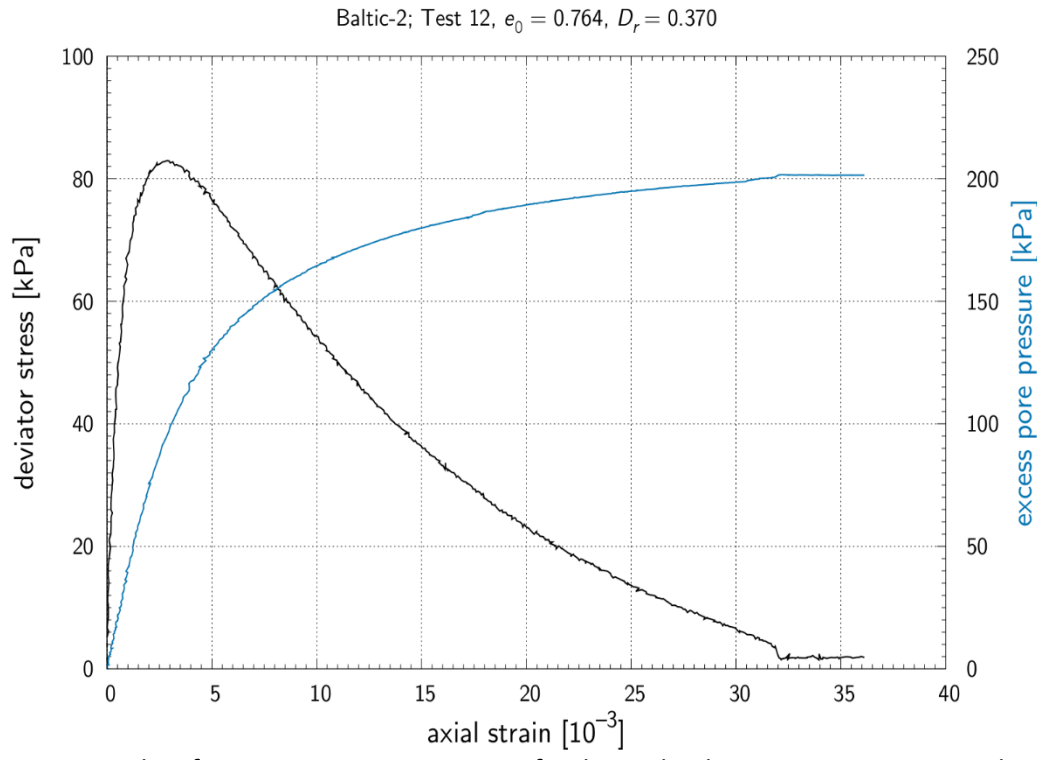


Fig.6.3.6 Results of monotonic test: response of soil sample: deviator stress vs. vertical strain – sample no 12.





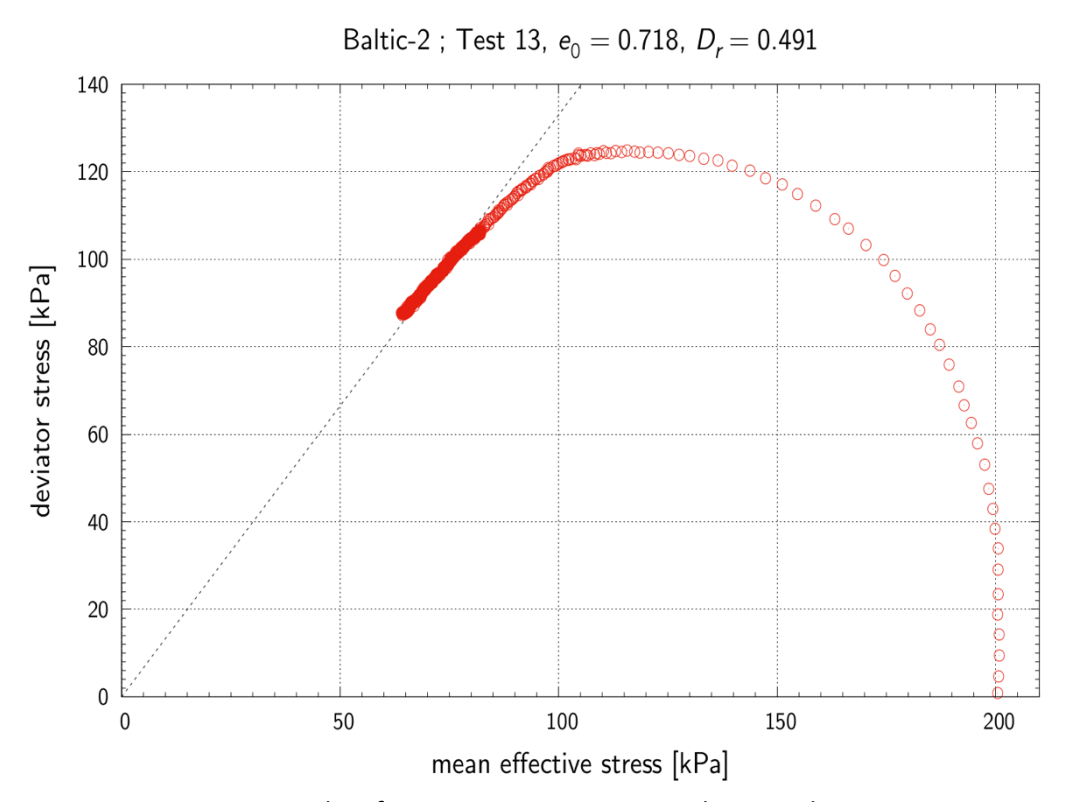


Fig.6.3.7 Results of monotonic test: stress path – sample no 13.

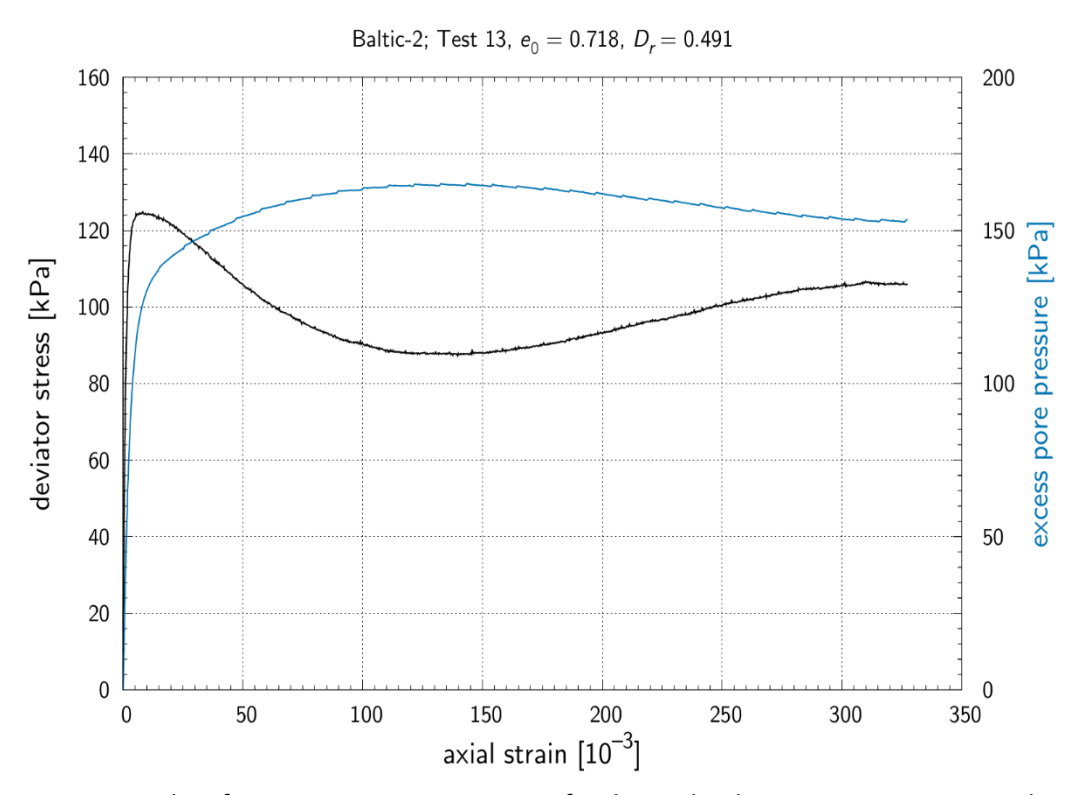


Fig.6.3.8 Results of monotonic test: response of soil sample: deviator stress vs. vertical strain – sample no 13.





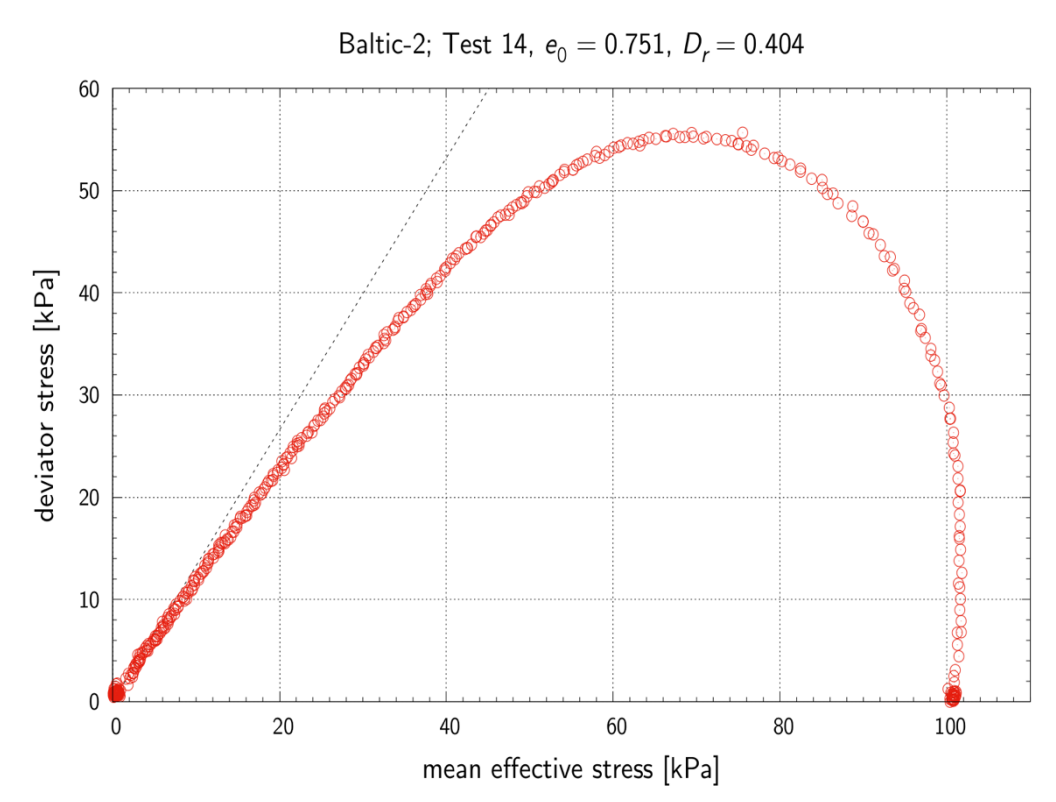


Fig. 6.3.9 Results of monotonic test: stress path – sample no 14.

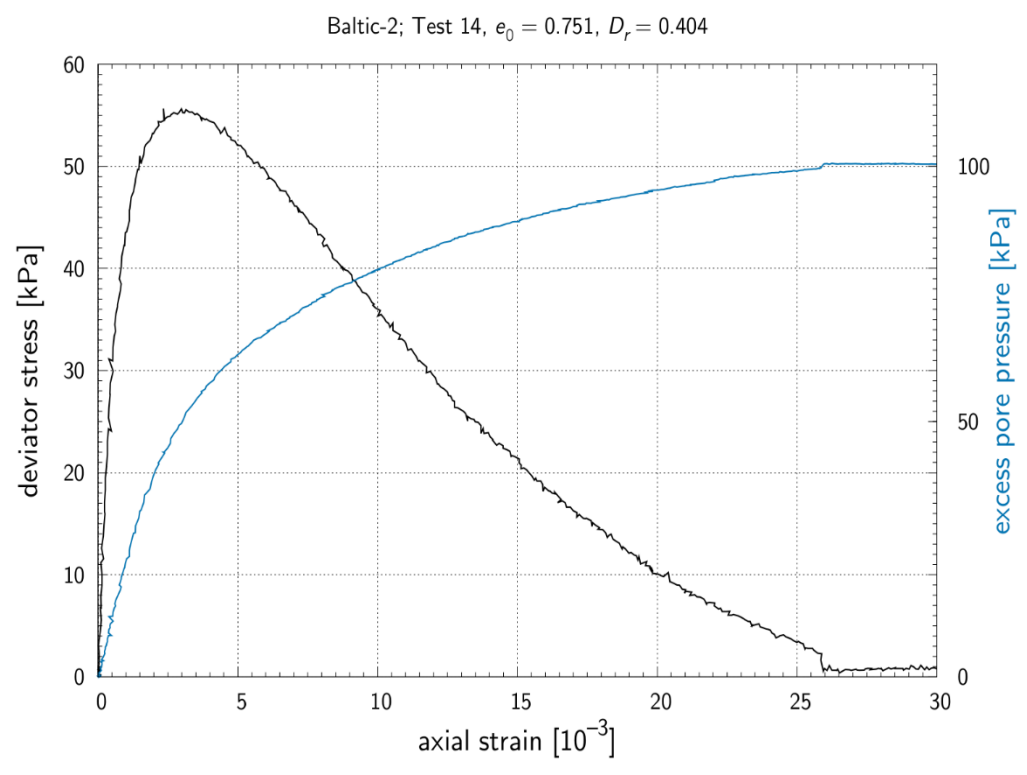


Fig.6.3.10 Results of monotonic test: response of soil sample: deviator stress vs. vertical strain – sample no 14.





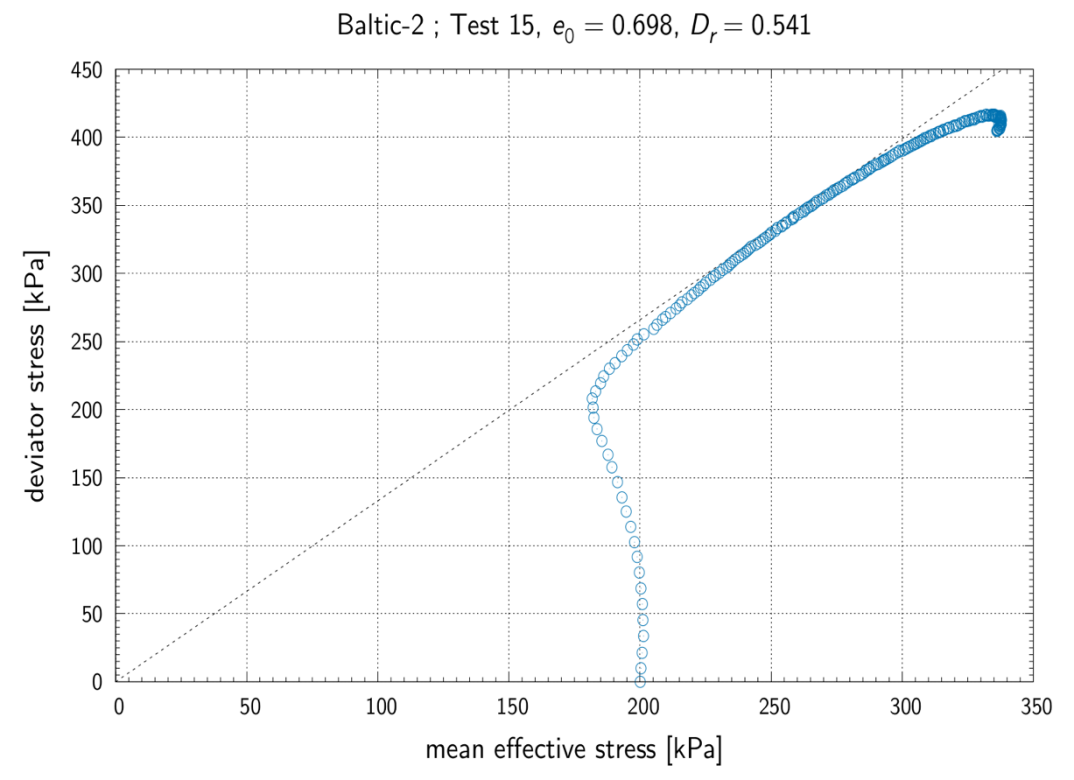


Fig.6.3.11 Results of monotonic test: stress path – sample no 15.

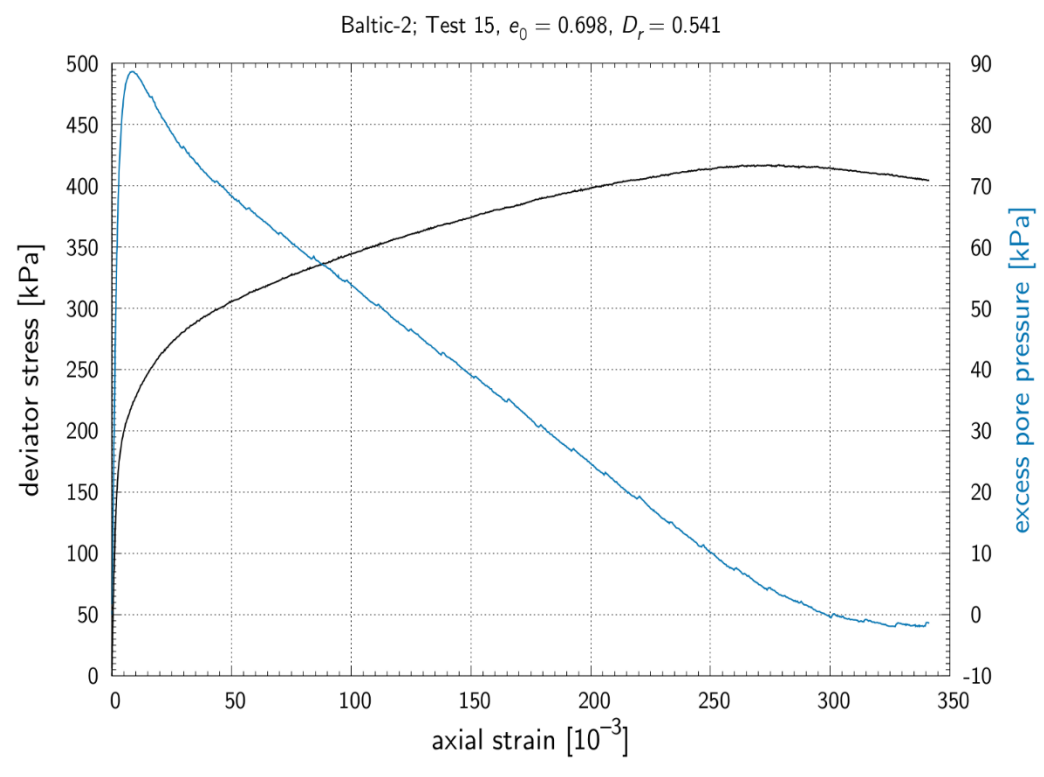


Fig.6.3.12 Results of monotonic test: response of soil sample: deviator stress vs. vertical strain – sample no 15.





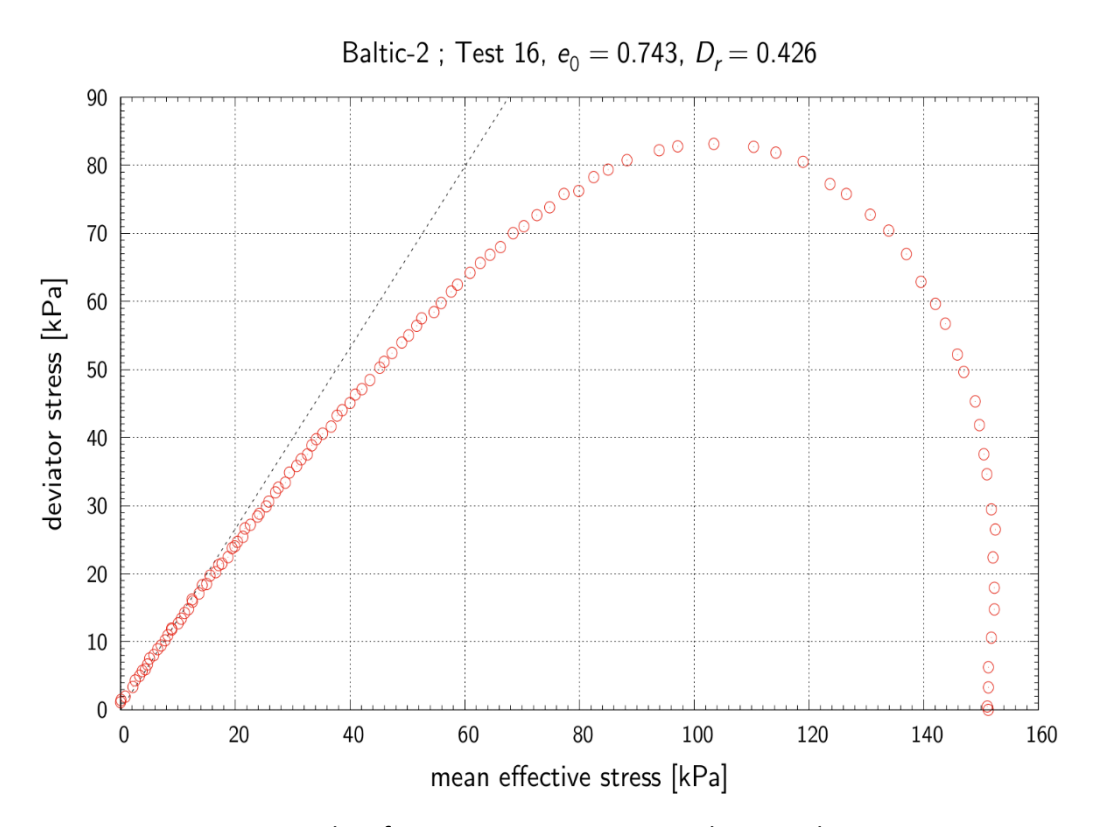


Fig.6.3.13 Results of monotonic test: stress path – sample no 16.

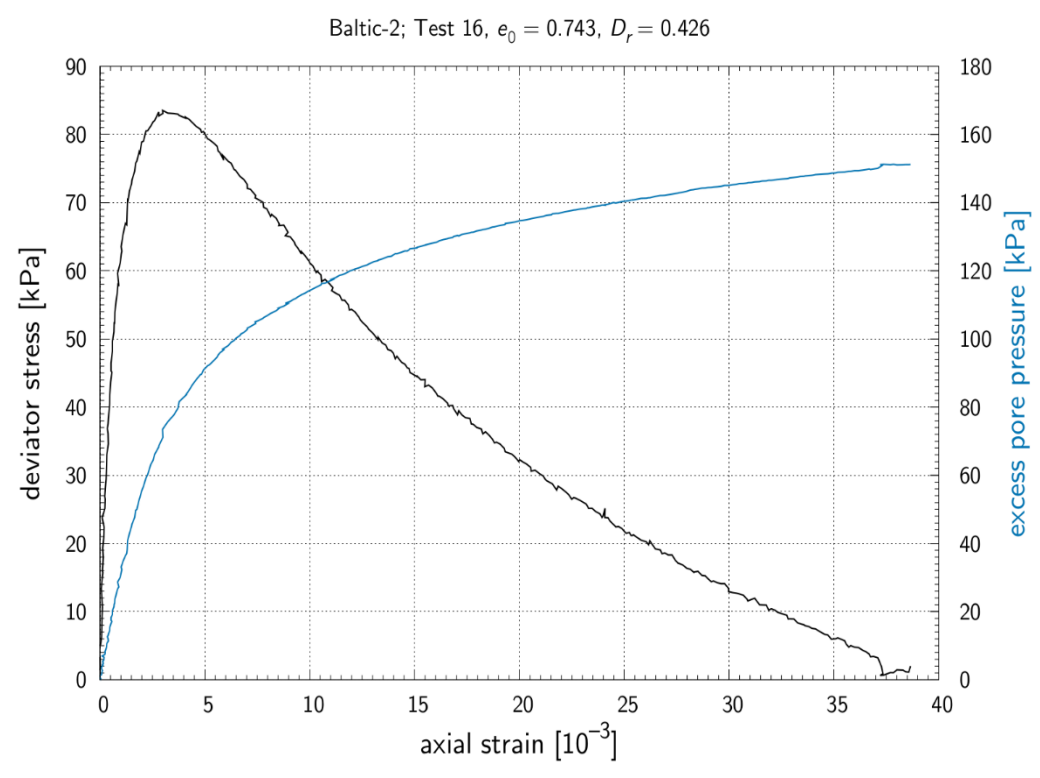


Fig 6.3.14 Results of monotonic test: response of soil sample: deviator stress vs. vertical strain – sample no 16.





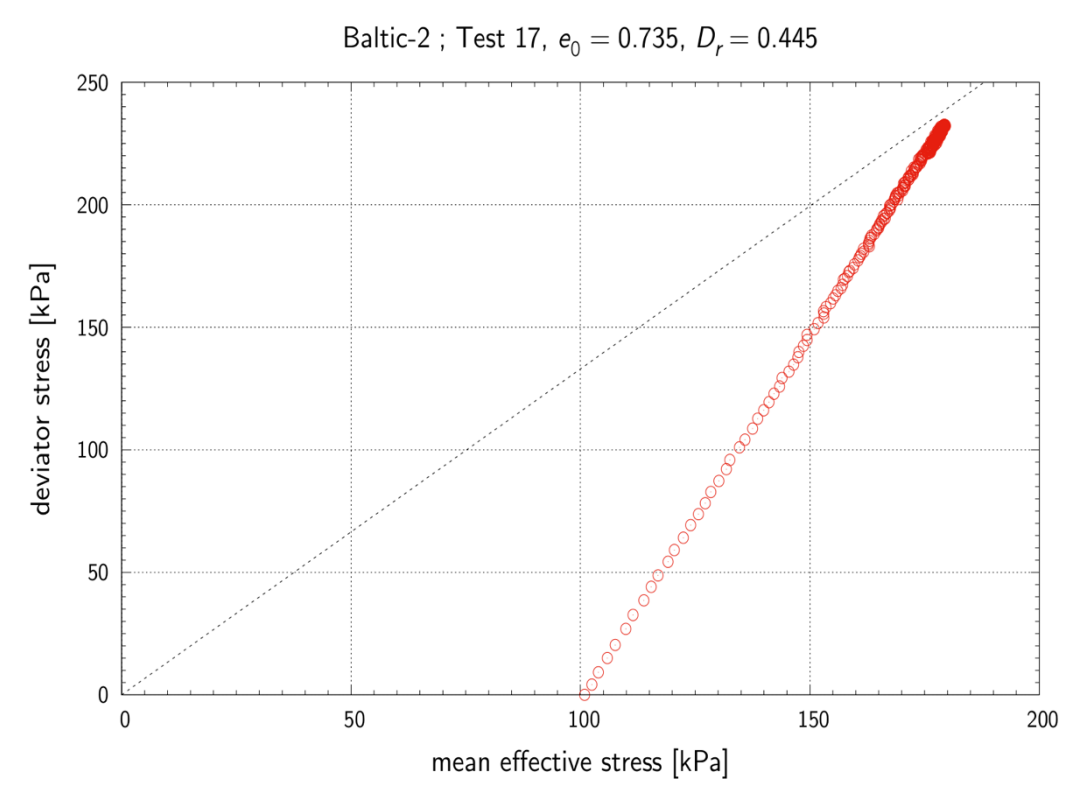


Fig.6.3.15 Results of monotonic test: stress path – sample no 17.

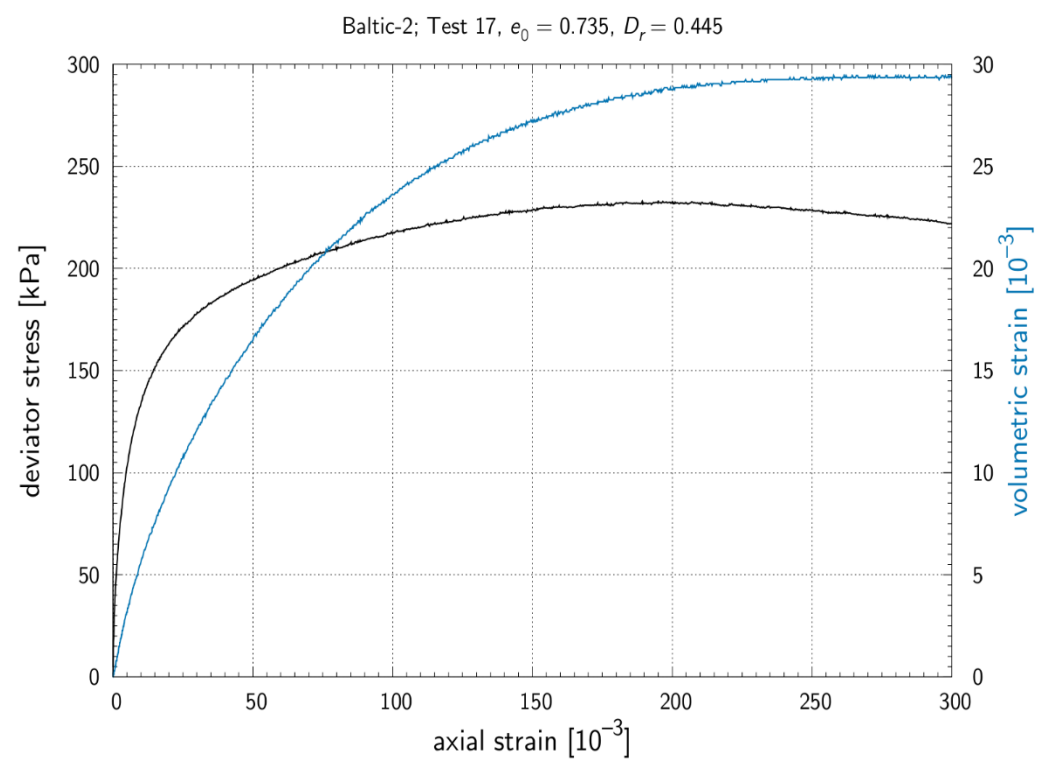


Fig.6.3.16 Results of monotonic test: response of soil sample: deviator stress vs. vertical strain – sample no 17.





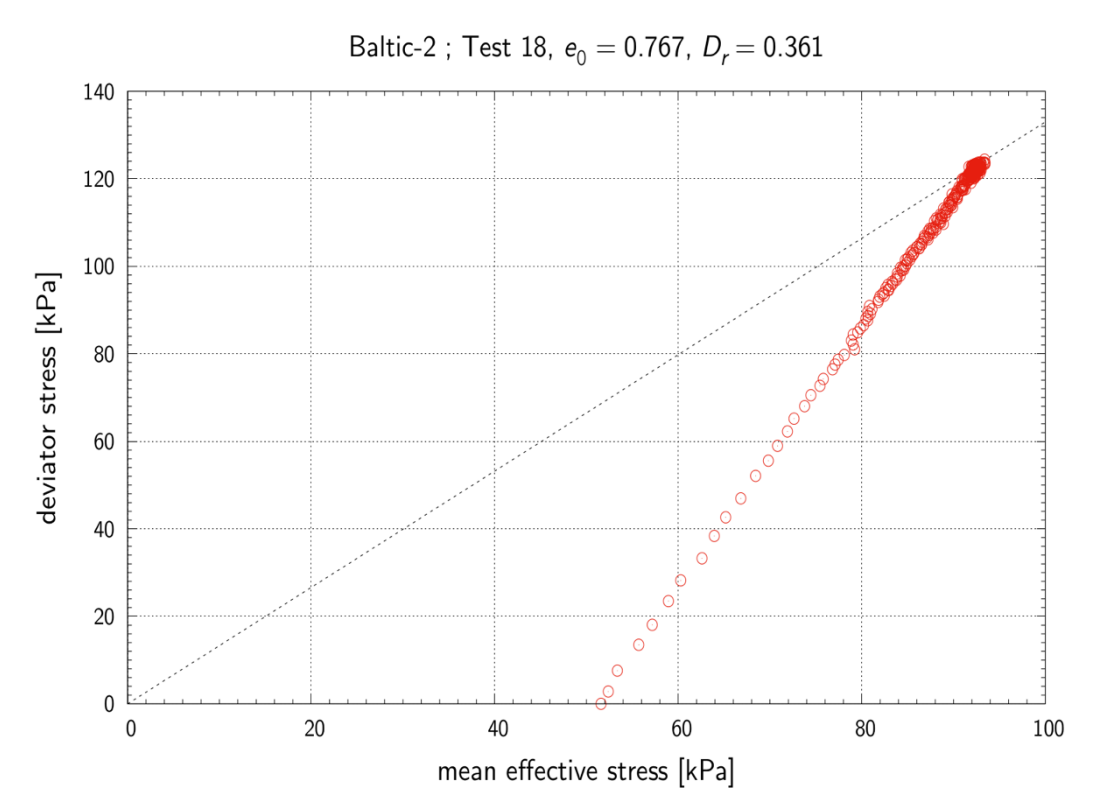


Fig.6.3.17 Results of monotonic test: stress path – sample no 18.

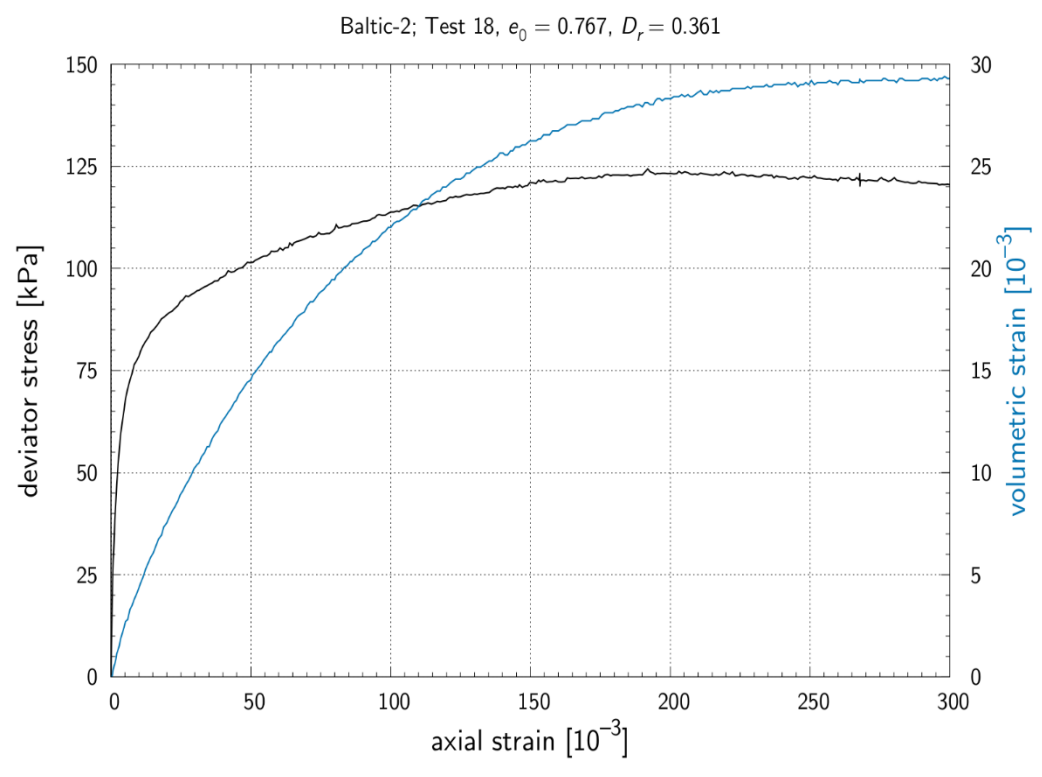


Fig. 6.3.18 Results of monotonic test: response of soil sample: deviator stress vs. vertical strain – sample no 18.





3. Results of cyclic triaxial tests.

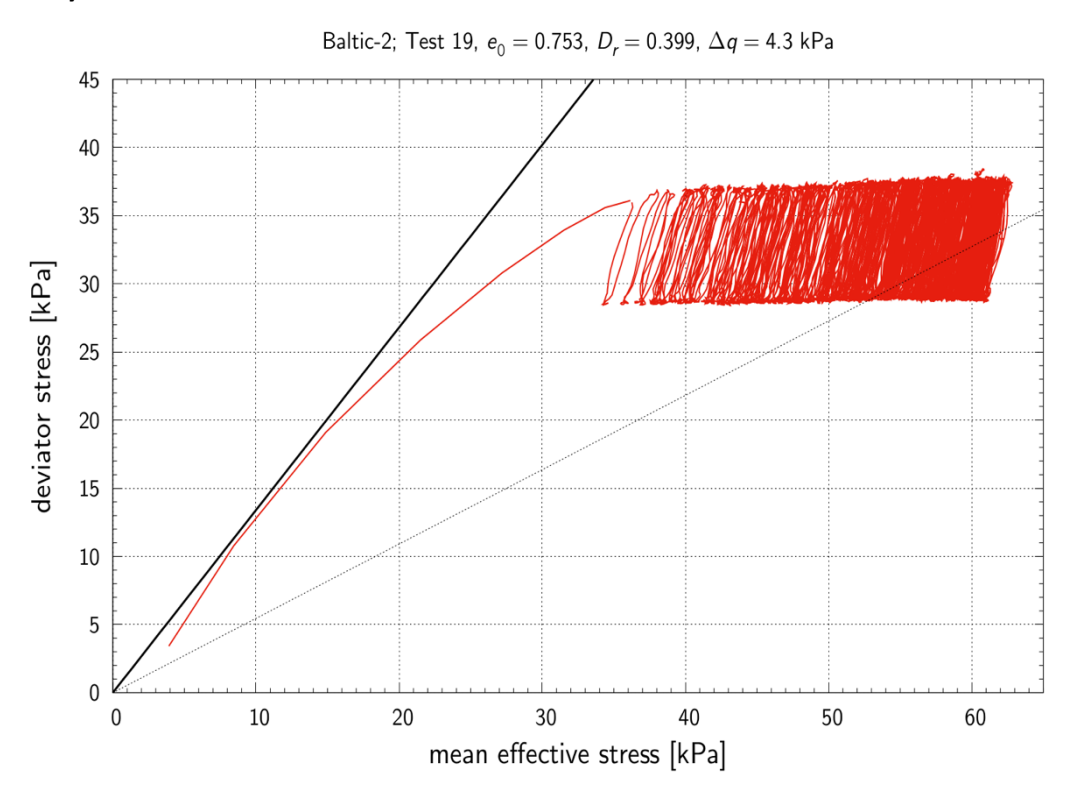


Fig. 6.3.19 Results of cyclic test: stress path - sample no 19.

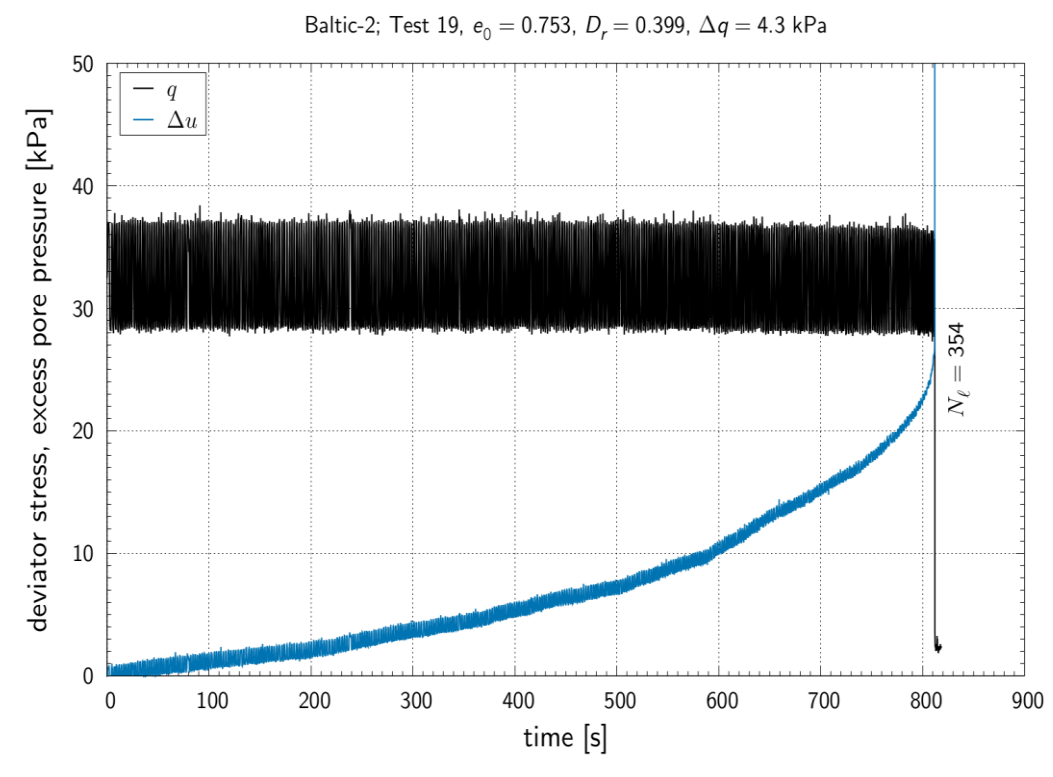


Fig.6.3.20 Results of cyclic test: generation of pore-water pressure and changes of axial strain versus number of loading cycles – sample no 19.





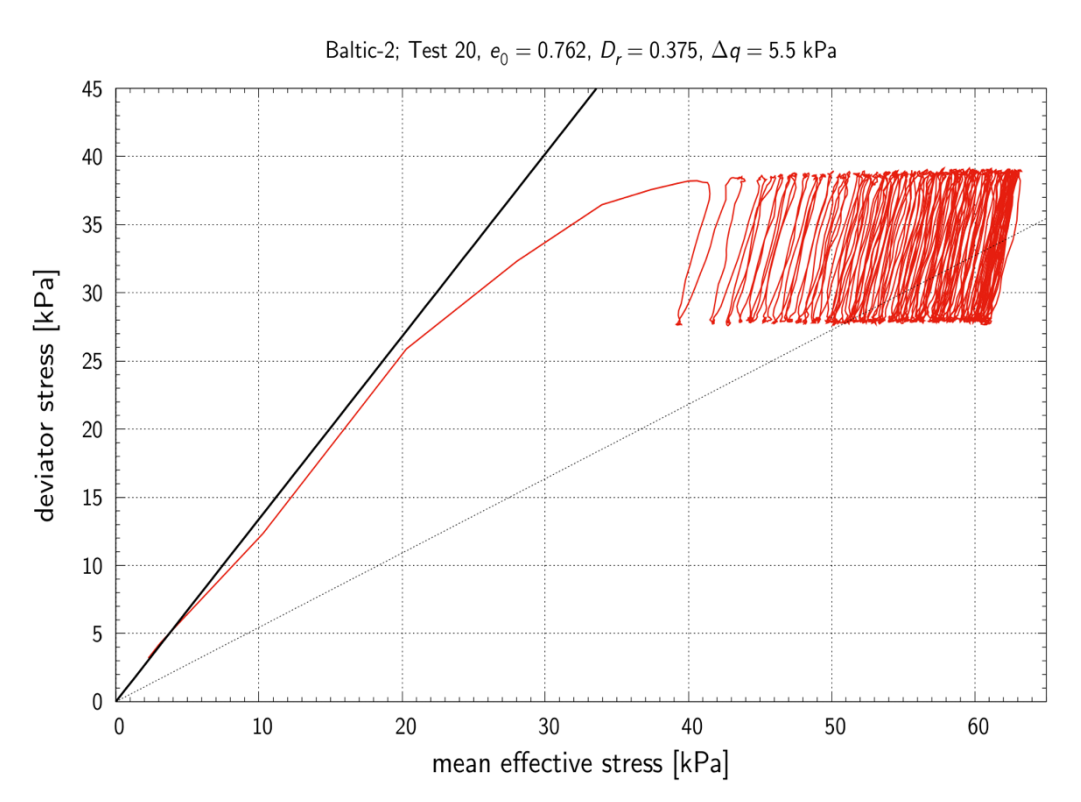


Fig.6.3.21 Results of cyclic test: stress path - sample no 20.

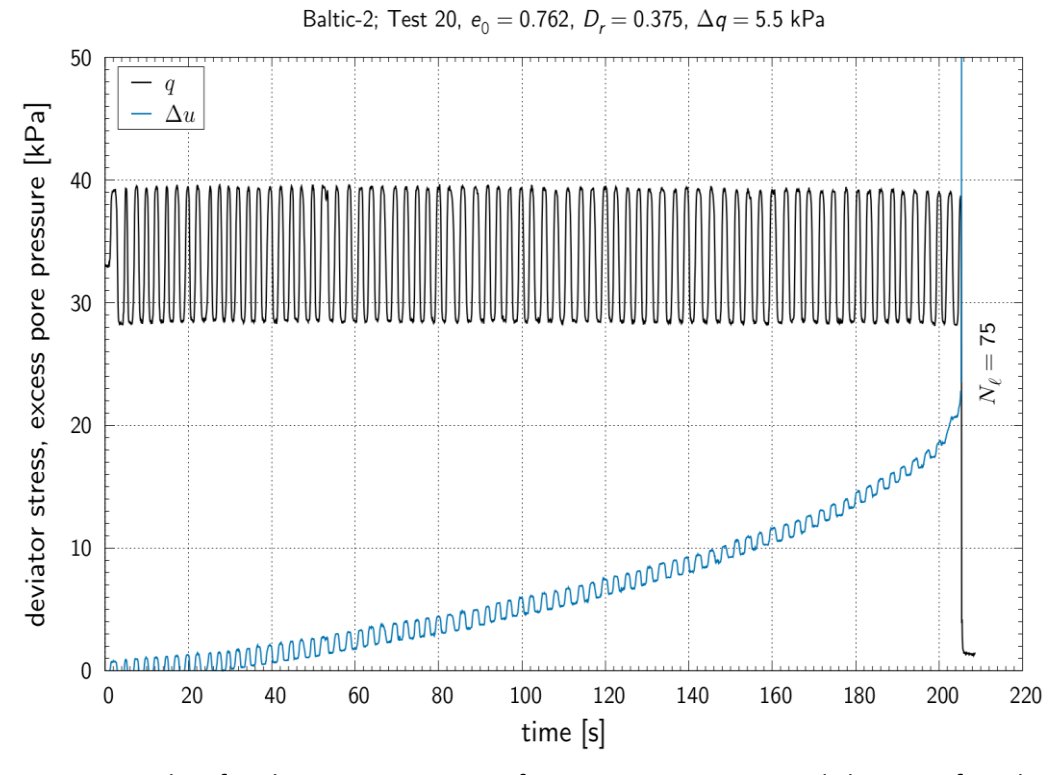


Fig.6.3.22 Results of cyclic test: generation of pore-water pressure and changes of axial strain versus number of loading cycles – sample no 20.





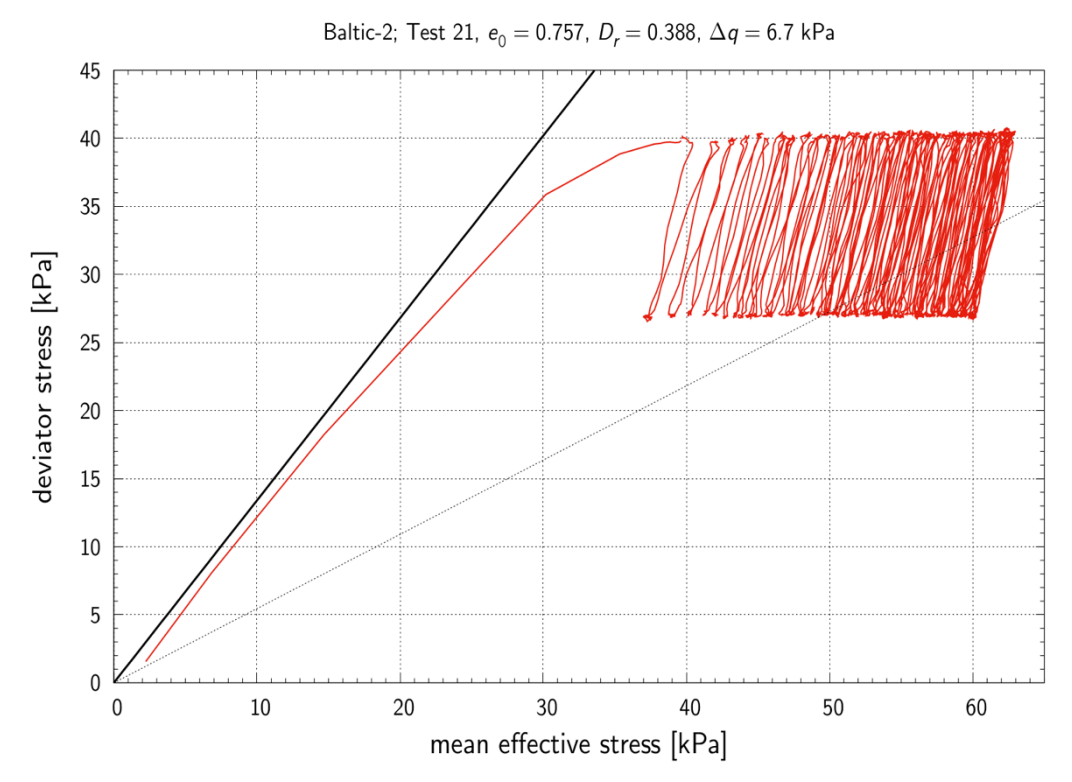


Fig.6.3.23 Results of cyclic test: stress path - sample no 21.

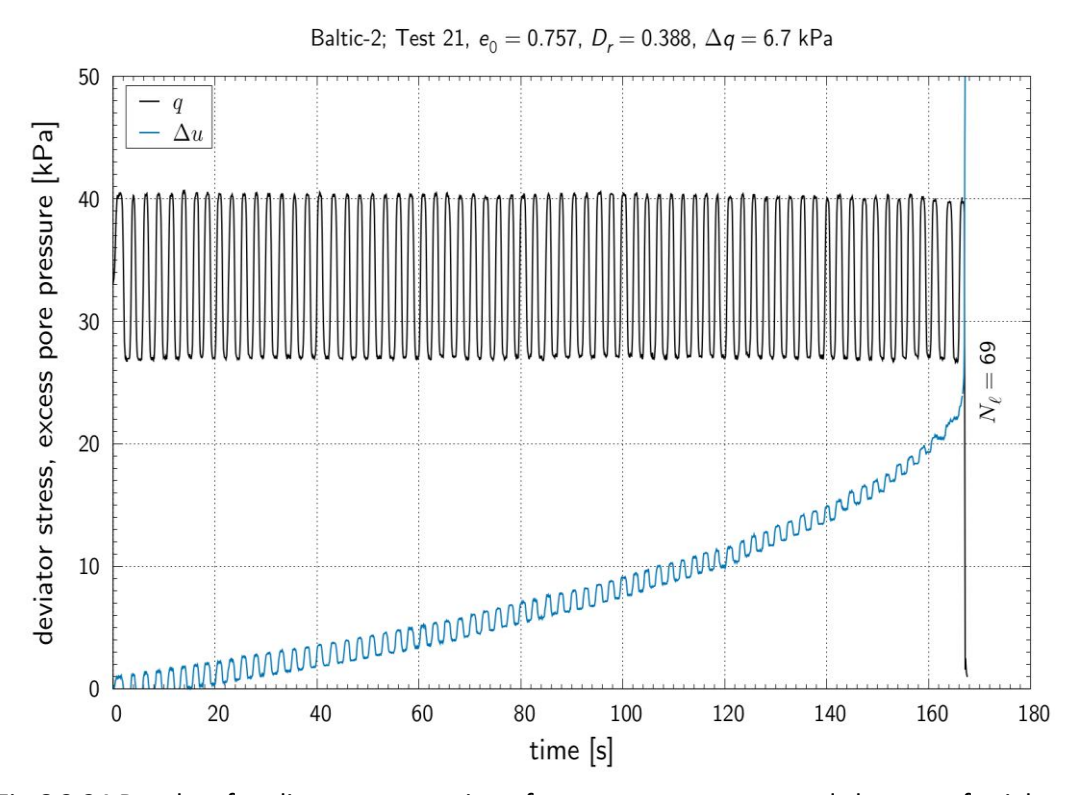


Fig.6.3.24 Results of cyclic test: generation of pore-water pressure and changes of axial strain versus number of loading cycles – sample no 21.





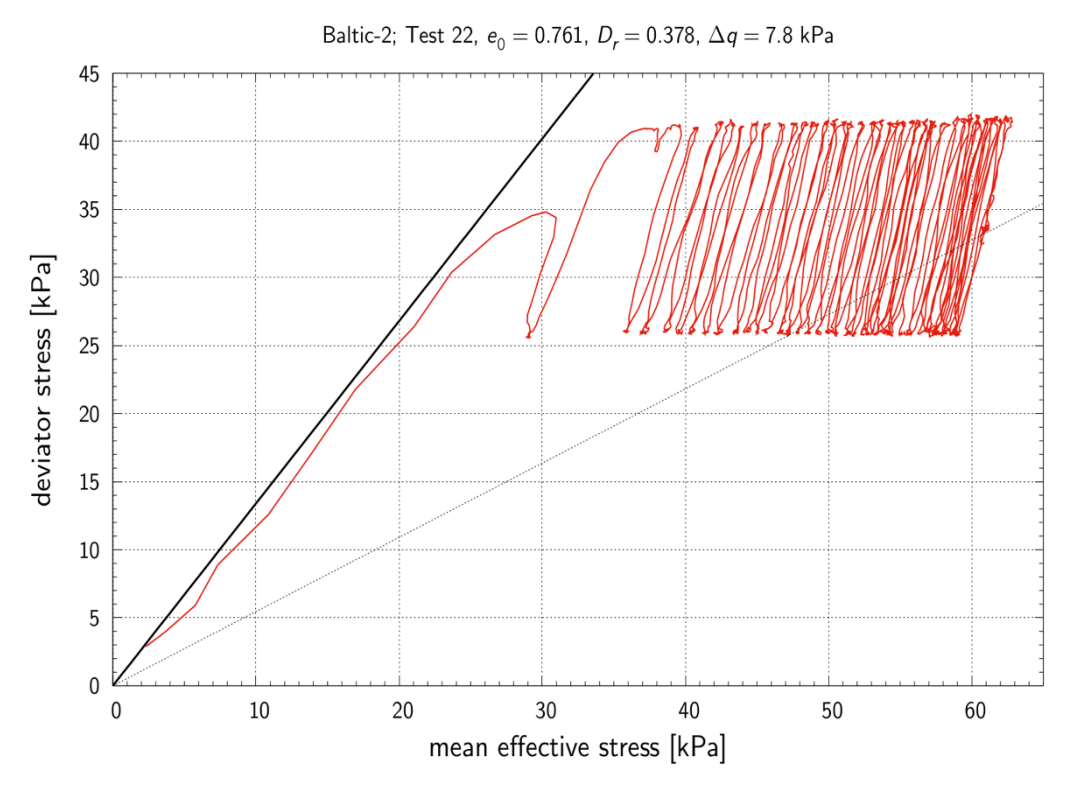


Fig.6.3.25 Results of cyclic test: stress path - sample no 22.

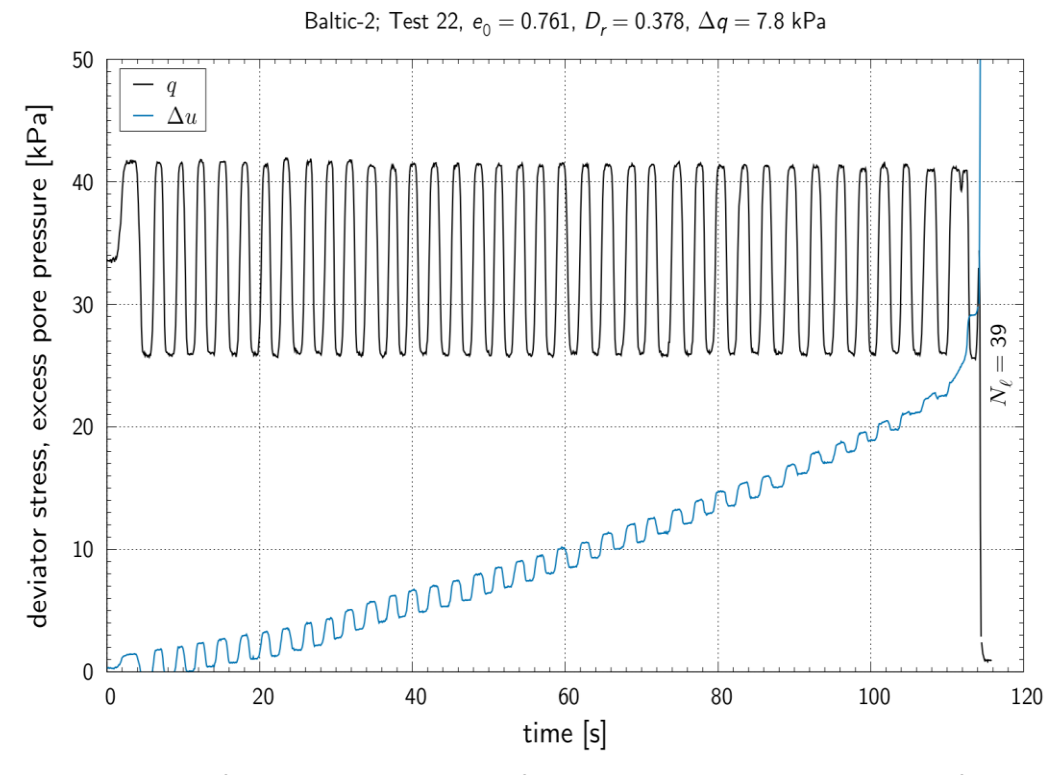


Fig.6.3.26 Results of cyclic test: generation of pore-water pressure and changes of axial strain versus number of loading cycles – sample no 22.





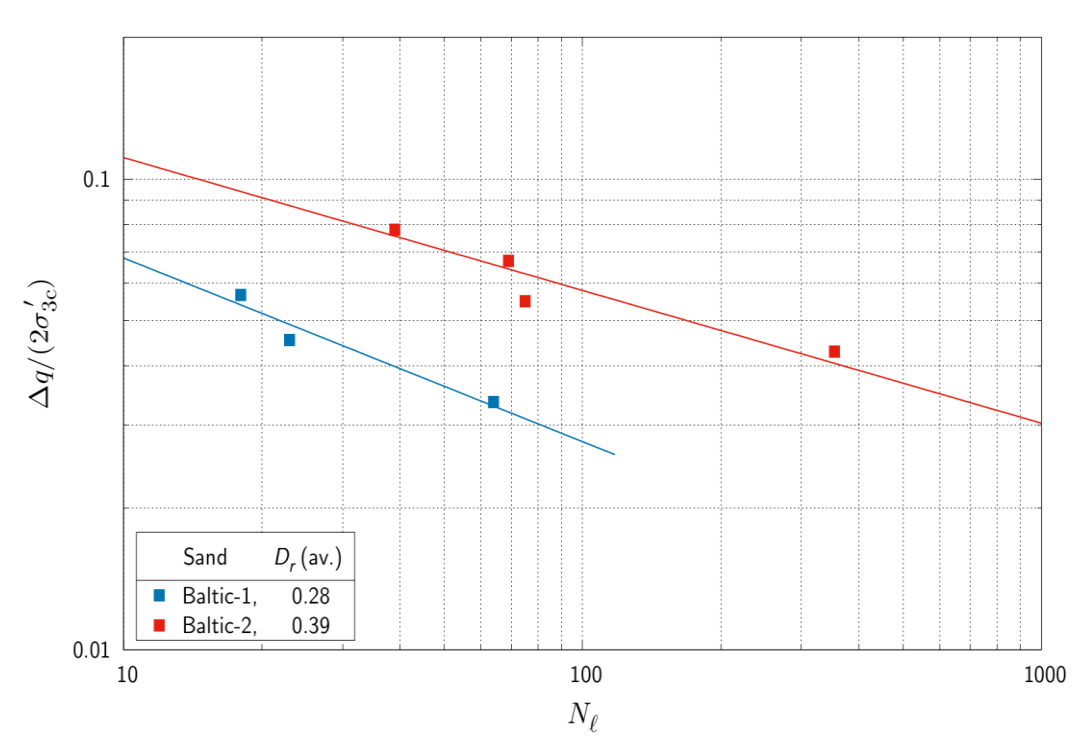


Fig.6.3.27 Normalized amplitude of the shear stress vs. the number of cycles to liquefaction.



6.4 Appendix nr 4 - Results of soil samples collected from Baltic Sea; Soil type: Scottish 1

1. Sampling locations and View of the samples under the microscope.





Fig.6.4.1 Sampling location.





Fig.6.4.2 View of the samples under the microscope.



2. Results of monotonic triaxial tests.

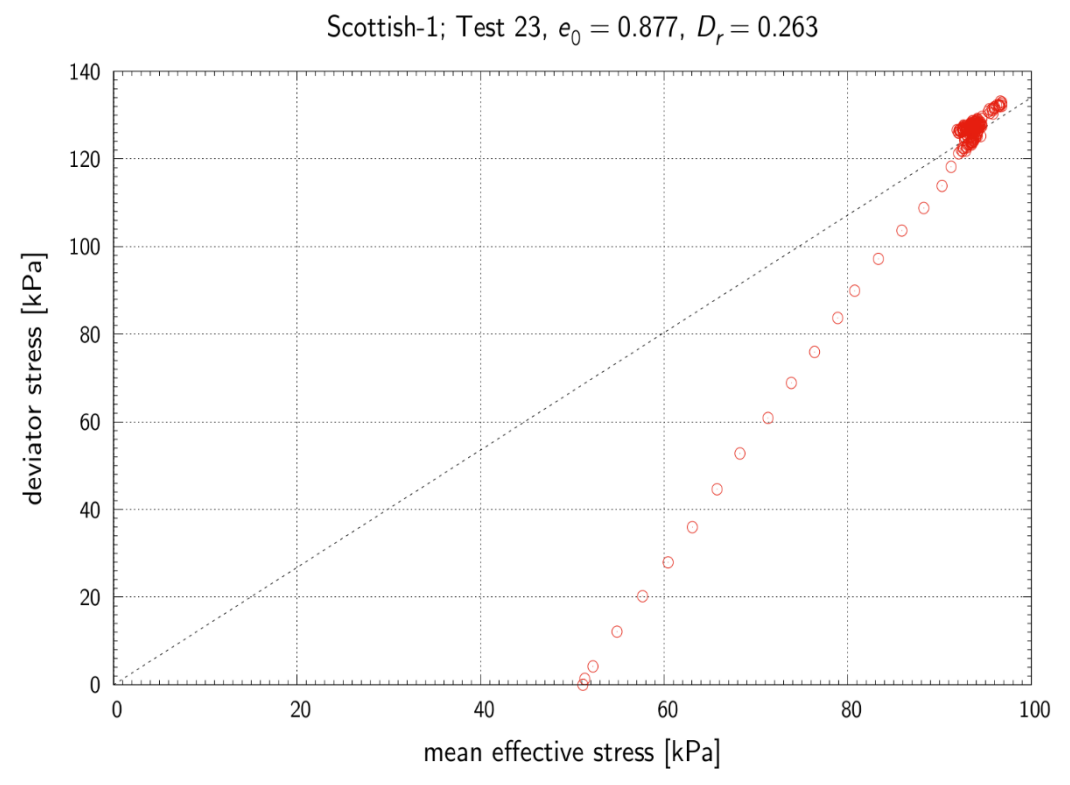


Fig.6.4.3 Results of monotonic test: stress path – sample no 23.

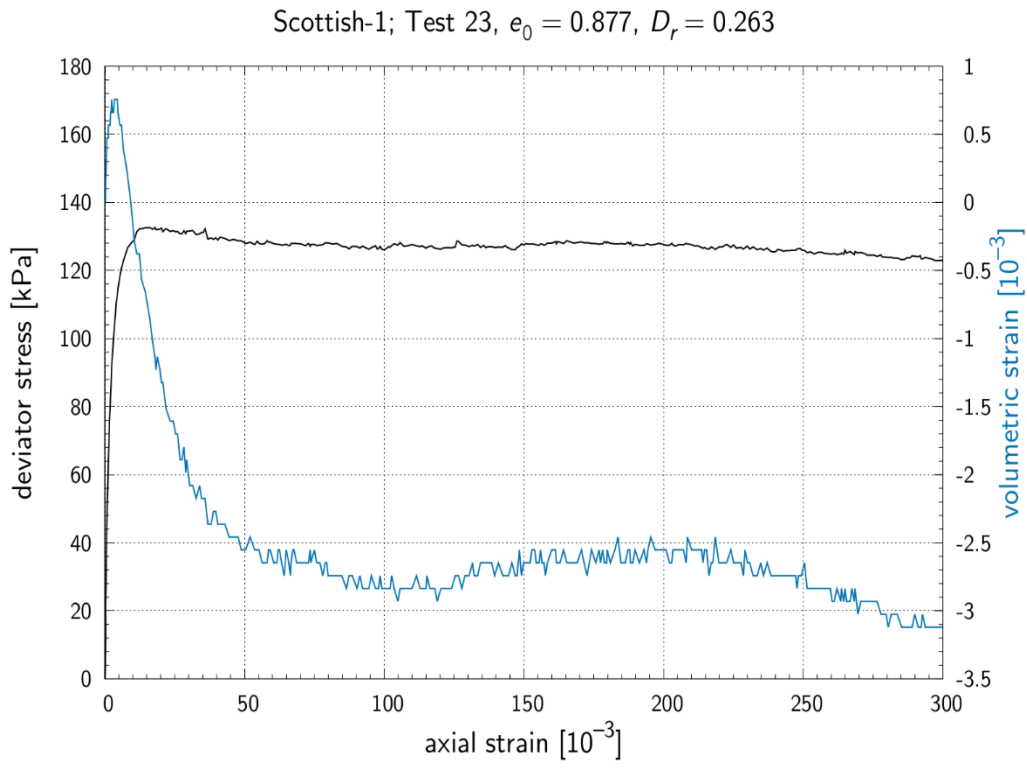


Fig .6.4.4 Results of monotonic test: response of soil sample: deviator stress vs. vertical strain – sample no 23.





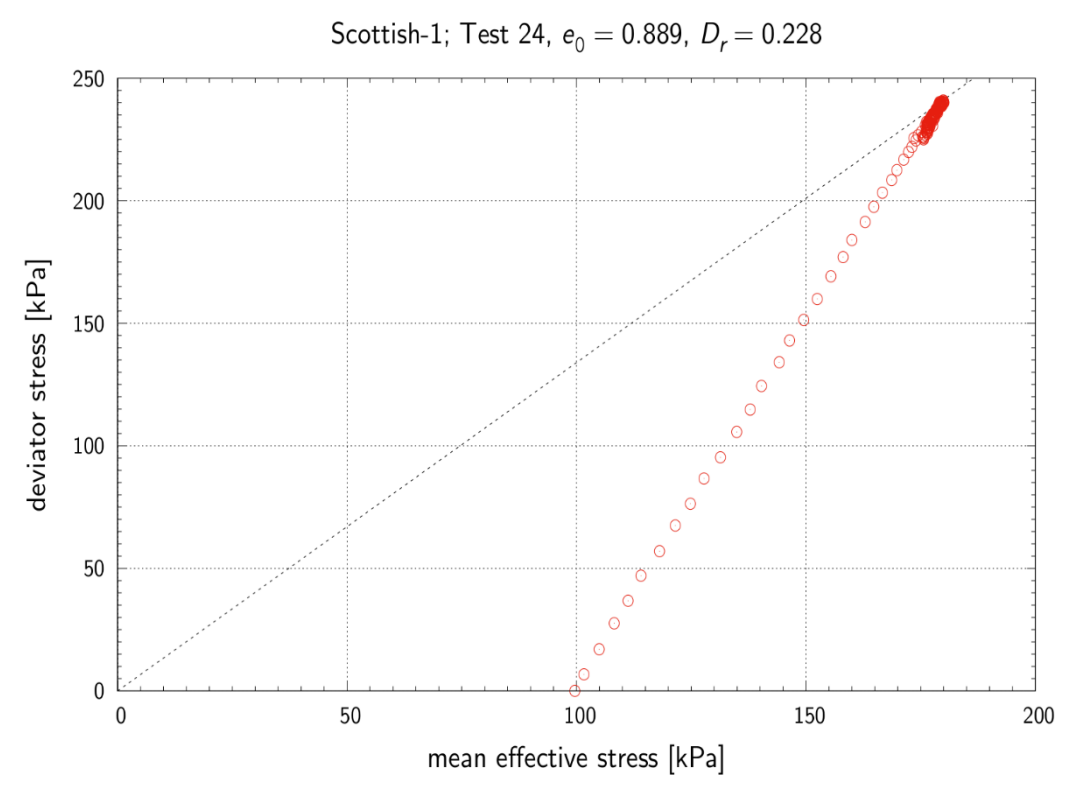


Fig. 6.4.5 Results of monotonic test: stress path – sample no 24.

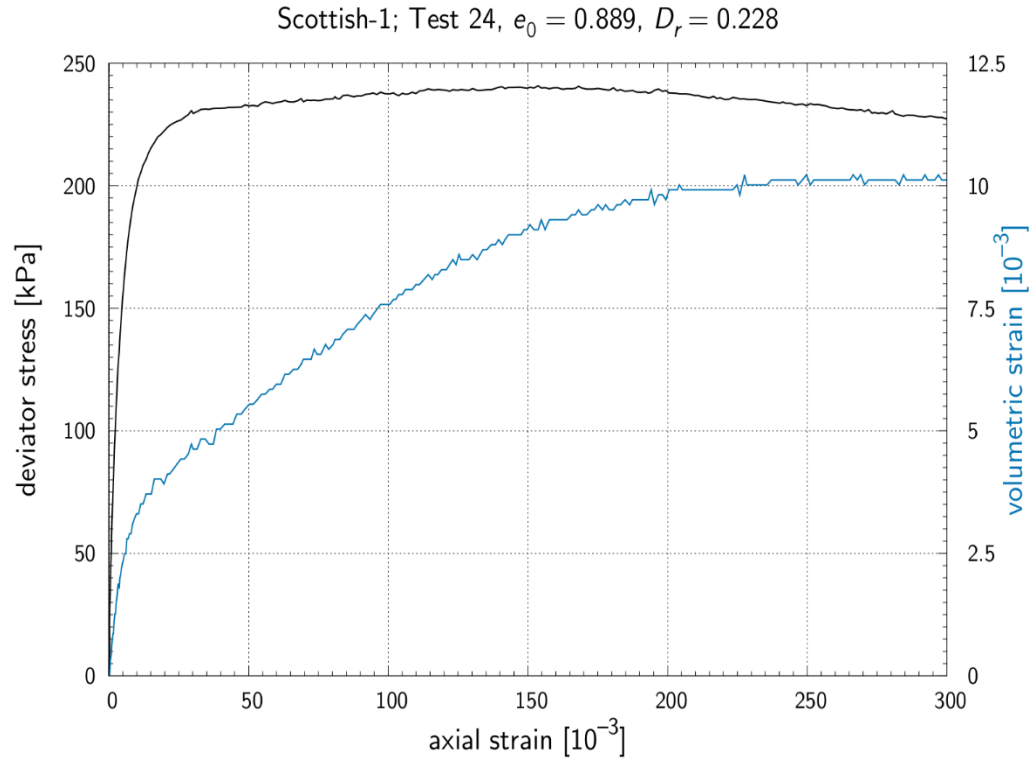


Fig.6.4.6 Results of monotonic test: response of soil sample: deviator stress vs. vertical strain – sample no 24.





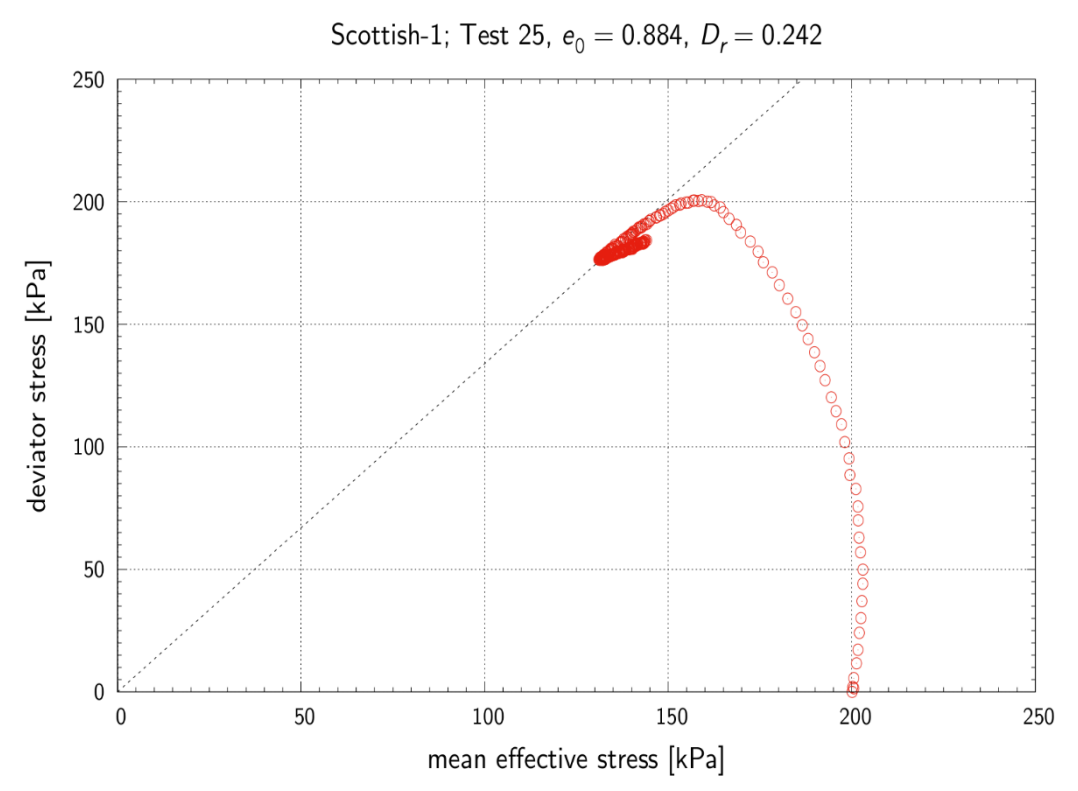


Fig.6.4.7 Results of monotonic test: stress path – sample no 25.

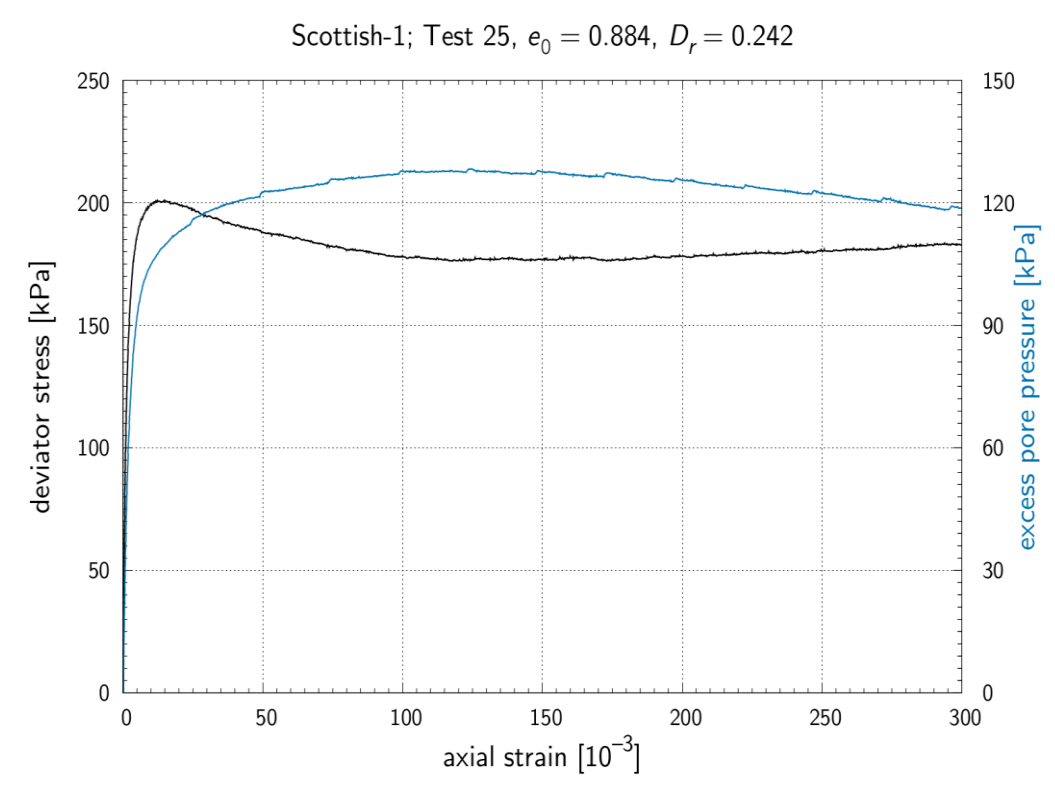


Fig.6.4.8 Results of monotonic test: response of soil sample: deviator stress vs. vertical strain – sample no 25.





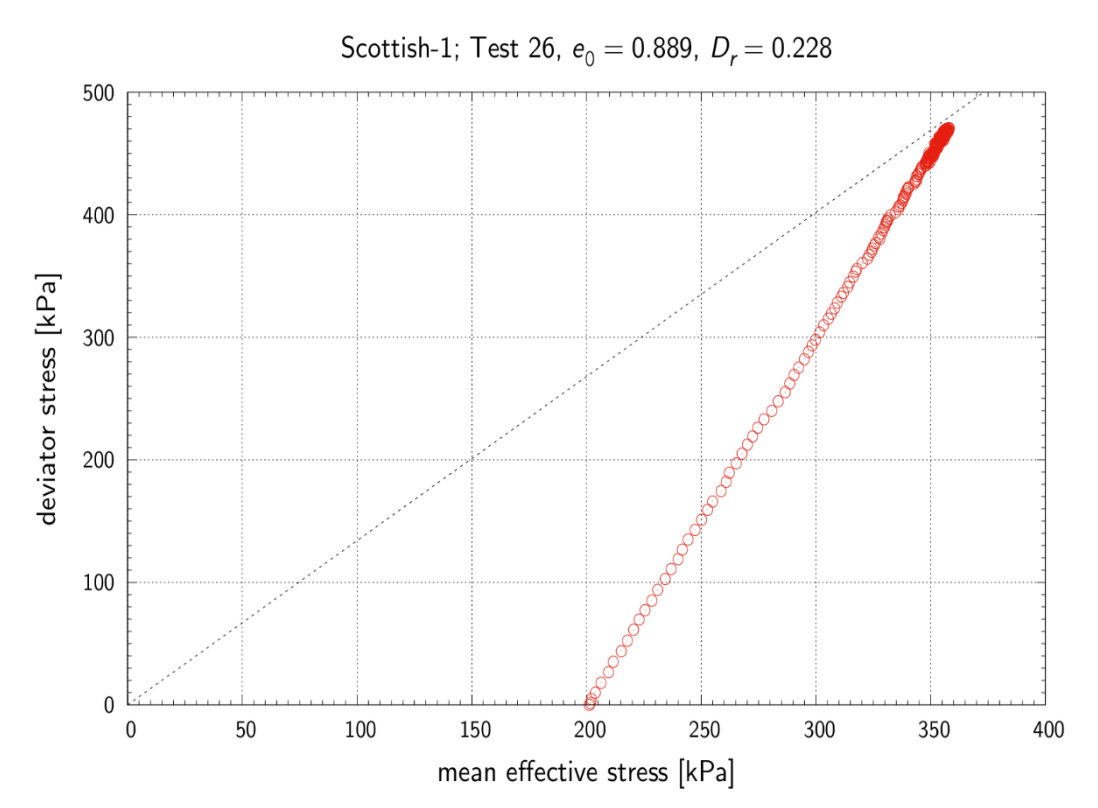


Fig. 6.4.9 Results of monotonic test: stress path – sample no 26.

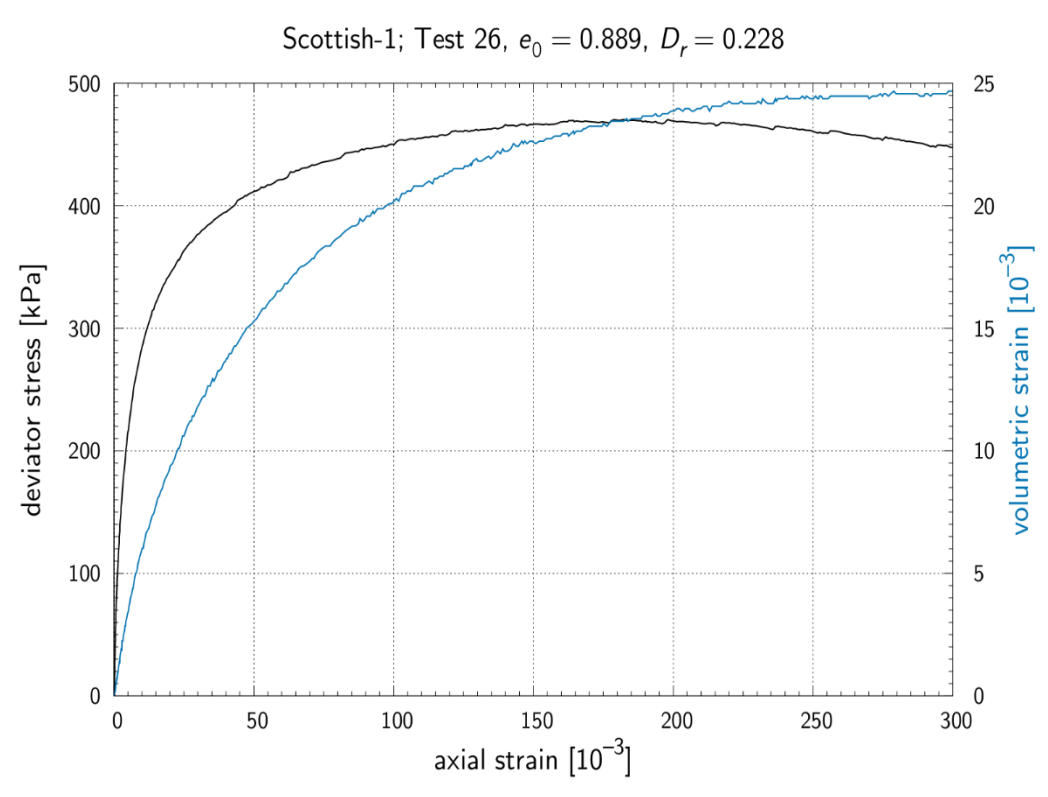


Fig. 6.4.10 Results of monotonic test: response of soil sample: deviator stress vs. vertical strain – sample no 26.





3. Results of cyclic triaxial tests.

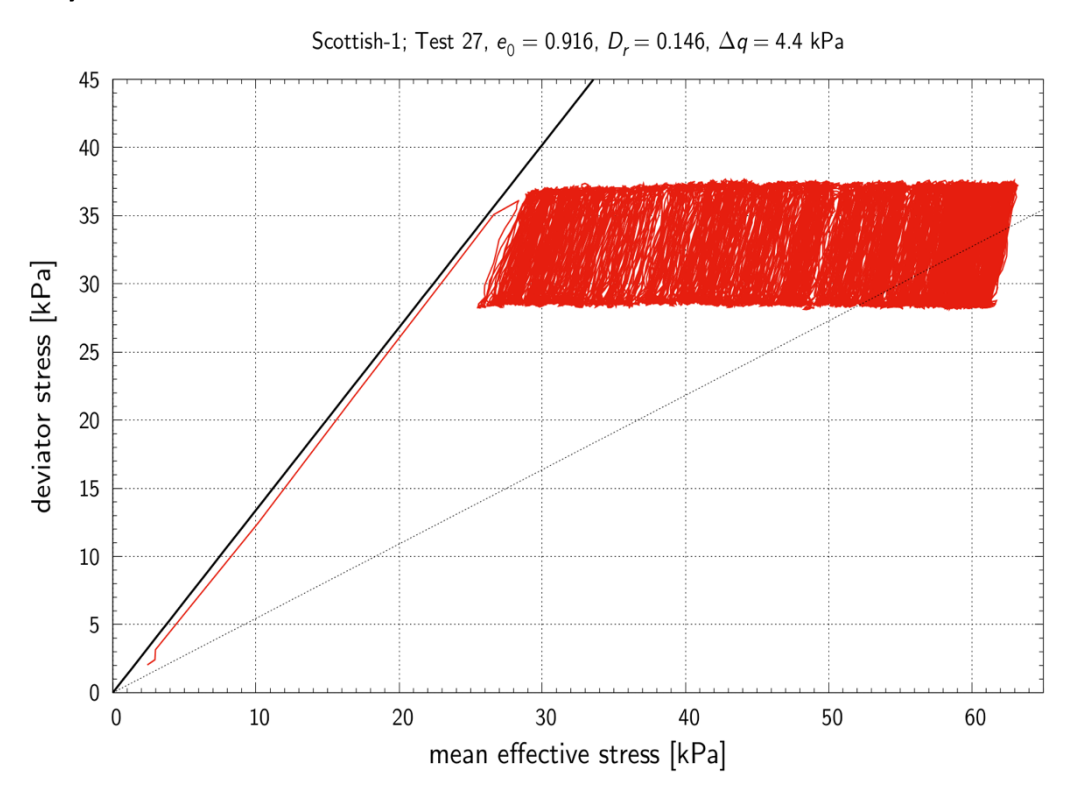


Fig.6.4.11 Results of monotonic test: stress path – sample no 27.

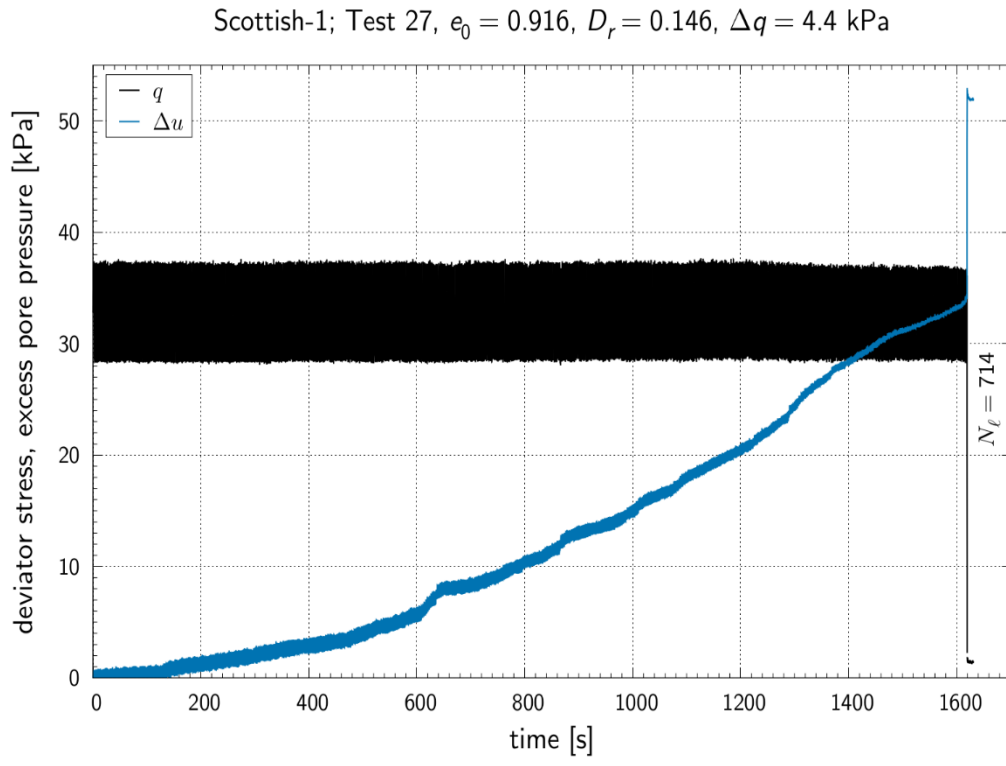


Fig.6.4.12 Results of monotonic test: response of soil sample: deviator stress vs. vertical strain - sample no 27.



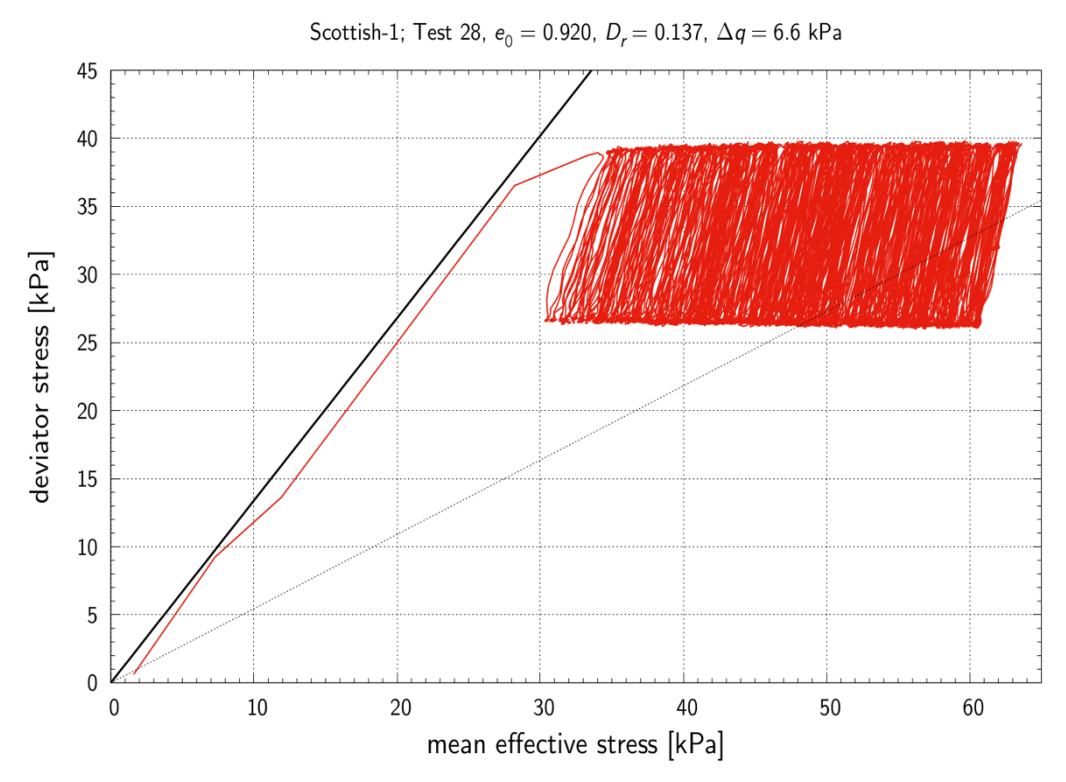


Fig. 6.4.13 Results of cyclic test: stress path - sample no 28.

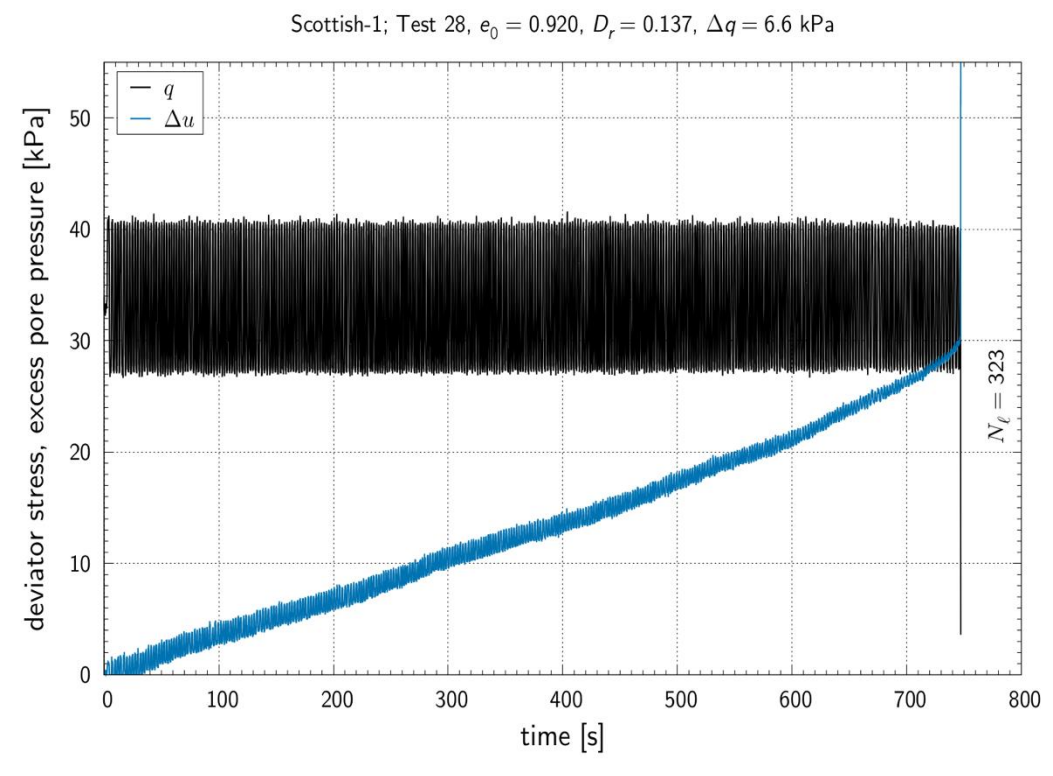


Fig. 6.4.14 Results of cyclic test: generation of pore-water pressure and changes of axial strain versus number of loading cycles – sample no 28.





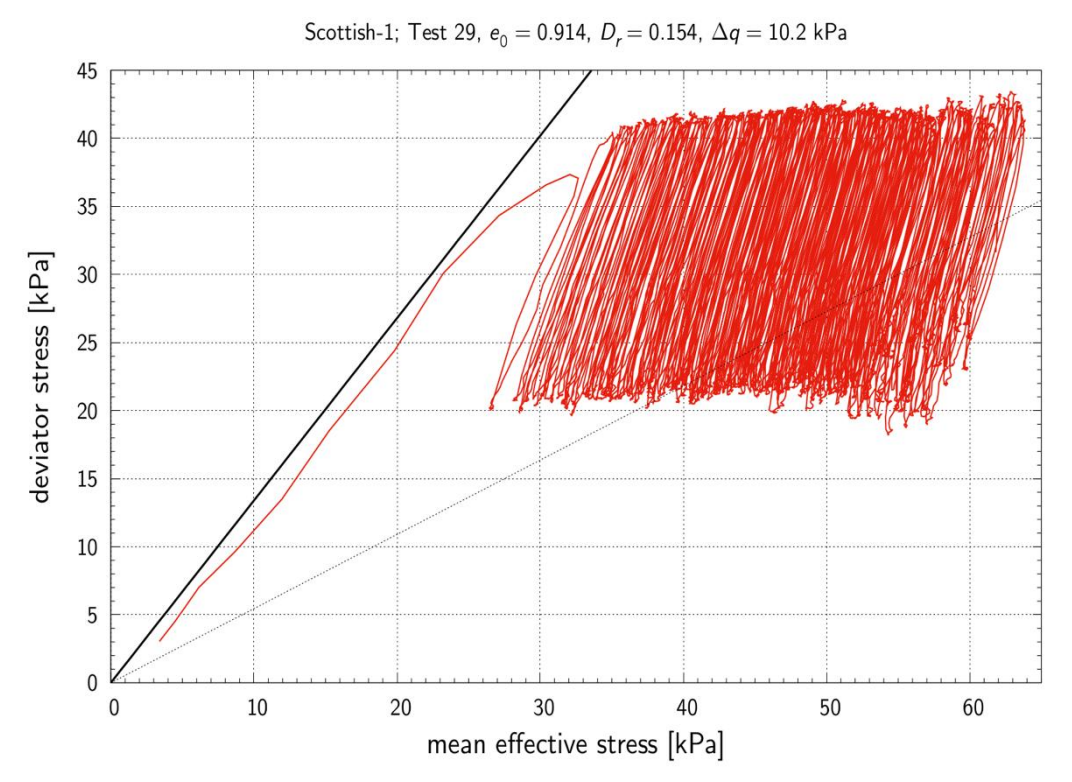


Fig. 6.4.15 Results of cyclic test: stress path - sample no 29.

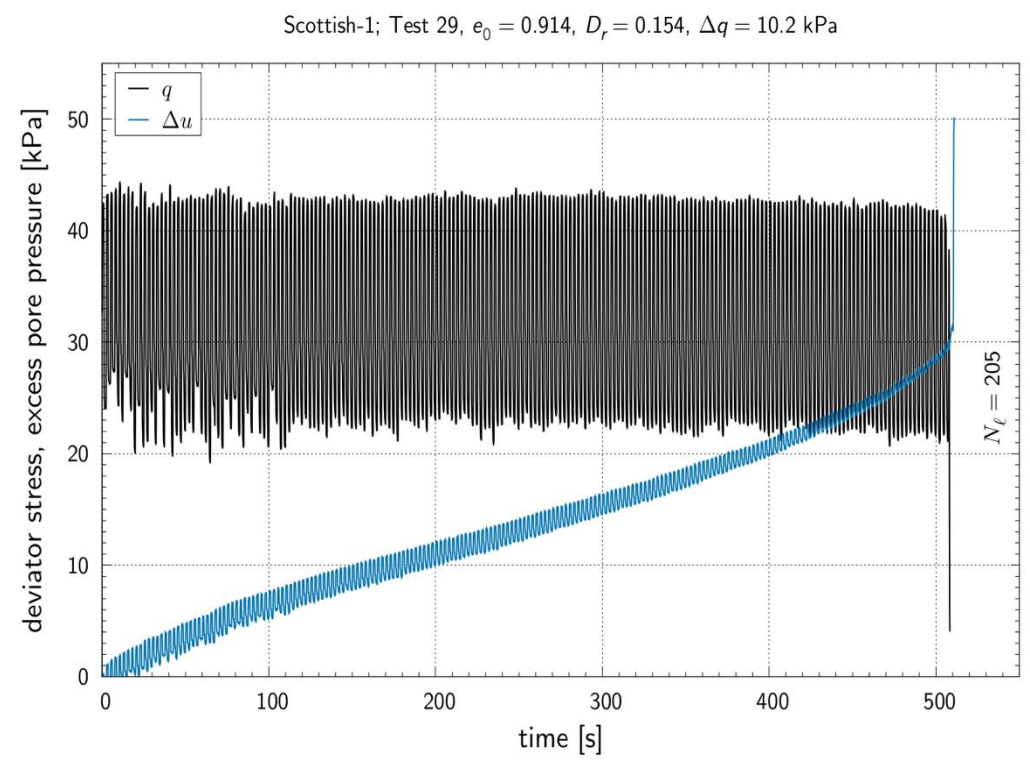


Fig. 6.4.16 Results of cyclic test: generation of pore-water pressure and changes of axial strain versus number of loading cycles – sample no 29.





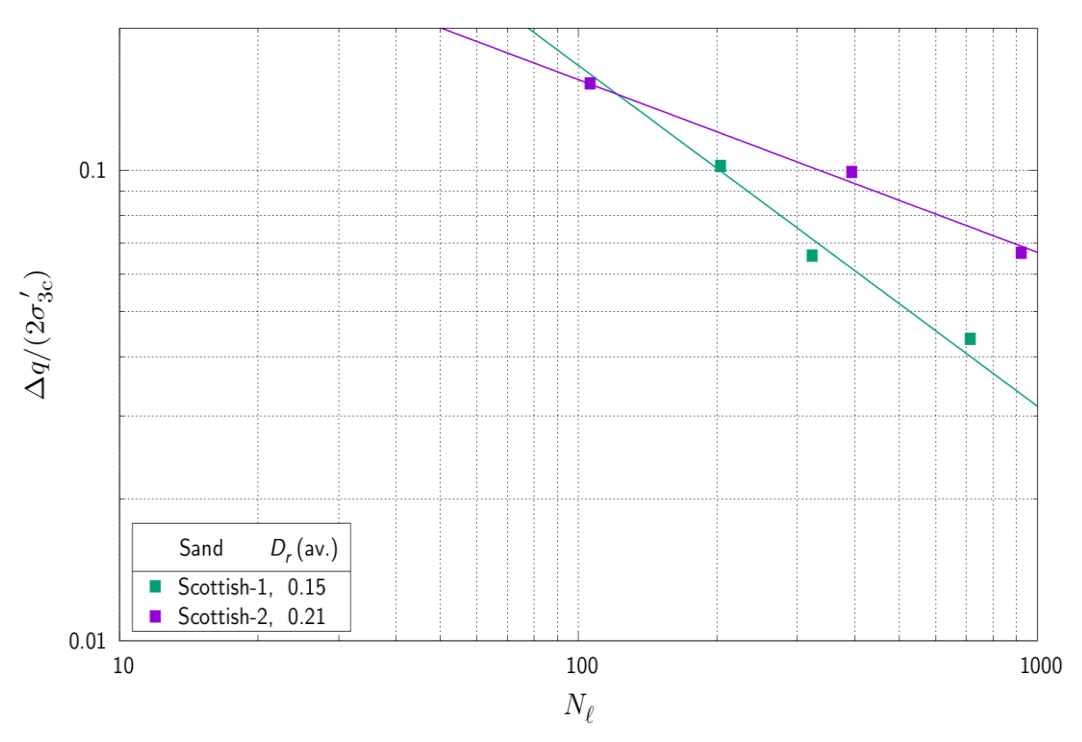


Fig.6.4.17 Normalized amplitude of the shear stress vs. the number of cycles to liquefaction.



6.5 Appendix nr 5 - Results of soil samples collected from Baltic Sea; Soil type: Scottish 2

1. Sampling locations and View of the samples under the microscope.



Fig.6.5.1 Sampling location.

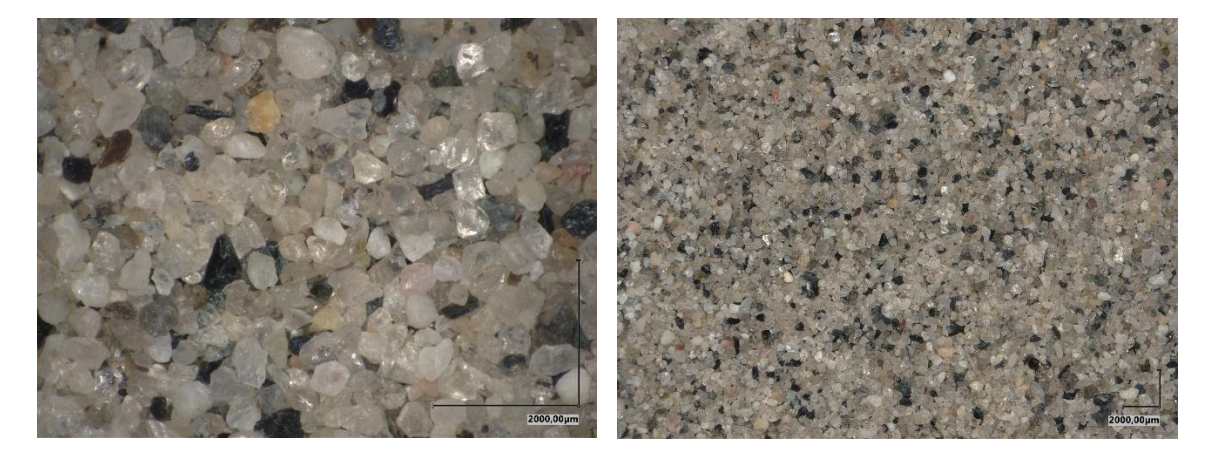


Fig. 6.5.2 View of the samples under the microscope.



2. Results of monotonic triaxial tests.

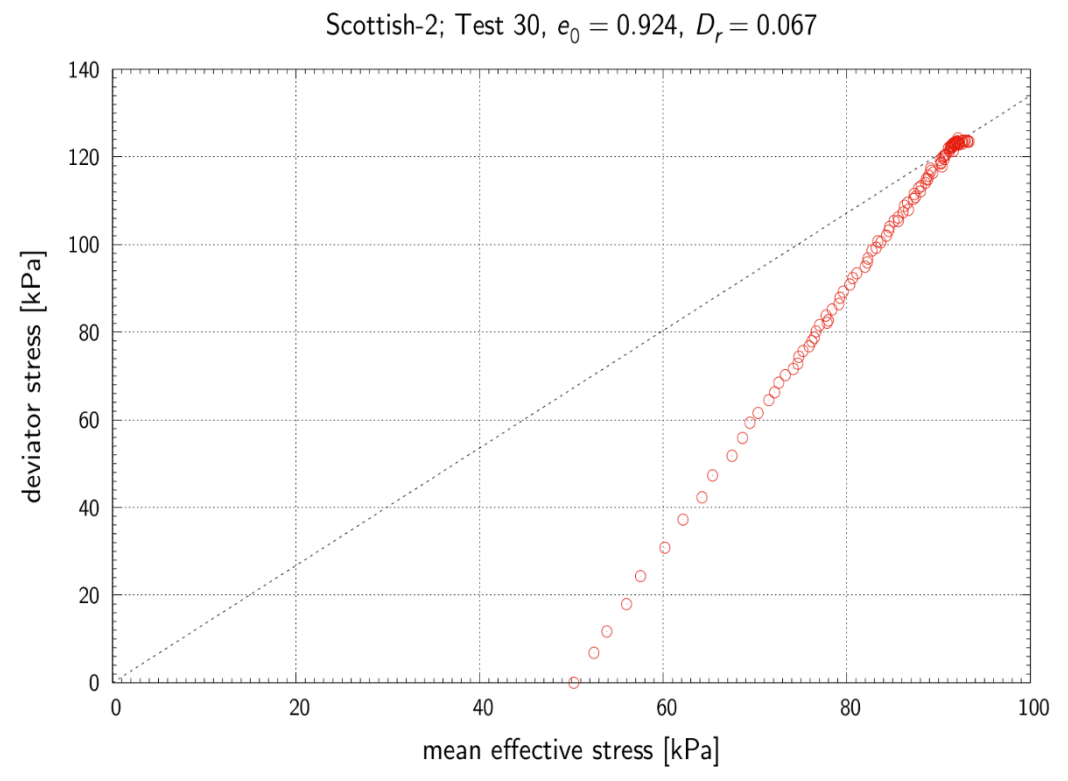


Fig.6.5.3 Results of monotonic test: stress path - sample no 30.

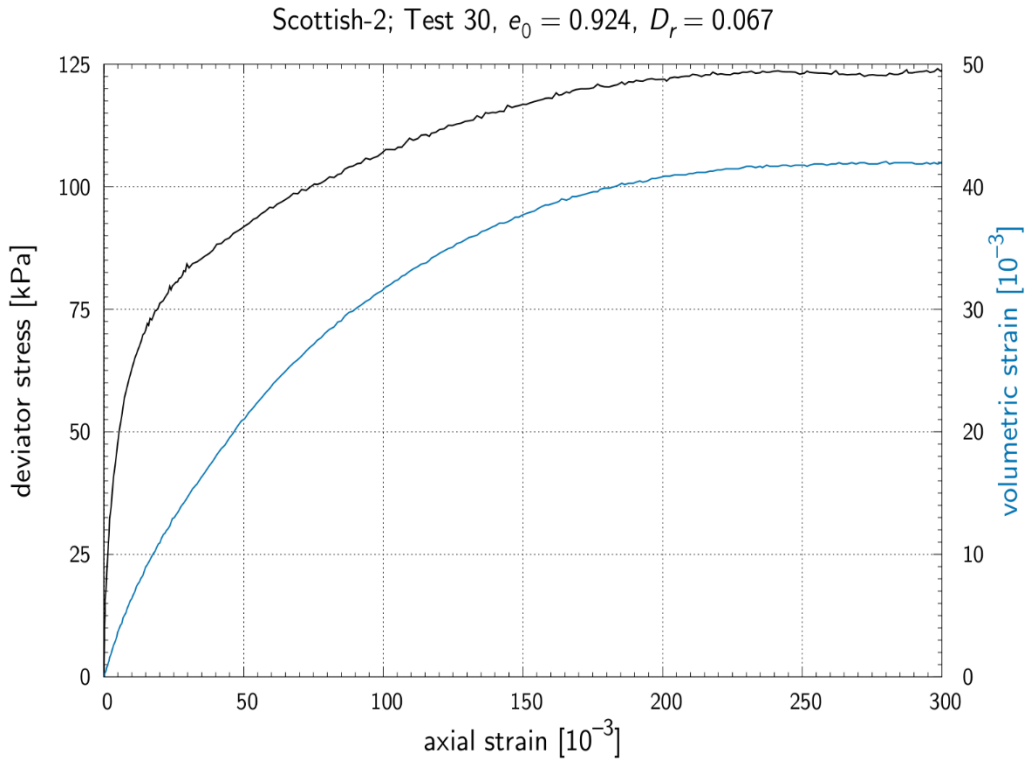


Fig.6.5.4 Results of monotonic test: response of soil sample: deviator stress vs. vertical strain – sample no 30.



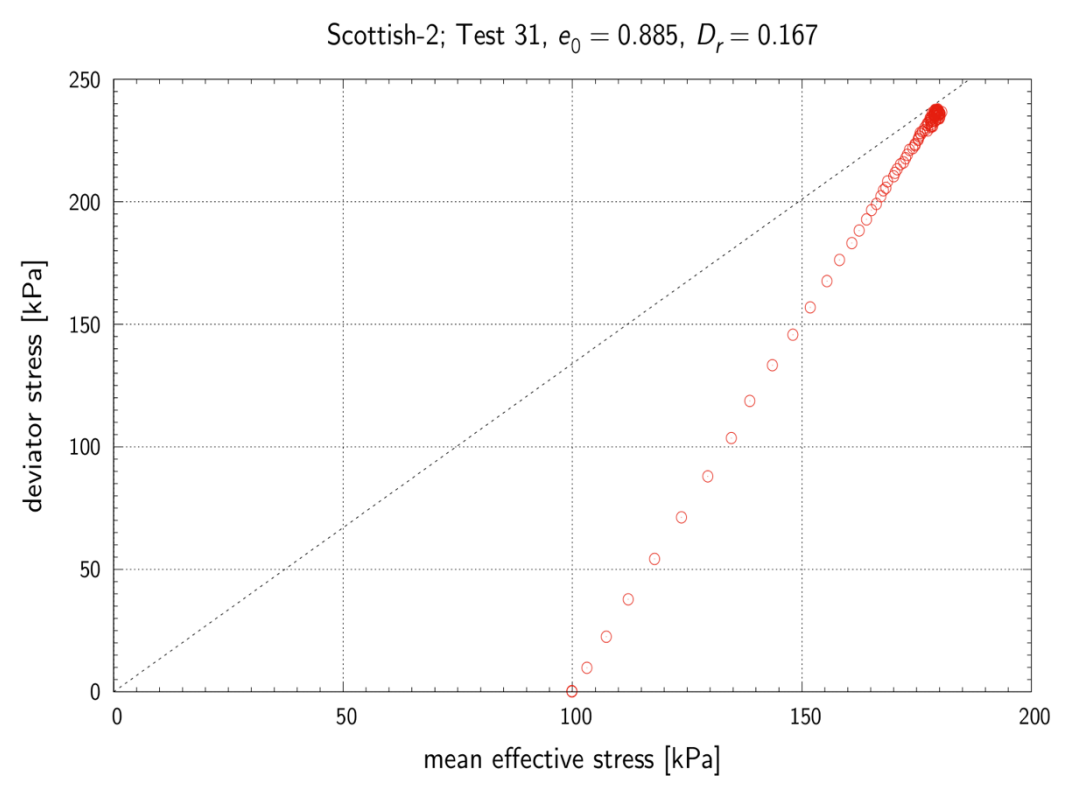


Fig.6.5.5. Results of monotonic test: stress path - sample no 31.

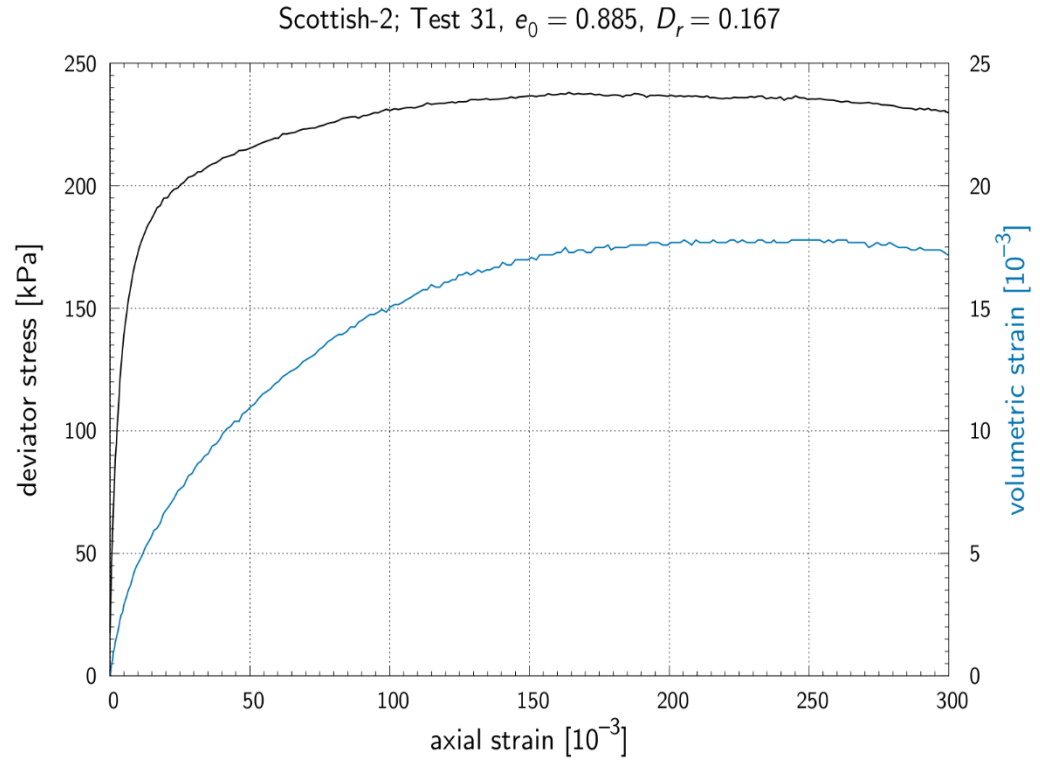


Fig.6.5.6 Results of monotonic test: response of soil sample: deviator stress vs. vertical strain – sample no 31.





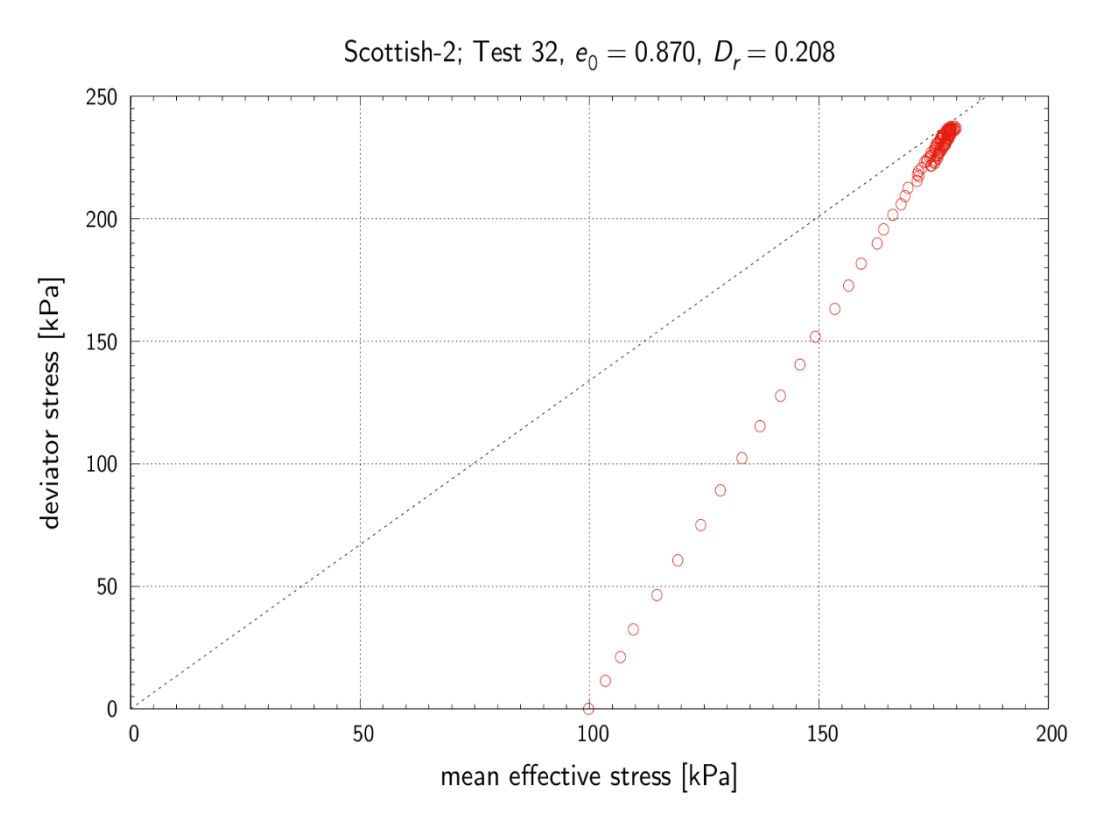


Fig.6.5.7 Results of monotonic test: stress path - sample no 32.

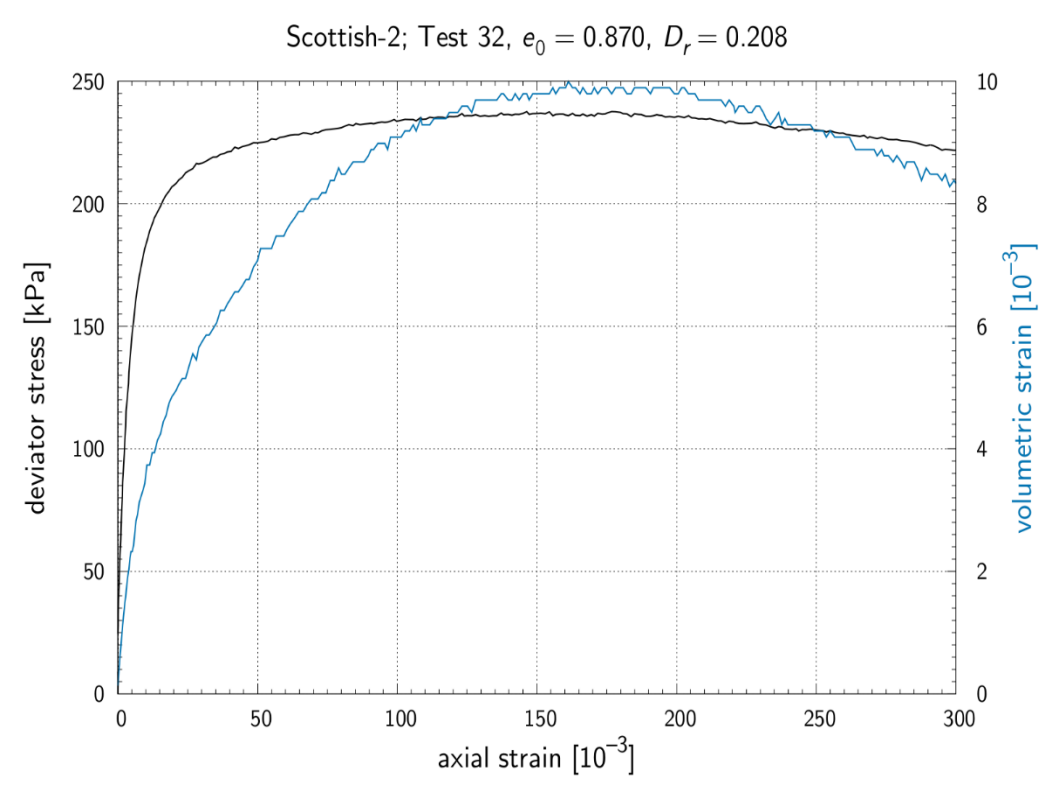


Fig.6.5.8 Results of monotonic test: response of soil sample: deviator stress vs. vertical strain – sample no 32.





3. Results of cyclic triaxial tests.

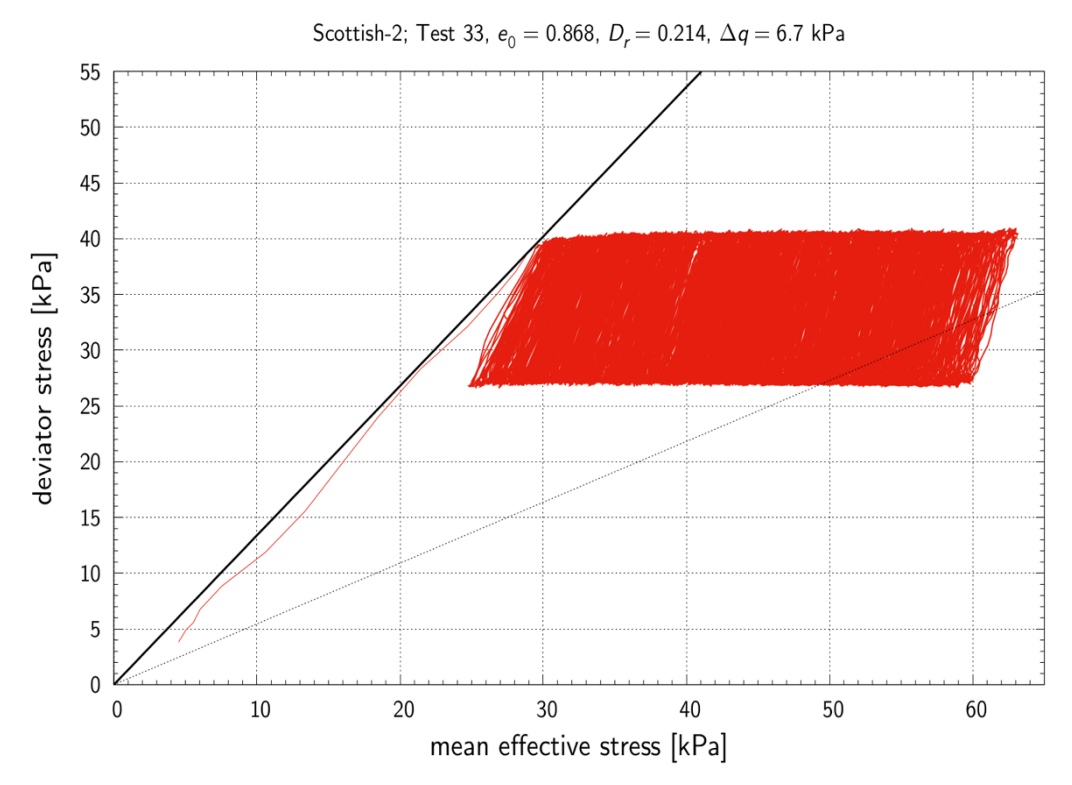


Fig. 6.5.9 Results of cyclic test: stress path - sample no 33.

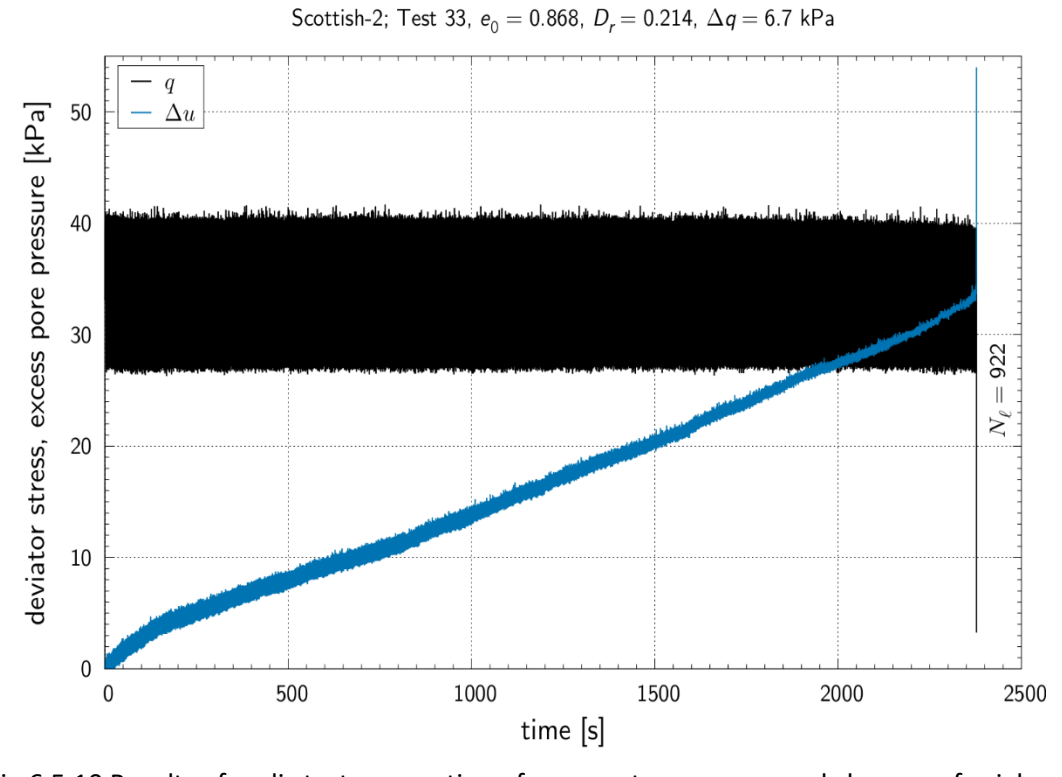


Fig.6.5.10 Results of cyclic test: generation of pore-water pressure and changes of axial strain versus number of loading cycles – sample no 33.





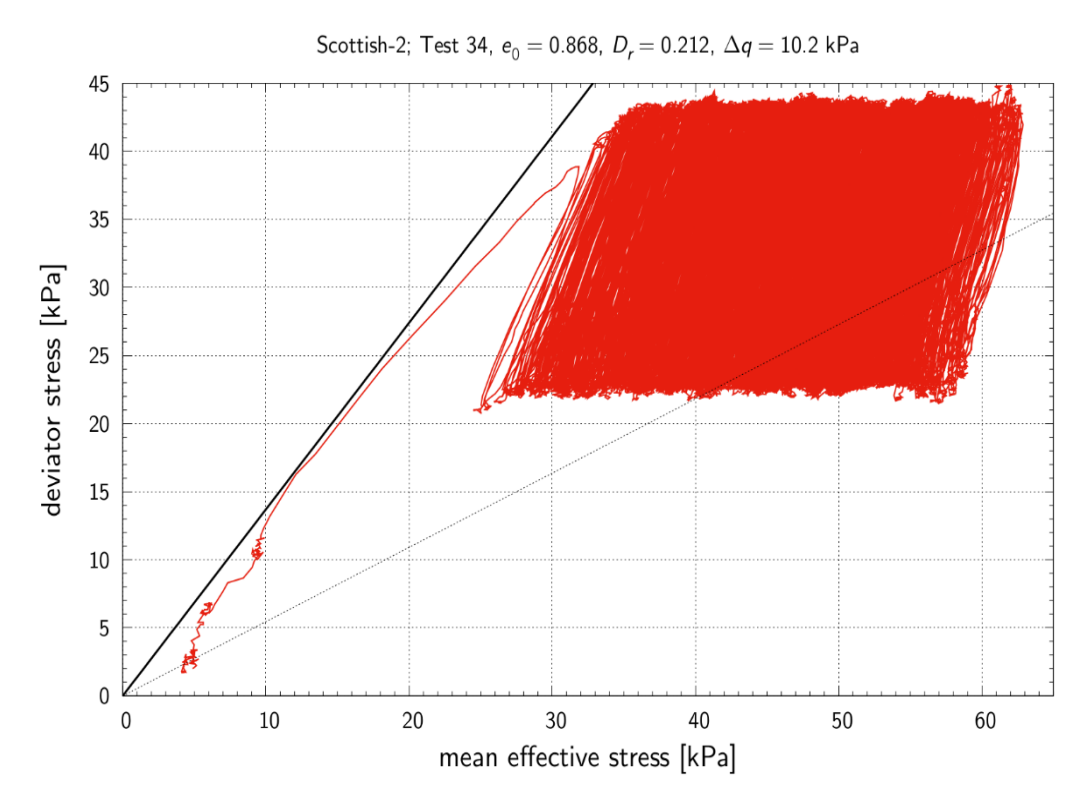


Fig. 6.5.11 Results of cyclic test: stress path - sample no 34.

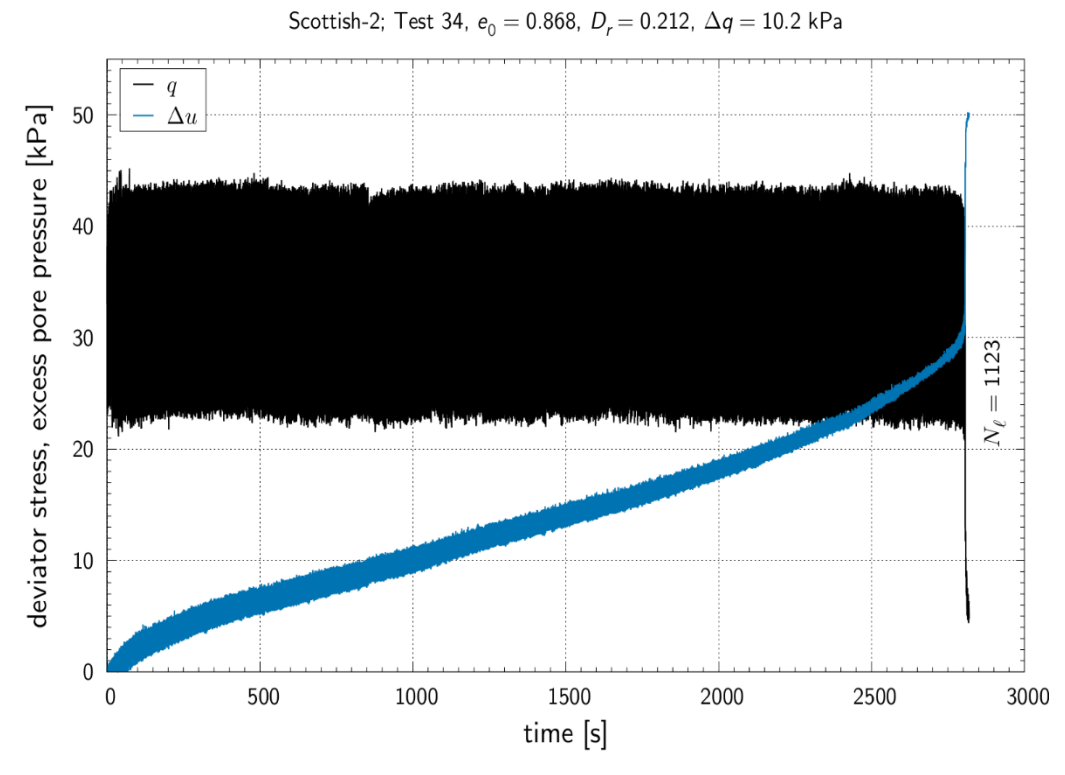


Fig.6.5.12 Results of cyclic test: generation of pore-water pressure and changes of axial strain versus number of loading cycles – sample no 34.





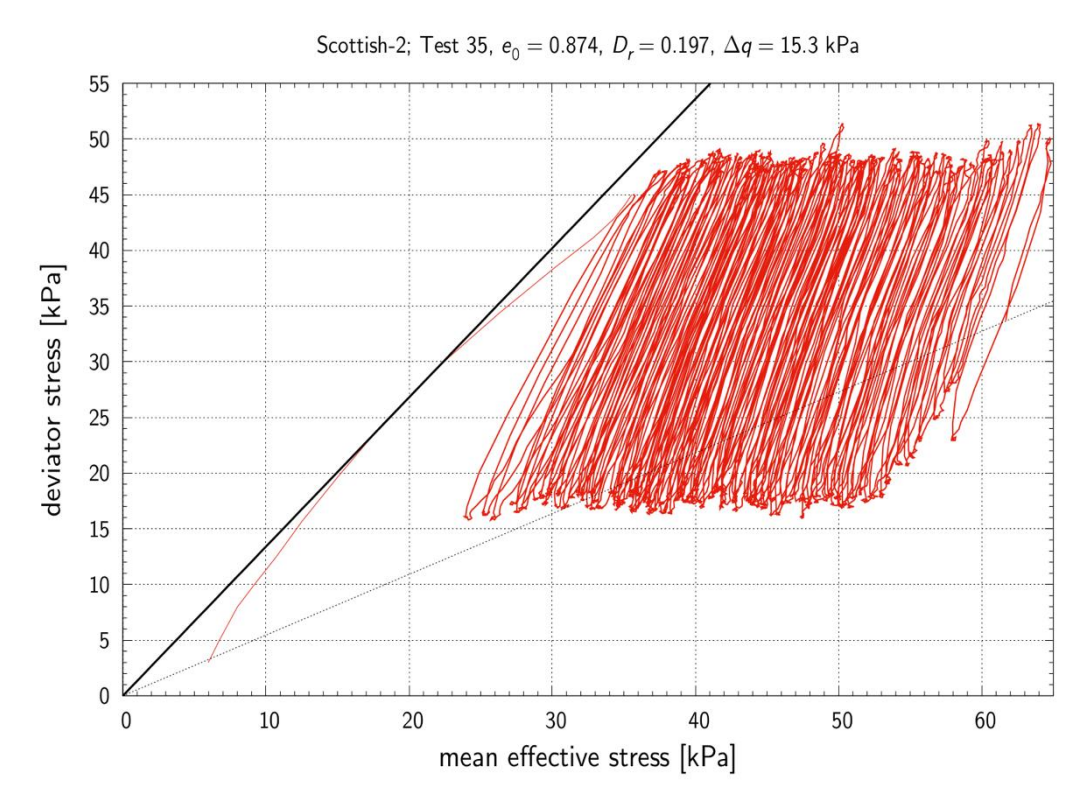


Fig. 6.5.13 Results of cyclic test: stress path - sample no 35.

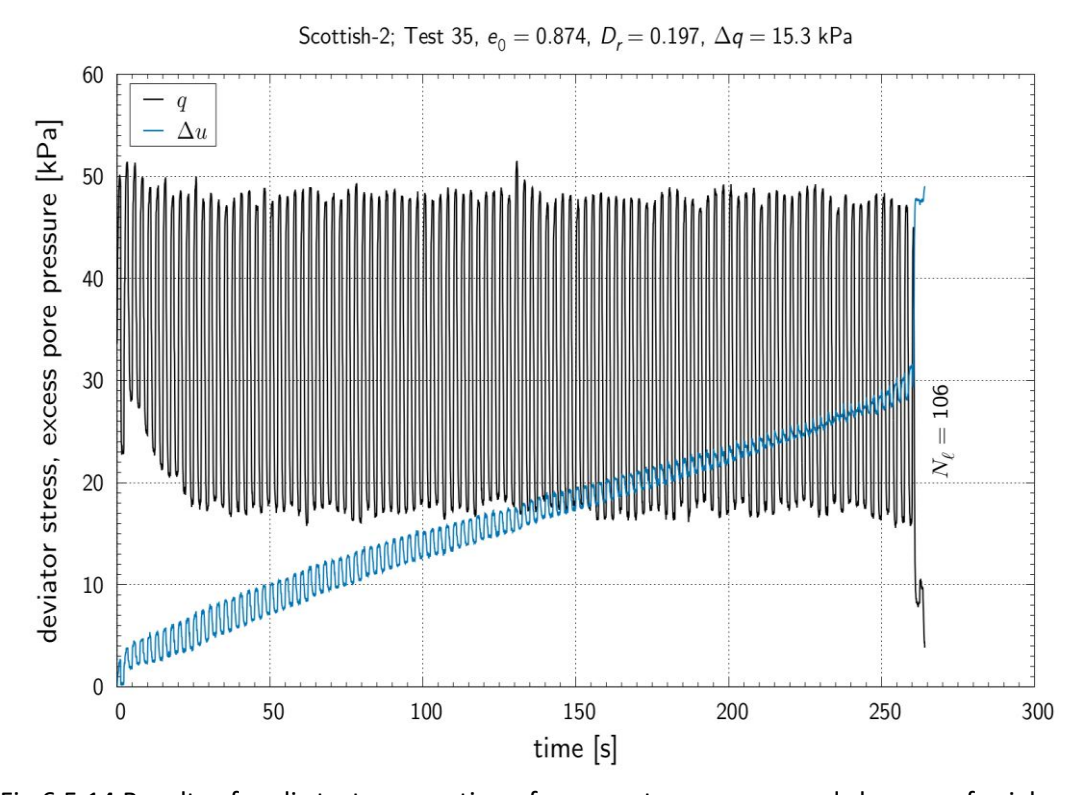


Fig.6.5.14 Results of cyclic test: generation of pore-water pressure and changes of axial strain versus number of loading cycles – sample no 35.





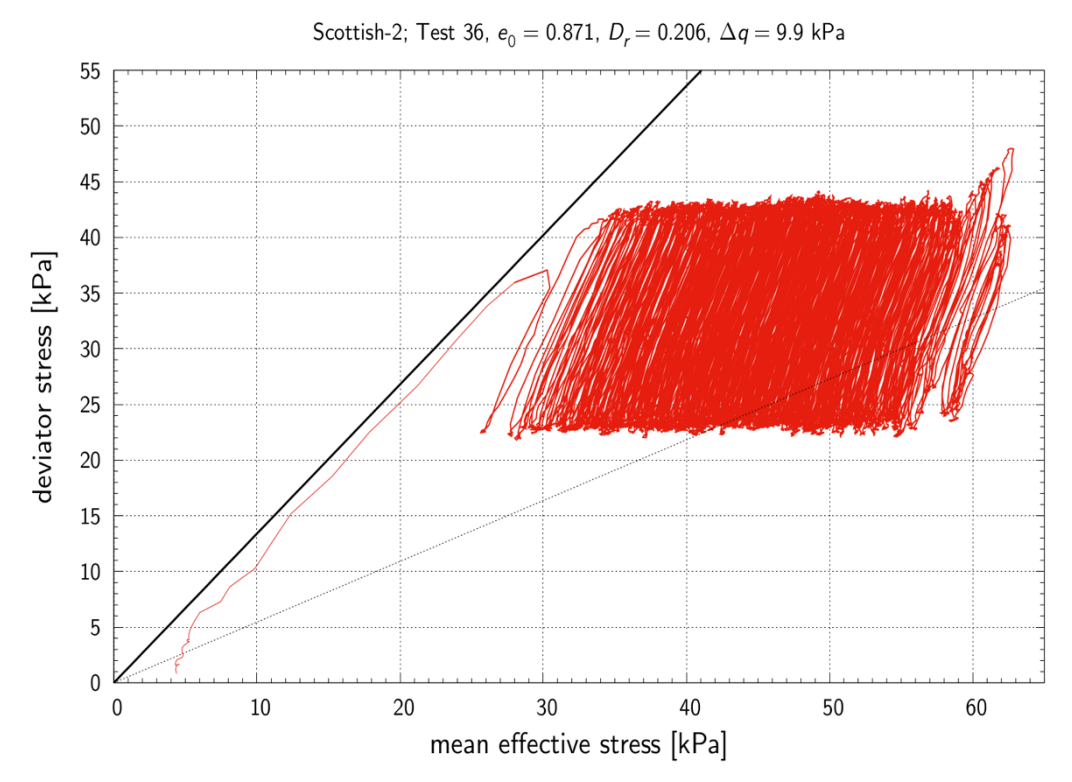


Fig. 6.5.15 Results of cyclic test: stress path - sample no 36.

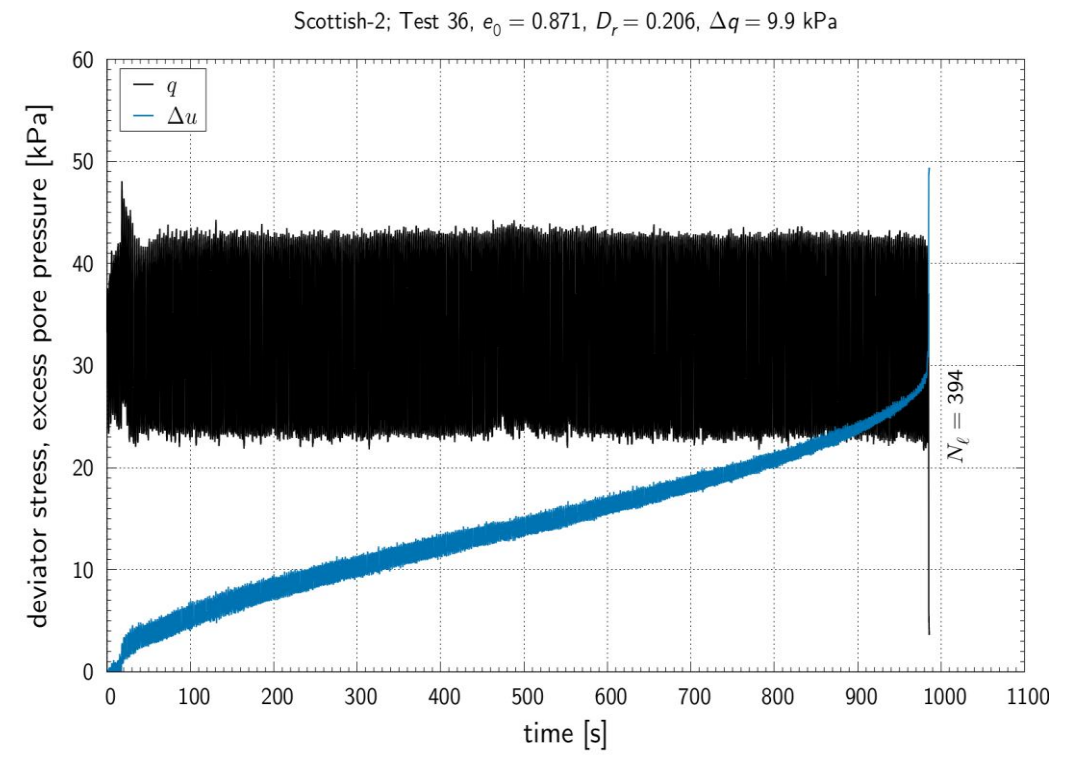


Fig.6.5.16 Results of cyclic test: generation of pore-water pressure and changes of axial strain versus number of loading cycles – sample no 36.





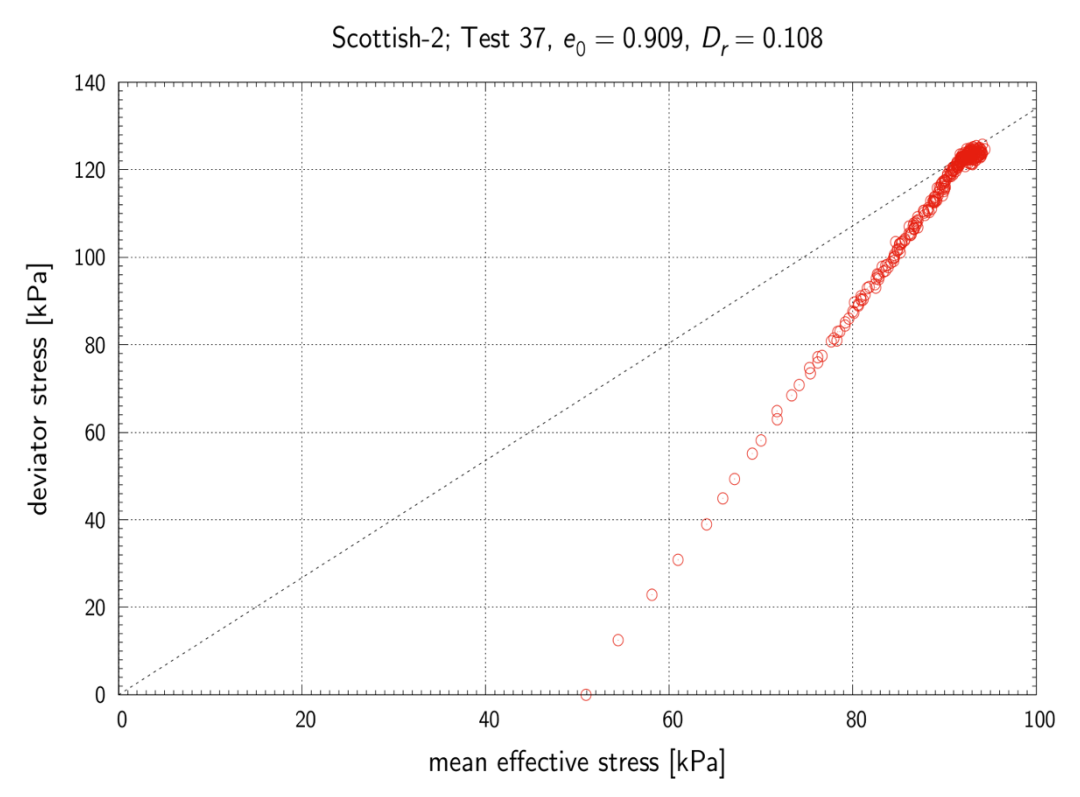


Fig.6.5.17 Results of cyclic test: stress path - sample no 37.

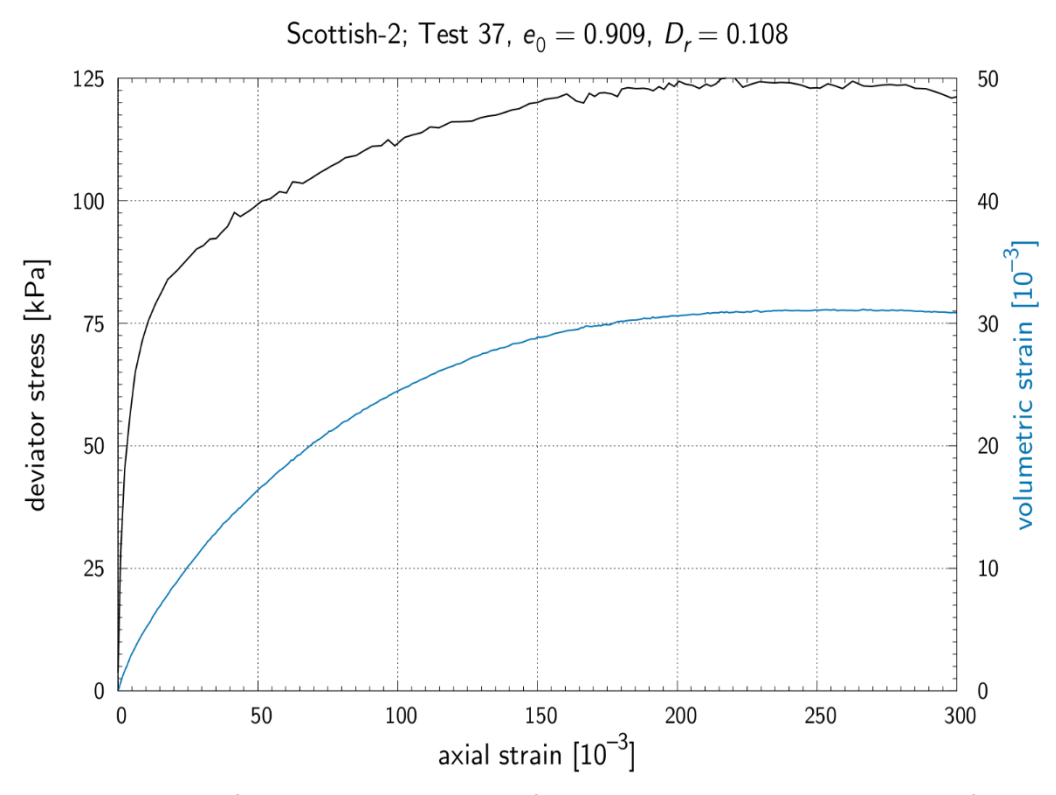


Fig.6.5.18 Results of cyclic test: generation of pore-water pressure and changes of axial strain versus number of loading cycles – sample no 37.





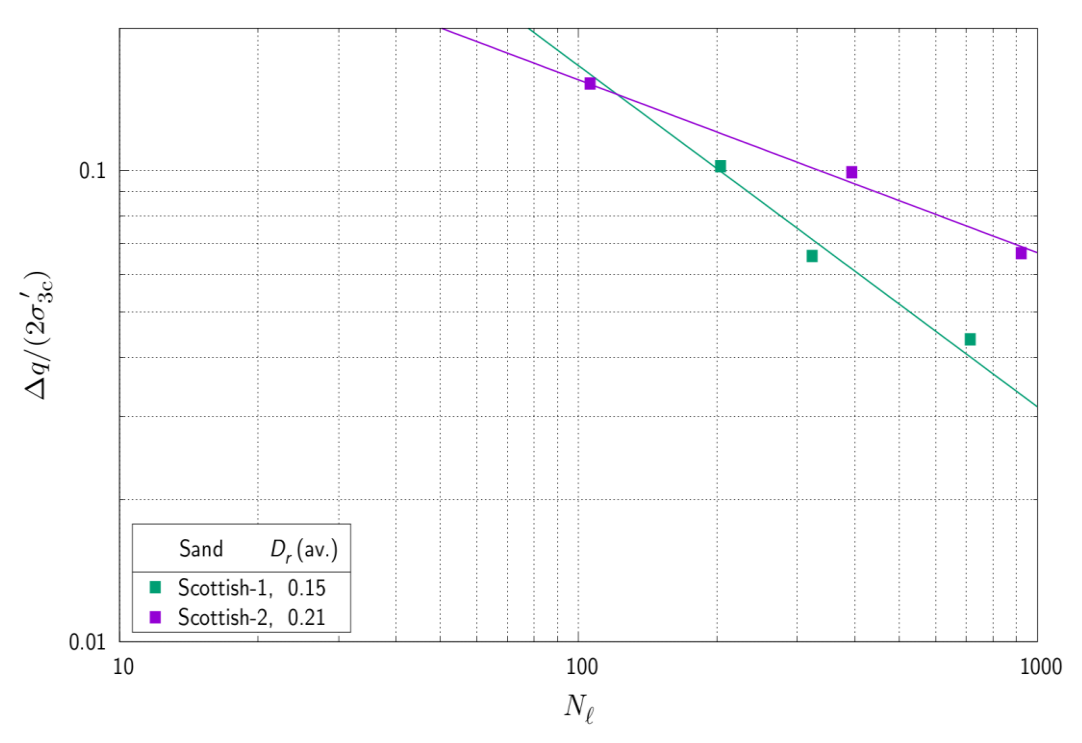


Fig.6.5.19 Normalized amplitude of the shear stress vs. the number of cycles to liquefaction.



6.6 Appendix nr 6 - Results of soil samples collected from Adriatic Sea; Soil type: Adriatic 1

1. Sampling locations and view of the samples under the microscope.



Fig.6.6.1 Sampling location.



Fig. 6.6.2 View of the samples under the microscope.



2. Results of monotonic triaxial tests.

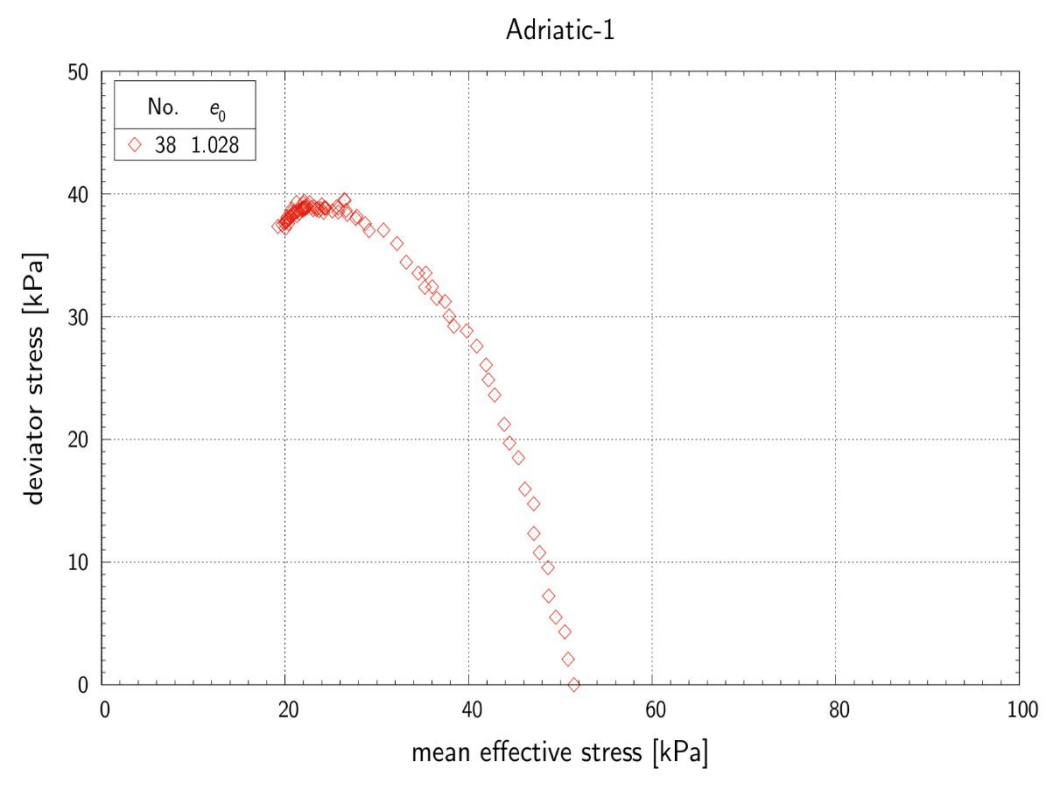


Fig.6.6.3 Results of monotonic test: stress path – sample no 38.

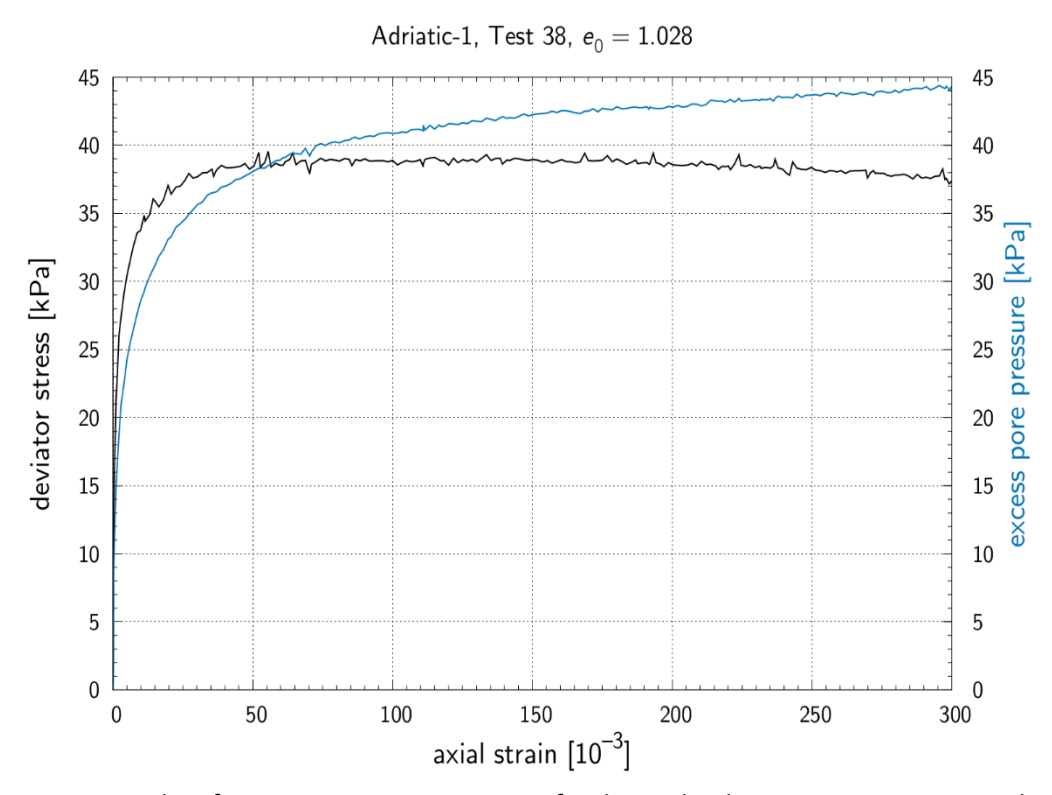


Fig.6.6.4 Results of monotonic test: response of soil sample: deviator stress vs. vertical strain – sample no 38.



6.7 Appendix nr 7 - Results of soil samples collected from Adriatic Sea; Soil type: Adriatic 2

1. Sampling locations and View of the samples under the microscope.



Fig.6.7.1 Sampling location.

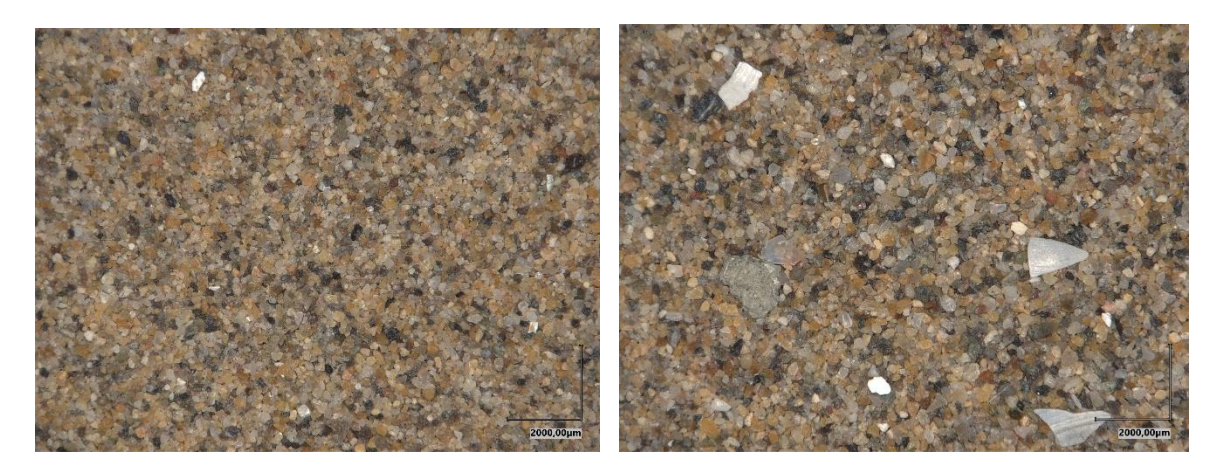


Fig.6.7.2 View of the samples under the microscope.





2. Results of monotonic triaxial tests.

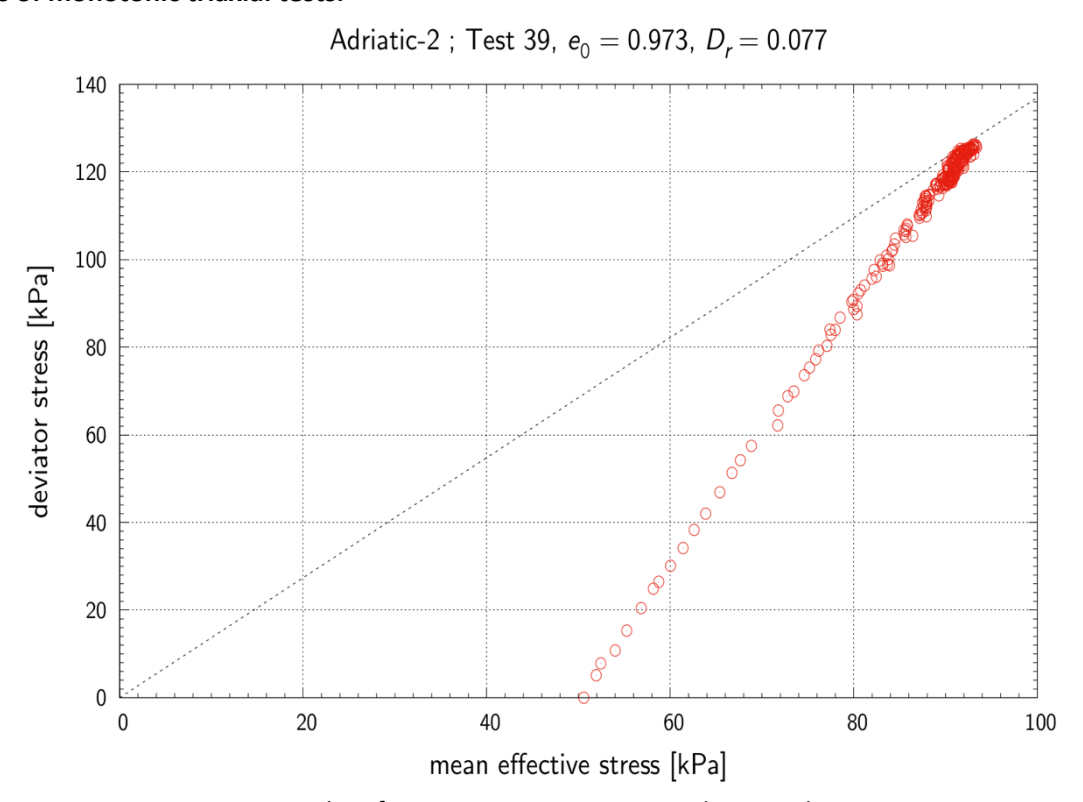


Fig.6.7.3 Results of monotonic test: stress path - sample no 39.

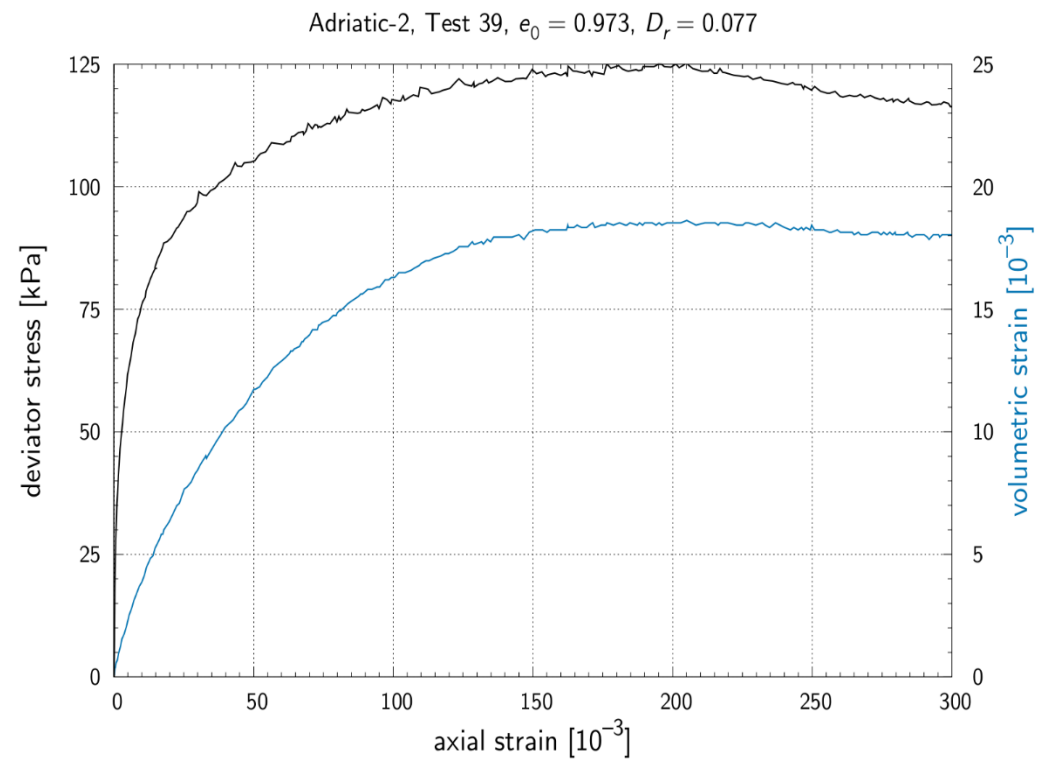


Fig.6.7.4 Results of monotonic test: response of soil sample: deviator stress vs. vertical strain – sample no 39.





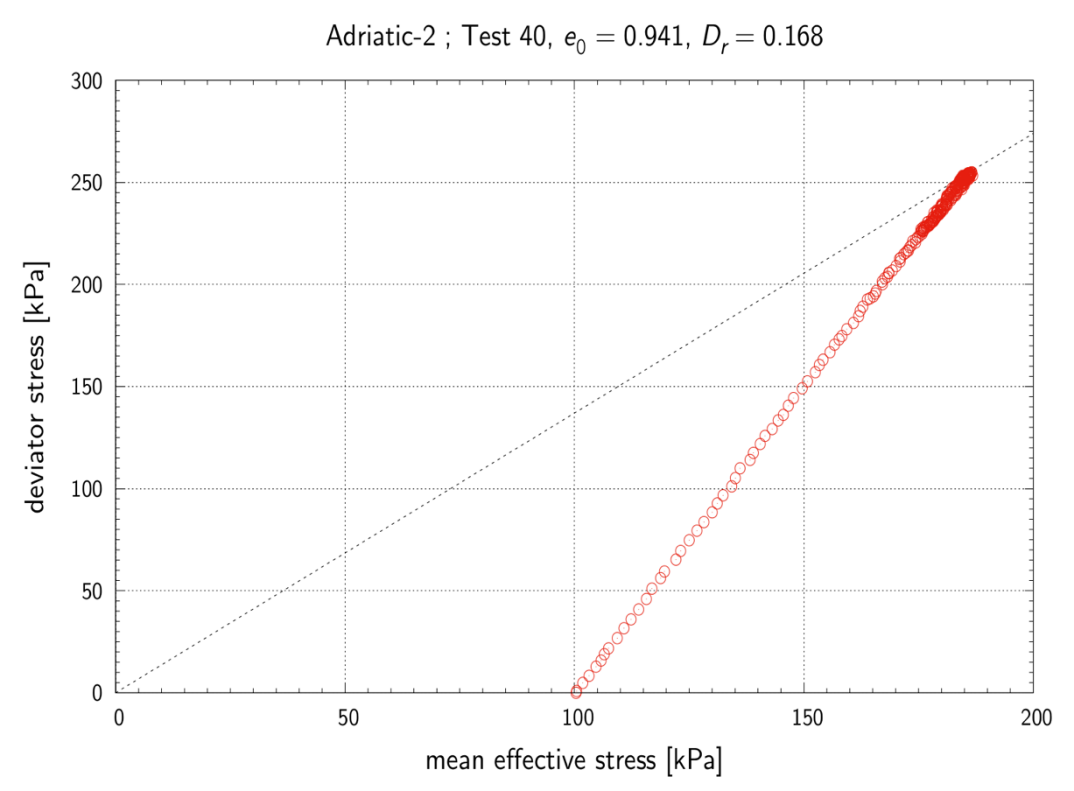


Fig.6.7.5 Results of monotonic test: stress path - sample no 40.

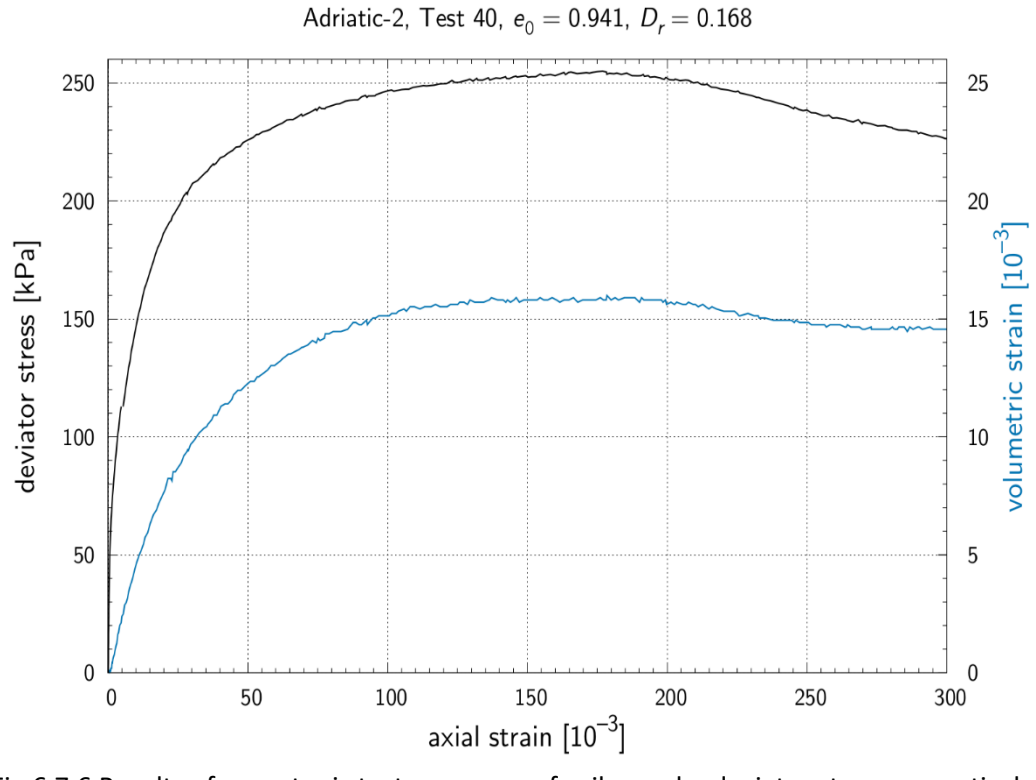


Fig.6.7.6 Results of monotonic test: response of soil sample: deviator stress vs. vertical strain – sample no 40.





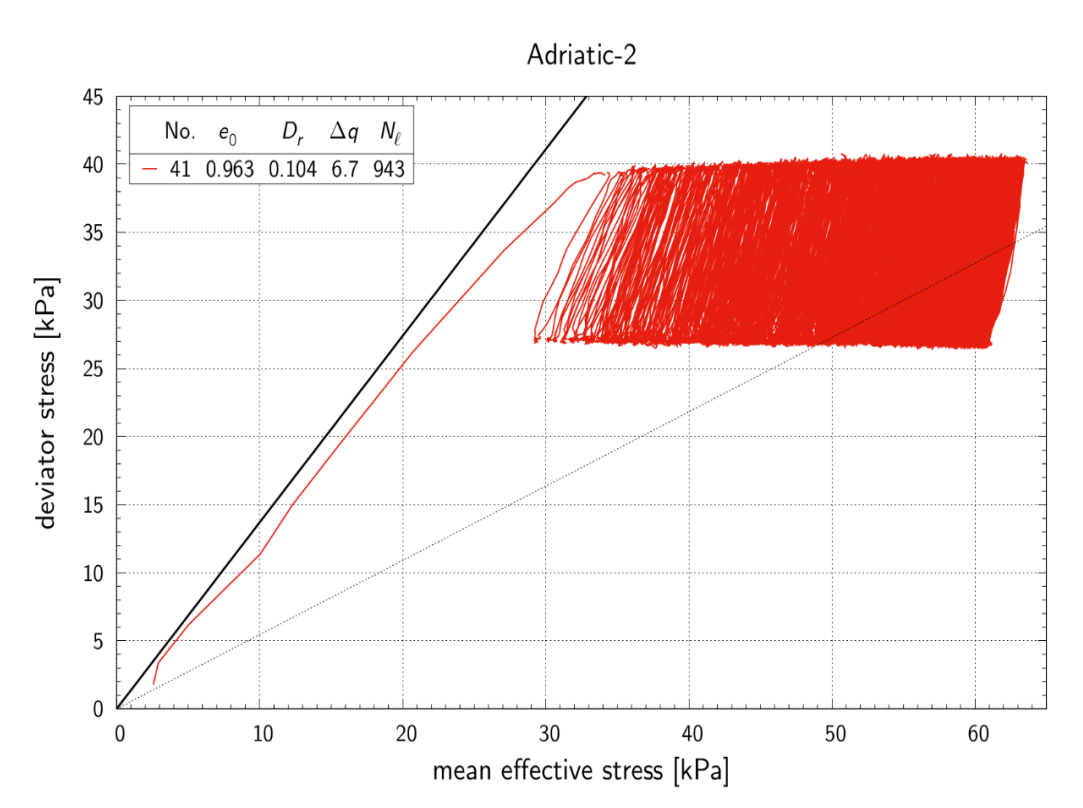


Fig.6.7.7 Results of cyclic test: stress path - sample no 41.

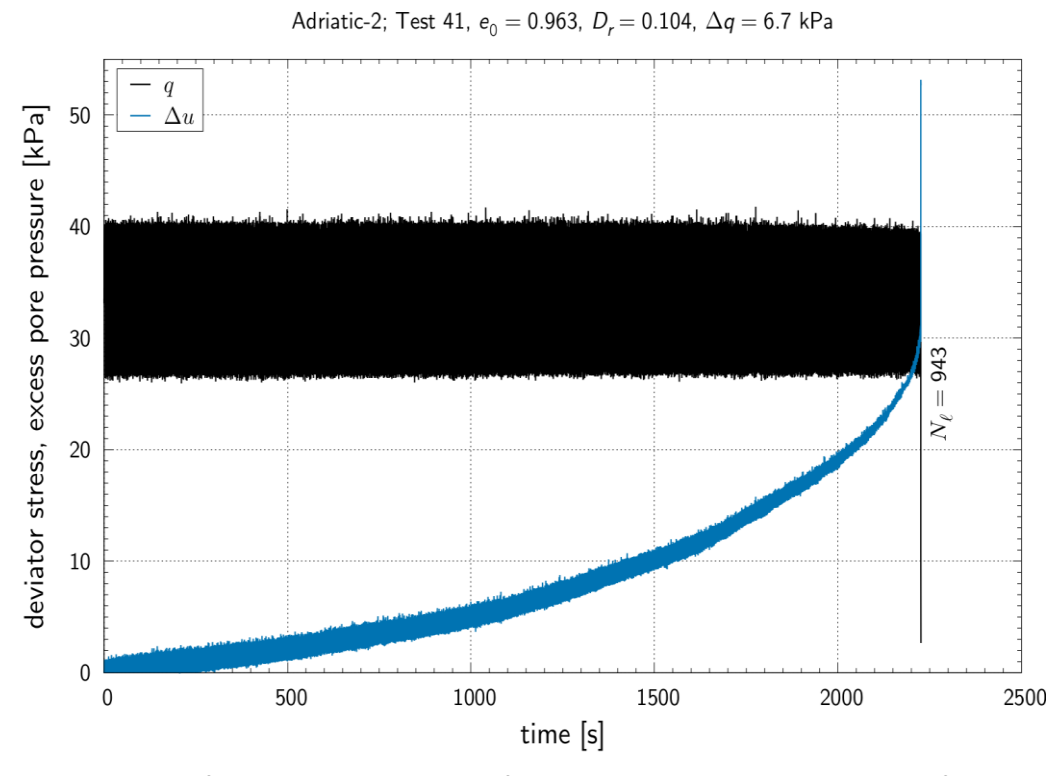


Fig.6.7.8 Results of cyclic test: generation of pore-water pressure and changes of axial strain versus number of loading cycles – sample no 41.





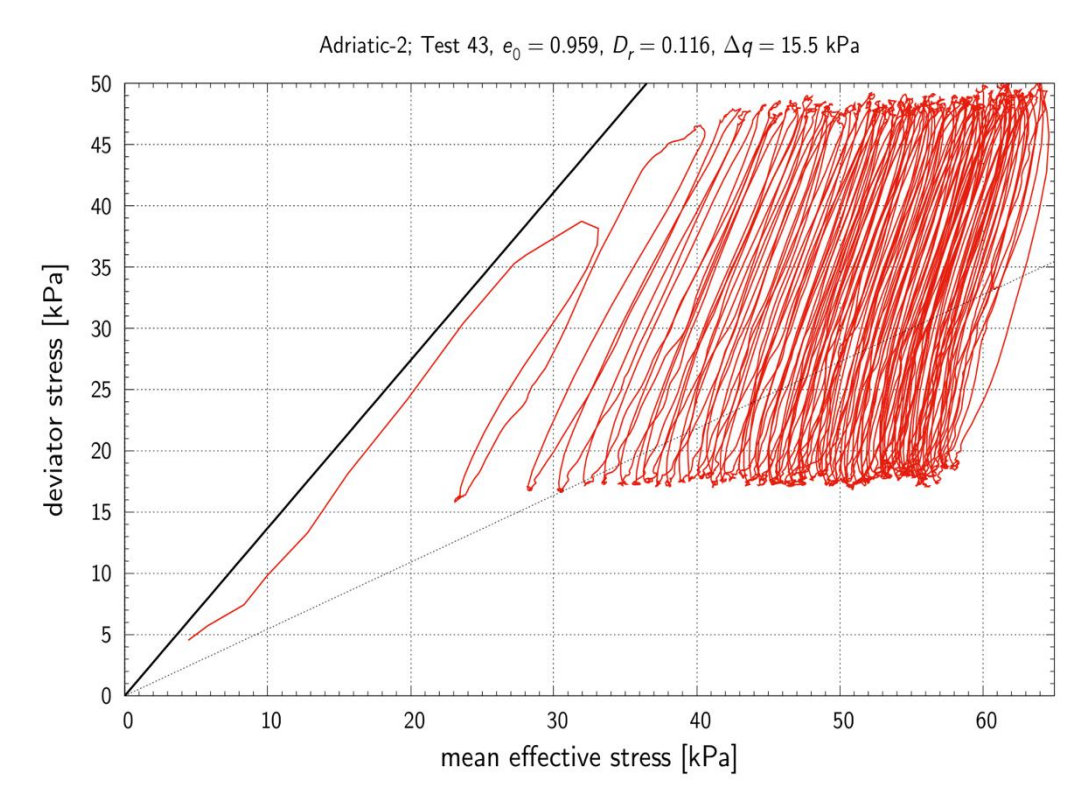


Fig.6.7.9 Results of cyclic test: stress path - sample no 43.

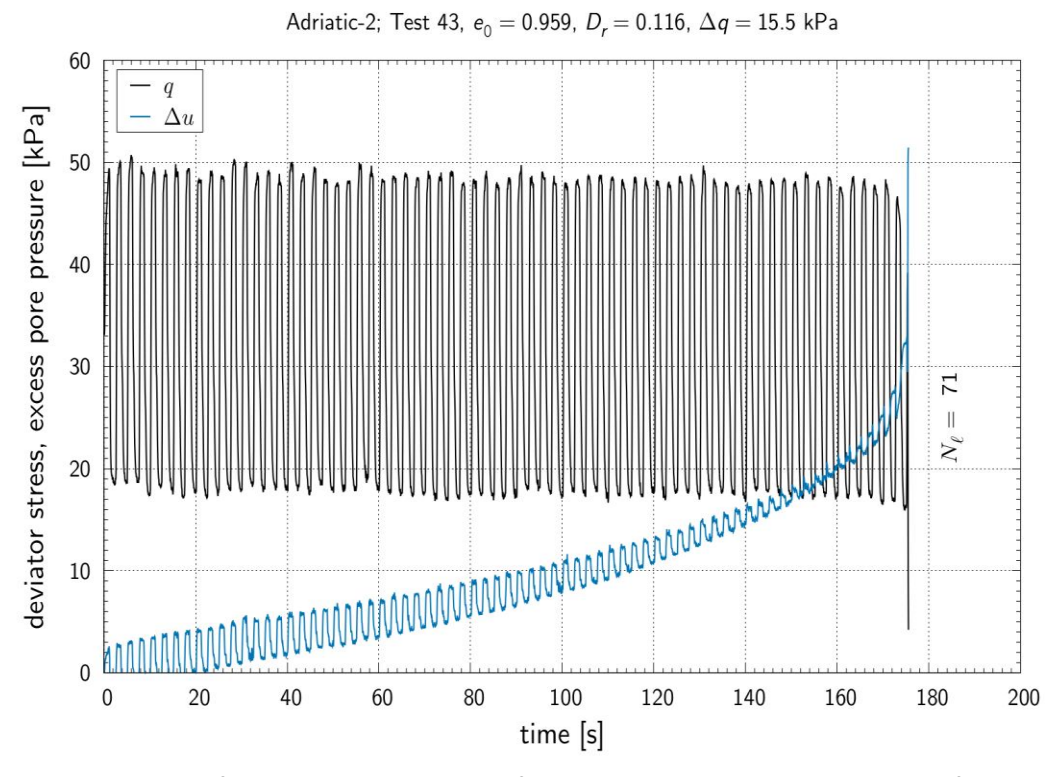


Fig.6.7.10 Results of cyclic test: generation of pore-water pressure and changes of axial strain versus number of loading cycles – sample no 43.





6.8 Appendix nr 8 - Triaxial tests: Elastic modulus

1. Young Modulus

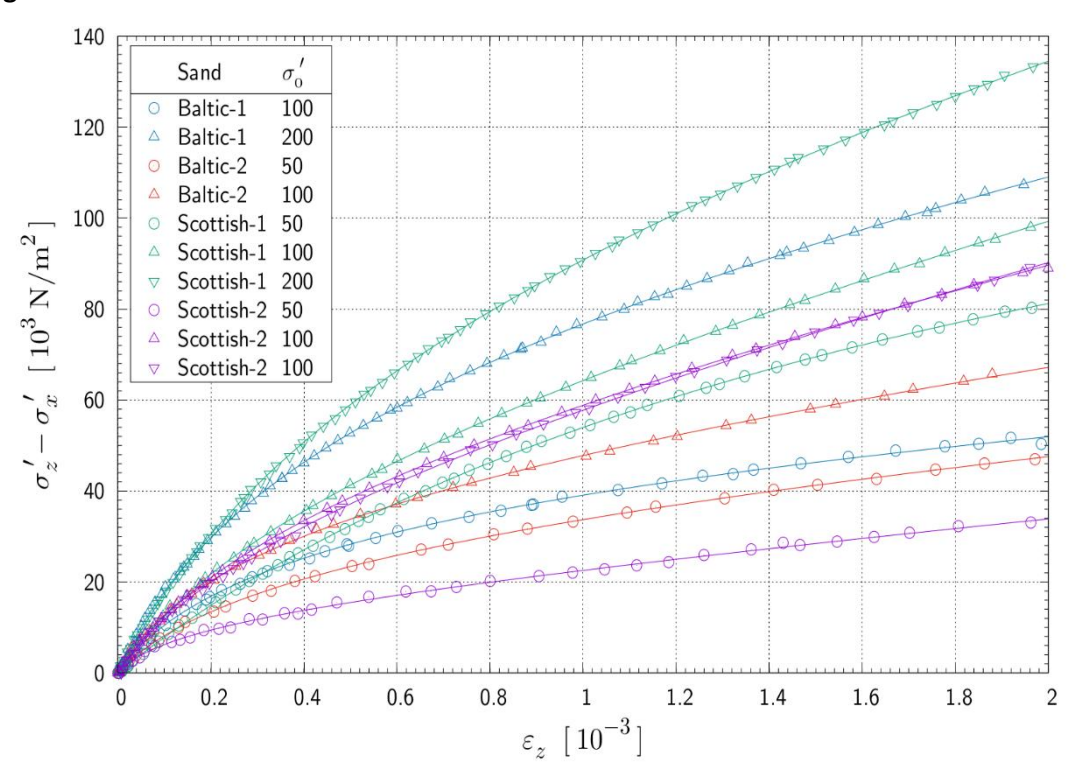


Fig. 6.8.1 The initial changes of the stress deviator q as a function of the axial strain.

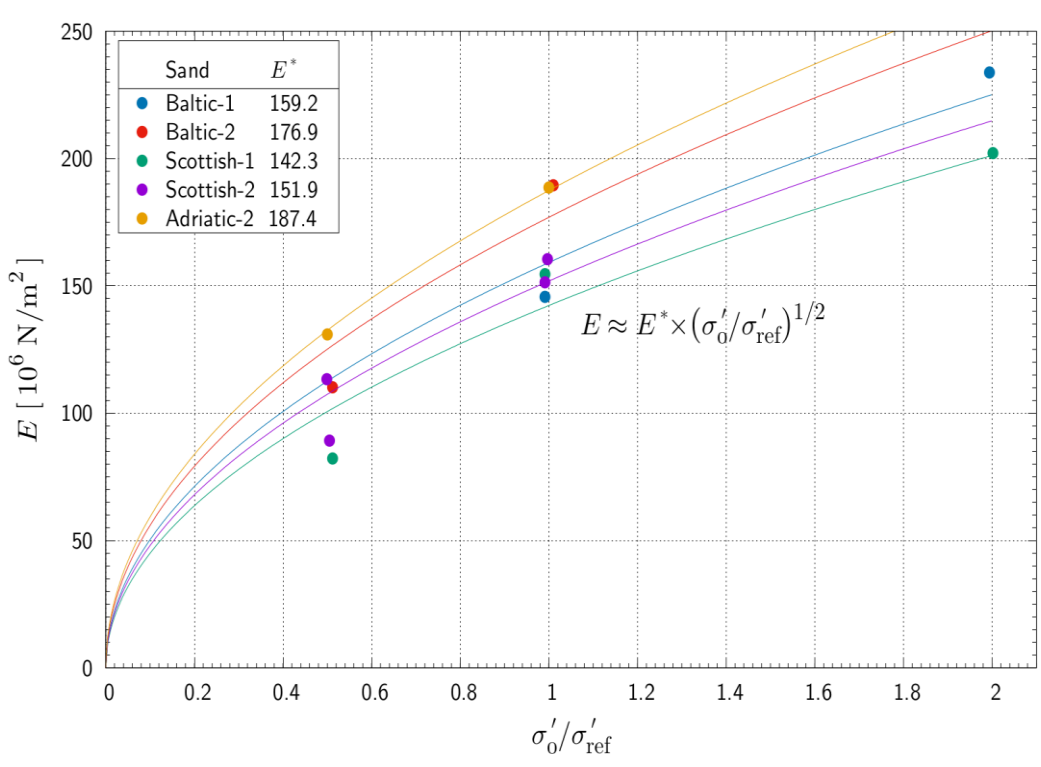


Fig. 6.8.2 Calculated values of modulus $\it E$ as functions of the initial effective stress.





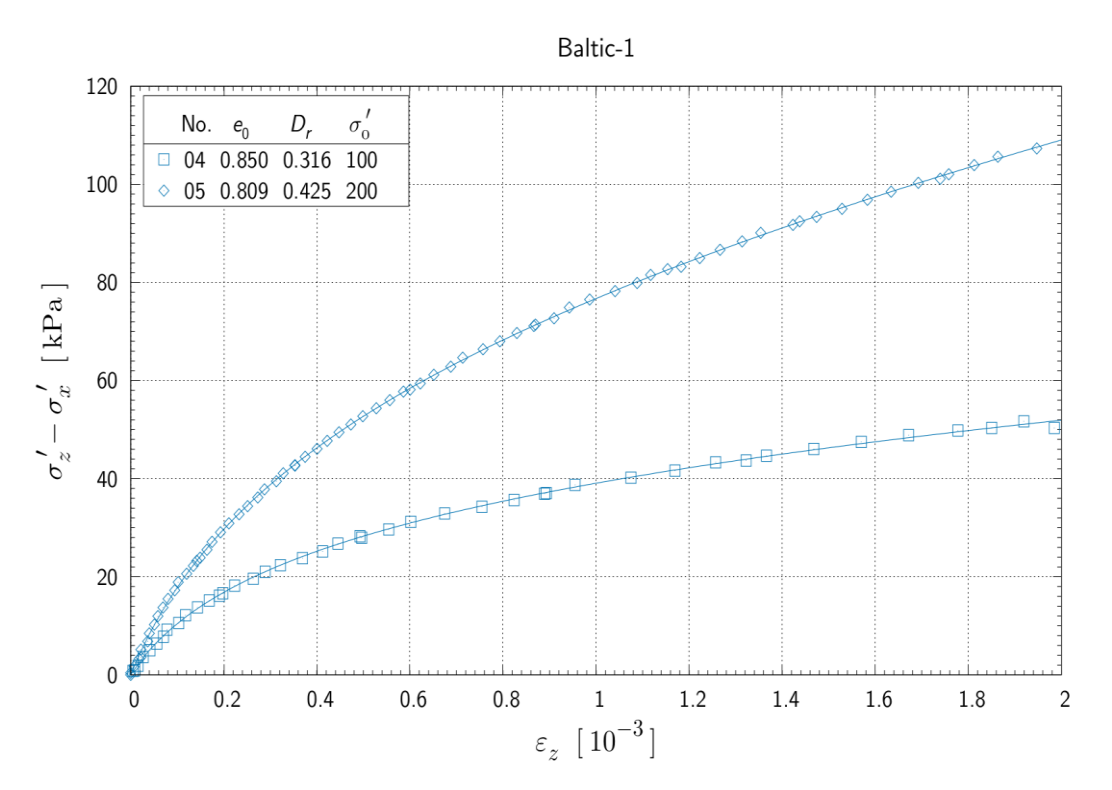


Fig.6.8.3 The initial changes of the stress deviator q as a function of the axial strain – Baltic 1.

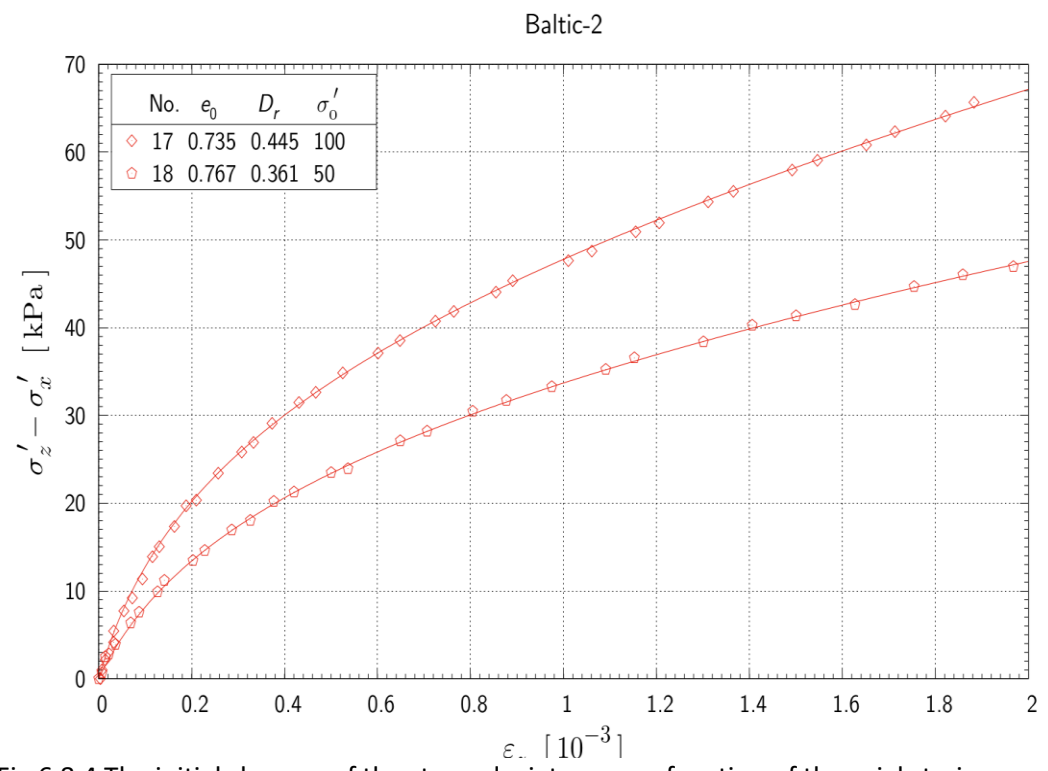


Fig. 6.8.4 The initial changes of the stress deviator q as a function of the axial strain – Baltic 2.





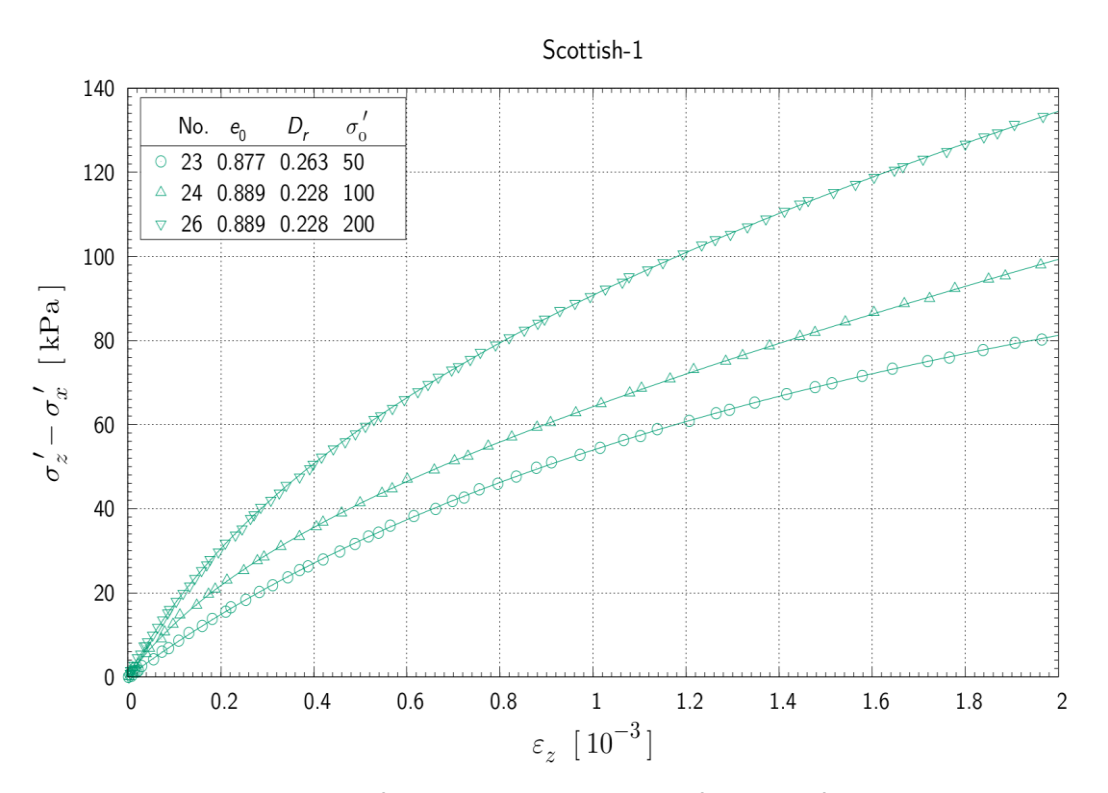


Fig. 6.8.5 The initial changes of the stress deviator q as a function of the axial strain – Scottish 1.

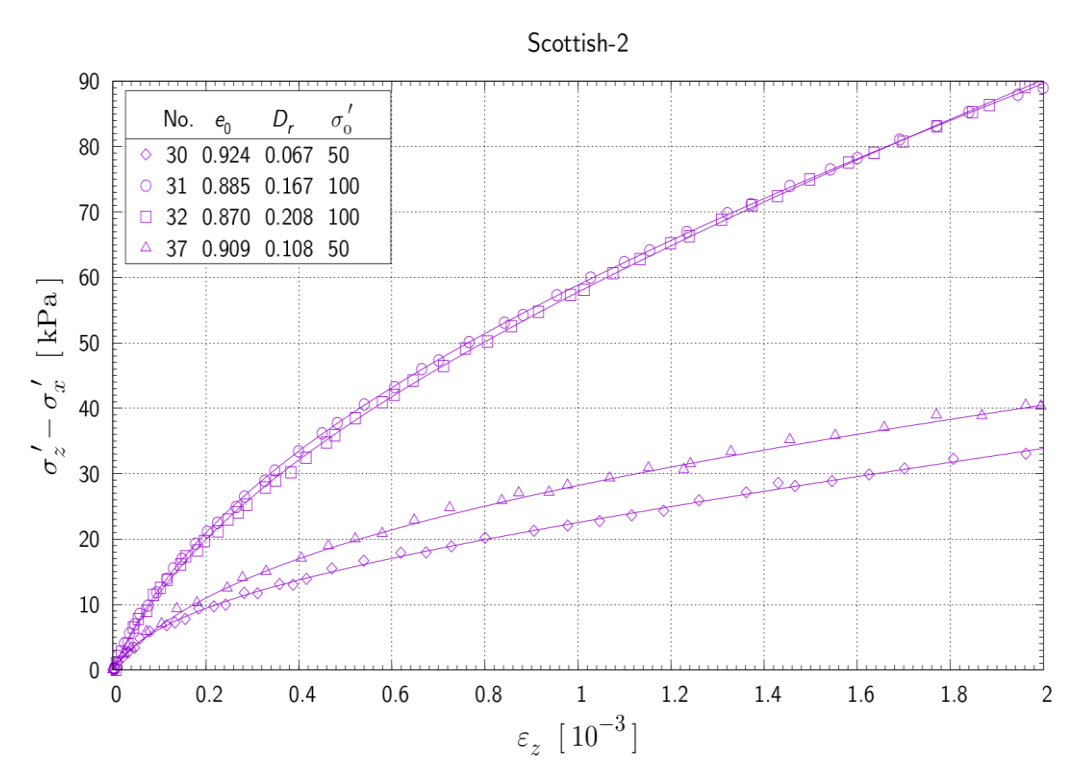


Fig. 6.8.6 The initial changes of the stress deviator q as a function of the axial strain – Scottish 2.





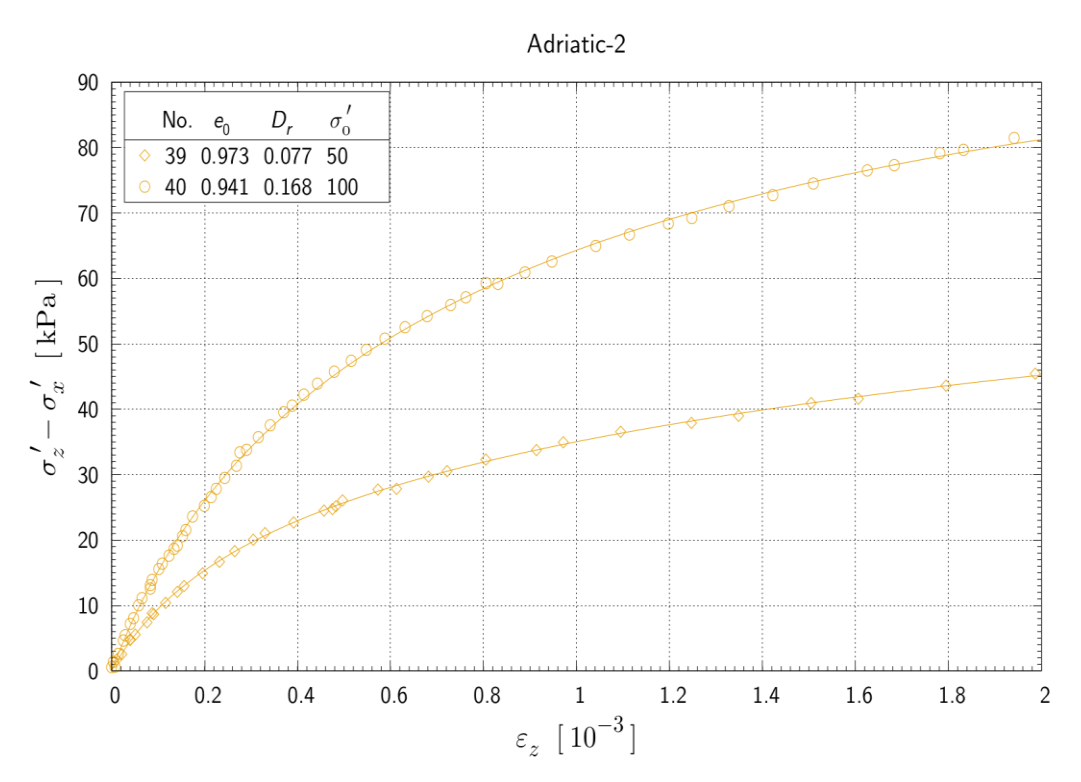


Fig. 6.8.7 The initial changes of the stress deviator q as a function of the axial strain – Adriatic 2.



2. Poisson ratio

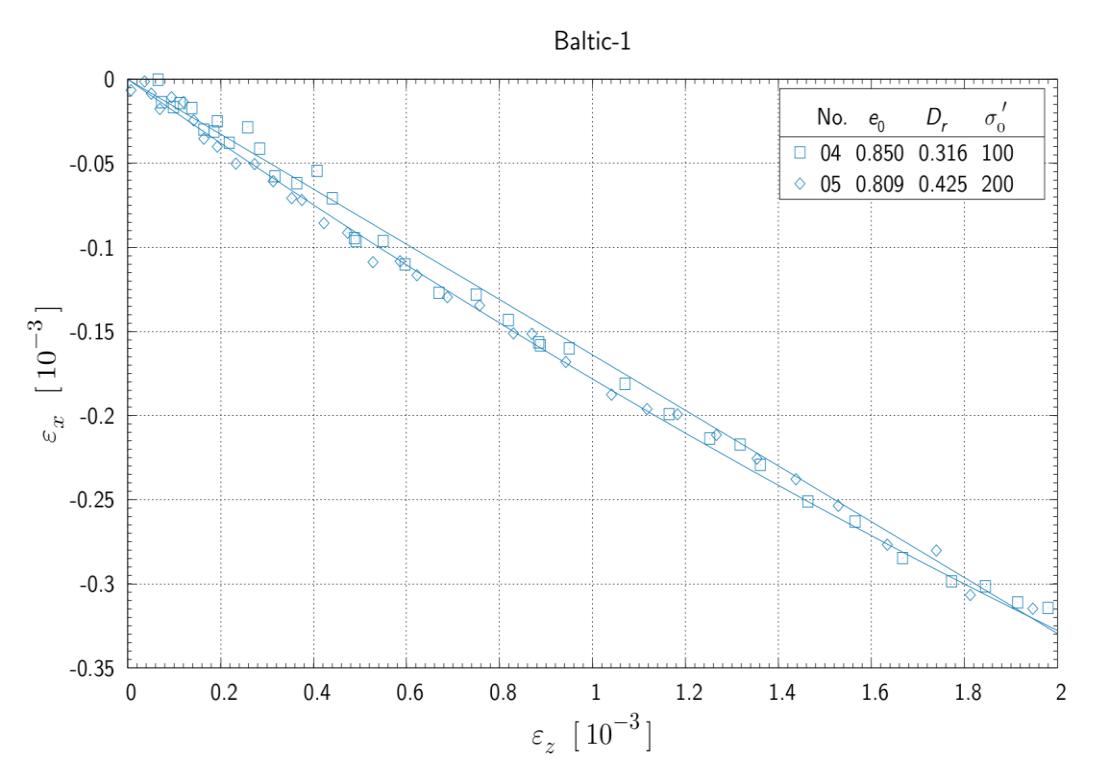


Fig. 6.8.8 Relationship between radial and axial strains - Baltic 1.

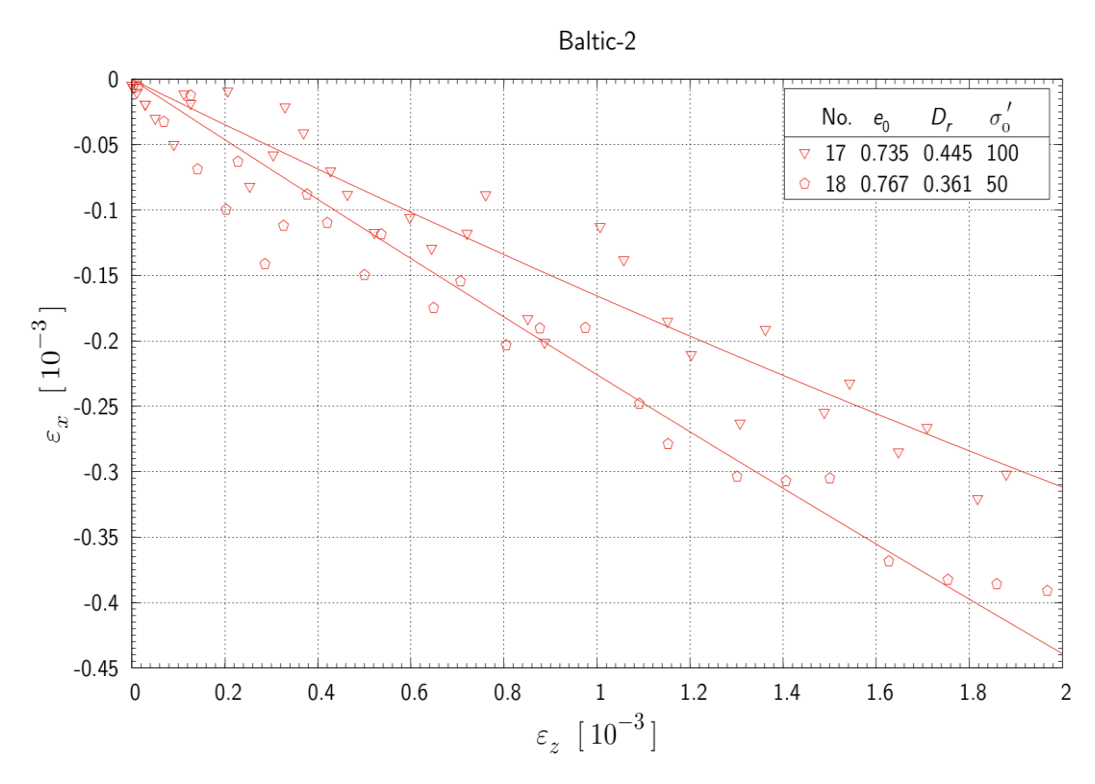


Fig.6.8.9 Relationship between radial and axial strains - Baltic 2.





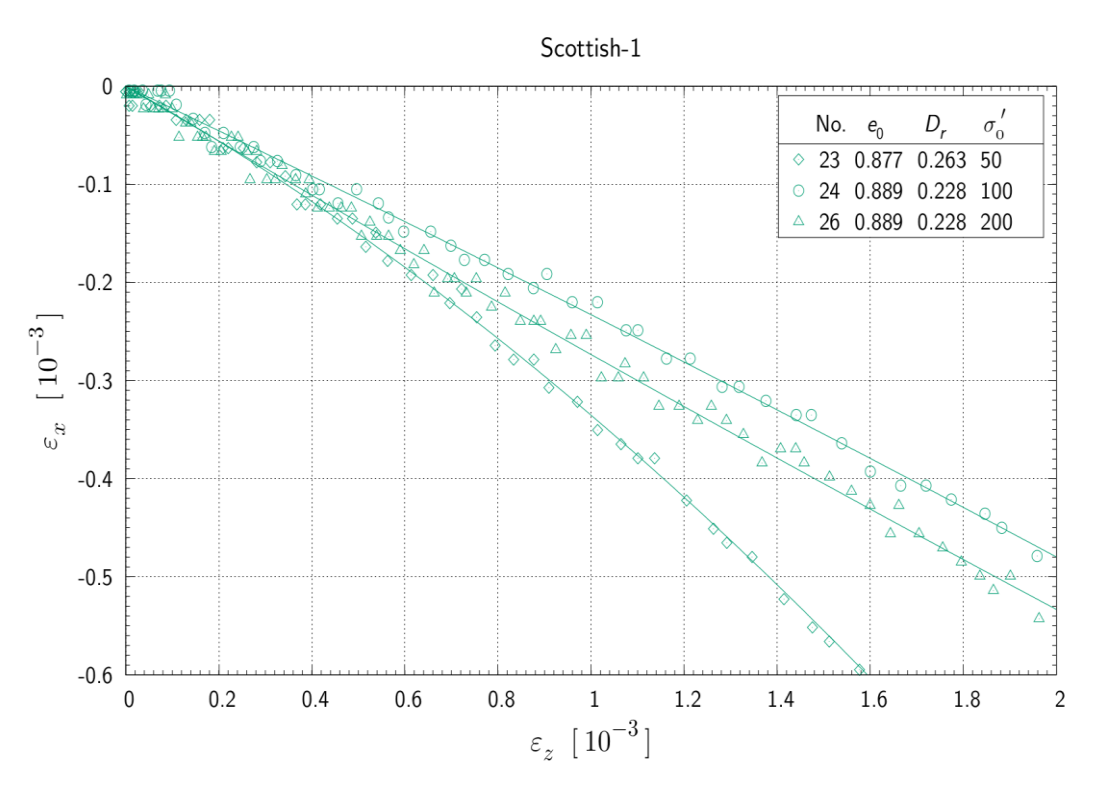


Fig. 6.8.10 Relationship between radial and axial strains - Scottish1.

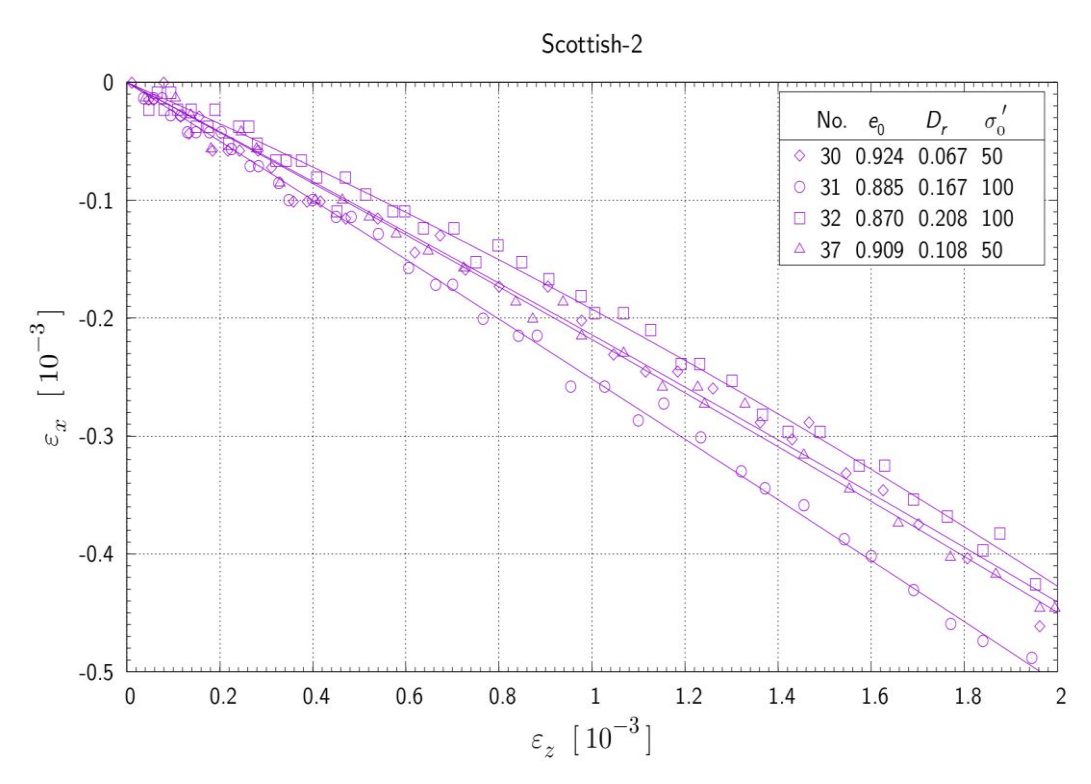


Fig. 6.8.11 Relationship between radial and axial strains - Scottish2.





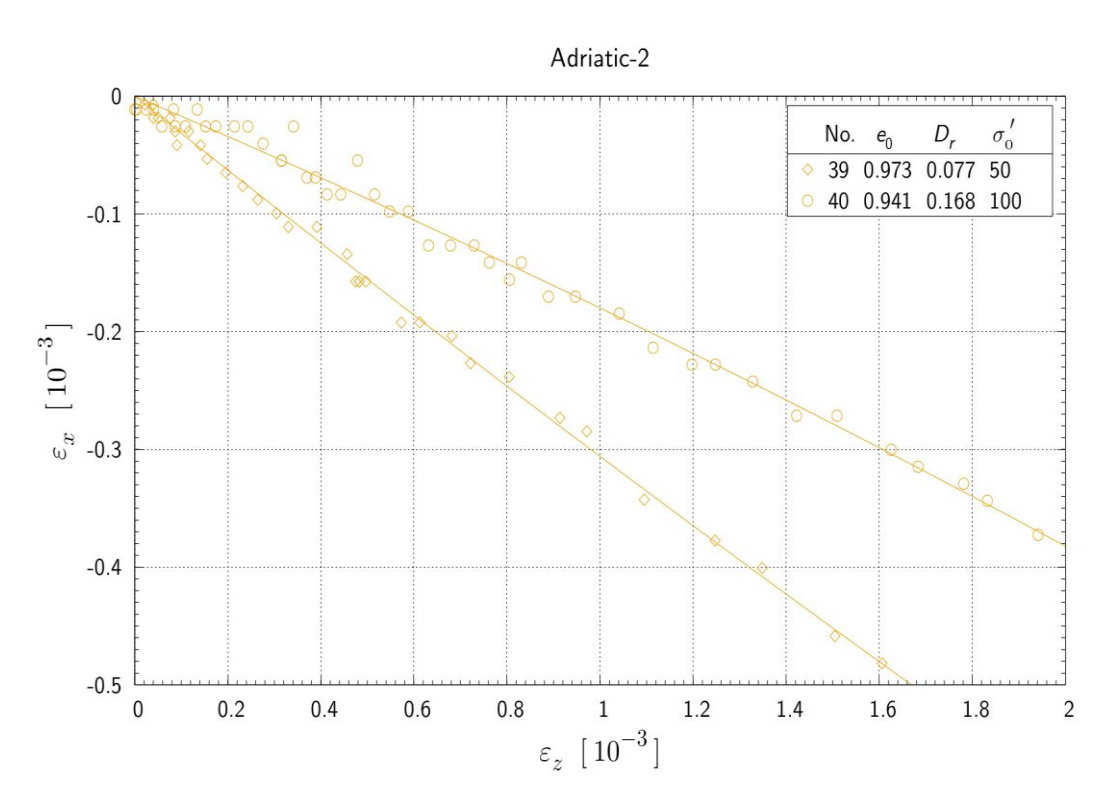


Fig.6.8.12 Relationship between radial and axial strains - Adriatic2.

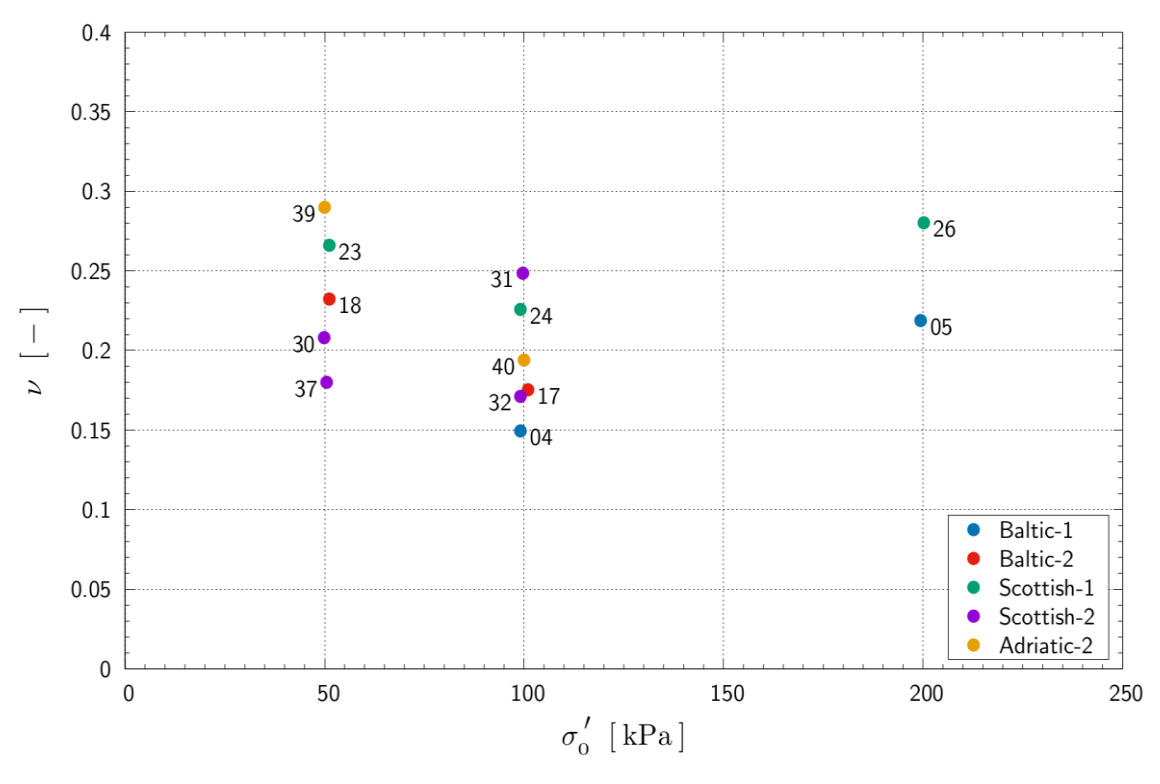


Fig.6.8.13 Values of Poisson ratio.

